

國立台灣大學電機資訊學院生醫電子與資訊學研究所



博士論文

Graduate Institute of Biomedical Electronics and Bioinformatics

College of Electrical Engineering and Computer Science

National Taiwan University

Doctoral Dissertation

信號複雜度於腦波與心電圖之相關性分析

Correlation analysis between ECG and EEG signals based
on signal complexity

林佩芬

Lin, Pei-Feng

指導教授：曹建和博士

Advisor: Tsao, Jen-Ho Ph.D.

中華民國104年1月

January, 2015

國立臺灣大學博士學位論文
口試委員會審定書

信號複雜度於腦波與心電圖之相關性分析
**Correlation analysis between ECG and EEG signals
based on signal complexity**

本論文係林佩芬君（學號 D99945002）在國立臺灣大學生醫
電子與資訊學研究所完成之博士學位論文，於民國 103 年 12 月
26 日承下列考試委員審查通過及口試及格，特此證明

口試委員：

曹建新

（指導教授）

郭柏宏

洪漢章

黃念祖

林啟萬

羅子亭

所長：

莊曜宇

誌謝 Acknowledgement



感謝所有費時費力配合檢查的受試叔伯、阿姨、朋友們。

感謝指導教授曹建和博士及研究夥伴們多年的指導與陪伴。

感謝口試委員張璞曾教授、林啟萬教授、郭柏齡教授、黃念祖教授及羅孟宗博士珍貴的指教。

感謝中研院院士黃鐸博士的指導與鼓勵。感謝成大蔡景仁教授、曾俊達教授的推薦與鼓勵。

感謝父親林世福及其他家人的支持與鼓勵。

感謝衛福部台南醫院及其新化分院，所有跟診本人門診以及神經科檢查室，各位護理師辛勞的協助。

感謝所有幫助我、鼓勵我的師長、同學、朋友和同事。因人數眾多無法一一列名，敬請海涵，鞠躬致歉。

In silence there is eloquence. Stop weaving and see how the pattern improves.— Rumi

中文摘要



緒論

生命的祕密至今無解。各種律動組成人體的運作，是維持生命的要素。這些律動彼此交互影響、形成迴路、並共同與擾動的、多變的環境發生應對。他們提供組成生命所需有序的功能。回顧歷史，心臟在許多不同文化裡被視為是情緒和智慧的本源。大多數的神經科學家認為意識及思考只是大腦及其相關的神經生理功能。然而，心臟在腦形成以前已經開始跳動。傳統說法，心與腦經由神經及荷爾蒙兩種路徑互相溝通，其溝通是否也能經由個別律動內所隱藏的動態變化，則令人好奇。心律變異是心臟自主神經系統的指標，腦波動態變化則被證明與意識活動有關。本論文始於複習非線性訊號分析。生物訊號屬於多尺度、非線性且非穩定性序列，混沌理論是否可行不需執著，非隨機的複雜性的確存在於生物信號中。我選擇以探討規則的統計為中心的複雜性分析來探討心腦連結問題。同步記錄及非同步記錄的腦波及心電圖都將被使用。實驗對象使用一群老人，基本上心臟功能健康、而意識功能則從健全到失智拉開分布。腦的電磁活動運轉非常迅速，類穩定的腦波信號是非常短的，處於幾十秒的尺度。因此我採用符號動力學方法來分析同步信號。腦波的來源至今未有定論，其中新近被討論的皮層慢電位，其頻率範圍接近心臟的。我採用非線性、直覺性的方法來著手探討皮層慢電位。並且對於腦波之電位及即時頻率兩個成分將分開探討。

研究方法及材料

實驗對象包含 89 個老年門診病患，分為三個族群，38 個血管型失智症、22 個阿茲海默症、以及 29 個智能健全的對照組。多尺度熵分析(Multiscale entropy)用以分析非同步的腦波心電圖，符號動力學方法用以分析同步的腦波心電圖。另外分散信號的方法用以將波幅及即時頻率分開。傅立葉頻譜低頻對高頻比(LF/HF)用以代表交感副交感神經平衡指數。



結果與討論

在非同步信號經由多尺度熵分析，我發現心腦信號之複雜動態間，的確存在線性關係。但短暫的同步信號之間並無關聯證據。這可能因為同步於腦波的心律變異太短，無法穩定表現個案特質。不過，符號動力學方法顯示：每個分散的腦波局部高峰，其電位值的變異與智能相關，但是腦波的及時頻率並不相關。這表是局部同步激發的皮質神經元數量而非其激發的時機與智能相關。熵的值，或說複雜度，亦即規則性的強弱並不代表健康度。不同方法測量的是生物信號的不同尺度。在腦波分析方面，分散信號的方法所得到的資訊，並不亞於全波形的分析。失智的病理表現可能是連續性而非階梯式的。

關鍵字


信號複雜性；心電圖；腦波；多尺度熵分析；符號動力學；振幅；及時頻率

ABSTRACT



Introduction

The secret of life remains extremely concealed. There are all sorts of rhythms in human bodies and they are central to life. The rhythms interact with each other as well as the outside fluctuating, noisy environment under the control of innumerable feedback systems. They provide an orderly function that enables life. The heart has been considered the source of emotional experience and wisdom in many cultures throughout the ages. Most neuroscientists consider consciousness or even thought is merely an epiphenomenon of the human brain function and its associated neurophysiology. However, the heart begins to beat before the brain is formed. Conventionally, both neural and humoral pathways connect the heart with the brain. Whether the interplay between the heart and brain could be explored through their rhythms is the question. Heart rate variability is recognized as the indicator of cardiac autonomic function. The dynamics of human electroencephalography (EEG) dynamics has been proved to be related to cognitive activities. This dissertation starts with reviewing the nonlinear methods in analyzing biological rhythms, which are multiscale, nonlinear and non-stationary. Regardless of whether chaos is present, deterministic complexity exists in biological rhythms. Regularity based complexity was chosen after comparisons. The goal is to find correlations between EEG and electrocardiography (ECG) through

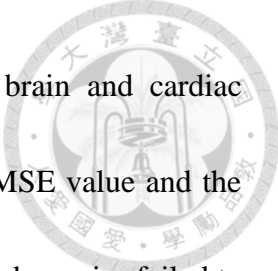


regularity based complexity analysis. Both simultaneous and non-simultaneous data would be examined. The experimental subjects are from a geriatric sample with varied cognitive abilities and basically healthy hearts. The electromagnetic activity of the brain works at an extremely fast speed, and the quasi-stationary epochs of EEG are, in general, short lasting, in the order of tens of seconds. Therefore symbolic techniques were introduced when exploring the very short simultaneous EEG and R-R interval (RRI) data. The origin of EEG remains unknown. Slow cortical potential (SCP), one component of EEG, is in the frequency range similar to that of the heart, and would be explored in an intuitive nonlinear way. In addition, the amplitude and instantaneous frequency of EEG would be separately approached.

Methods

The sample consisted of 89 geriatric outpatients in three patient groups: 38 fresh cases of vascular dementia (VD), 22 fresh cases of Alzheimer's disease (AD) and 29 controls. Multiscale entropy (MSE) analysis was applied to the non-simultaneous EEG and RRI data. Symbolic analysis was applied to the simultaneous EEG and RRI data. Discrete events (local peaks) of EEG were extracted to separate the amplitude and instantaneous frequency. The low-to-high frequency power (LF/HF) ratio of RRI was calculated to represent sympatho-vagal balance.

Results and Discussions



MSE revealed correlations between the signal complexity of brain and cardiac activities in non-simultaneous data. Linear correlation between the MSE value and the score of the mini-mental state examination was first found. Symbolic dynamics failed to correlate the heart to the brain. This is due to that the RRI is too short to represent the characteristics of a subject. The symbolic analysis revealed important information that the EEG dynamics which relates to either the cognitive functions or the underlying pathologies of dementia are embedded within the dynamics of the amount of but not the interval between each synchronized firing of adjacent cerebral neurons. Just like RRI of ECG, discrete events of EEG also provided important information. The relative value of complexity does not indicate health condition straightly. It depends on the method and the scale or dimension that particular method measures. Discrete events provide no less information than continuous waveforms of EEG. Pathological condition is continuous rather than stepwise.

Key words: signal complexity; ECG; EEG; Multiscale entropy; symbolic dynamics; amplitude; instantaneous frequency

CONTENTS



口試委員會審定書	ii
誌謝	iii
中文摘要	iv
ABSTRACT	vi
CONTENTS	ix
LIST OF TABLES	xv
LIST OF FIGURES	xvi
Chapter 1 Introduction	1
1.1 The Heart and the brain.....	1
1.2 Biological rhythms.....	6
1.3 Electroencephalography.....	8
1.3.1 Components and characteristics of EEG.....	9
1.3.2 Functional connectivity.....	11
1.3.3 Amplitude of EEG.....	12
1.4 Eelectrocardiography	14
1.5 Exploring a system.....	15
1.5.1 System thinking.....	15
1.5.2 System dynamics.....	17



1.5.3	Critical point.....	18
1.5.4	Complexity	18
1.6	Deterministic dynamics	21
1.6.1	Dynamics observation	21
1.6.2	Randomness and stochasticity.....	22
1.6.3	Law of nature	24
1.6.4	Fractals	26
1.6.5	Deterministic chaos	27
1.6.6	Chaos in medicine	30
1.6.7	Measures of chaos	33
1.6.8	Interpretation of the fractal dimension	37
1.6.9	Other fractal measurements.....	39
1.6.9.1	Rescaled range analysis	39
1.6.9.2	Detrended fluctuation analysis.....	40
1.6.10	Issues of embedding dimension	42
1.6.11	Multifractality	43
1.6.12	Lacunarity	44
1.6.13	Advantages of chaos in physiology.....	45
1.6.14	Non-stationarity.....	47



1.6.15	No guarantee of chaos	48
1.7	Entropy.....	50
1.7.1	Information entropy	52
1.7.2	Measures of entropy	53
1.7.2.1	Sample entropy and approximate entropy	53
1.7.2.2	Multiscale entropy	58
1.7.3	Network theory.....	60
1.7.4	Multiple attractors or single attractor	61
1.8	Symbolic dynamics	62
1.8.1	Symbolization or symbolic time-series analysis	62
1.8.2	Procedure of symbolization.....	65
1.8.3	Forbidden words.....	65
1.9	Surrogate data	66
1.10	Empirical mode decomposition	68
1.11	Dementia	70
Chapter 2	Experiments	71
2.1	Hypotheses	71
2.2	Material and Methods	71
2.2.1	Study population	71



2.2.2	Data collection	73
2.2.3	Data analysis	74
2.2.3.1	Filtering and detrending of EEG	74
2.2.3.2	LF/HF ratio	75
2.2.3.3	Multiscale entropy	75
2.2.3.4	Symbolic dynamics	75
2.2.3.4.1	Four sequences derived from EEG	75
2.2.3.4.2	Construction of symbolic sequences	77
2.2.3.4.3	Number of forbidden words and surrogate data.....	77
2.2.3.4.4	Steps and others.....	78
2.2.3.5	Statistical analysis	79
Chapter 3	Results	81
3.1	MSE analysis (non-simultaneous EEG and RRI)	81
3.1.1	Linear correlations between the MSE of EEG and RRI	81
3.1.2	Correlated data	84
3.2	Symbolic dynamics (simultaneous EEG and RRI).....	85
3.2.1	Discriminative power found only after the symbolization procedure.....	85
3.2.2	The local-peak voltage sequence of EEG shows the same	



dynamics in the EEG whole tracing.....	85
3.2.3 No correlations between simultaneous EEG and RRI.....	89
3.2.4 Correlated data	89
3.2.5 The number N of words used for estimation of the number of forbidden words	90
Chapter 4 Discussion.....	92
4.1 Inverse correlations between the signal complexity of cardiac and cerebral activities	92
4.2 The merits of symbolization and regularity based analysis	93
4.3 Study of the discrete events	94
4.4 Regularity based complexity study	96
4.5 The issue of more or less complexity	97
4.6 Photic stimulation amplified differences between groups	98
4.7 Nonlinear and non-stationary filters	100
4.8 Single or multichannel in EEG	101
4.9 Wide band or narrow band.....	102
4.10 Limitations	103
Chapter 5 Conclusion.....	104
Reference	107

English Abbreviation.....151



LIST OF TABLES

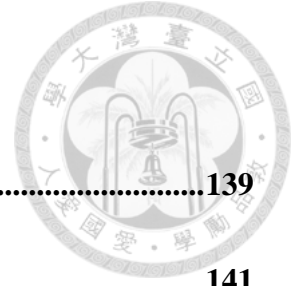


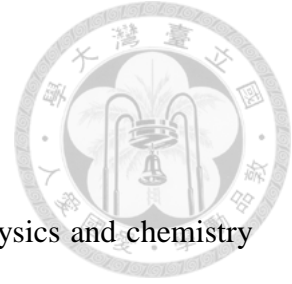
Table 1	139
Table 2	141

LIST OF FIGURES



Figure 1	143
Figure 2	144
Figure 3	145
Figure 4	146
Figure 5	147
Figure 6	148
Figure 7	149
Figure 8	150


Chapter 1 Introduction



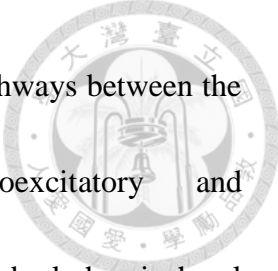
What is life? Alongside the development of modern science, physics and chemistry have been leading researches in biology, ranging from the molecular level to the entire organism. For example, individual atoms are combined to form molecules such as polypeptide chains, which then fold into protein. Protein, together with polysaccharides, nucleic acids, electrolytes, water, etc., confined by a sheet of lipid bi-layer called “membrane”, form the basic unit of living organism called “cell”. Contrary to religious legends, “life”, “intelligence”, and “consciousness” simply emerge from the interaction of those “inanimate” atoms. Nevertheless, these emergent phenomena remain outside the range of engineering-like sciences. Even when people are able to simulate a small organism like bacteria with a computer by putting all the chemical components together with rules of their interactions, it would probably far from manufacturing life itself. What is the essence of life? What are the laws of nature? Are there lawgivers? People ask all sorts of questions with desire to manipulate “life” on the background of the fear of “death”.

1.1 The Heart and the brain

The prenatal development of heart activity starts at the 3rd week, while the neural activity of the human brain starts between the 17th and 23rd week of prenatal

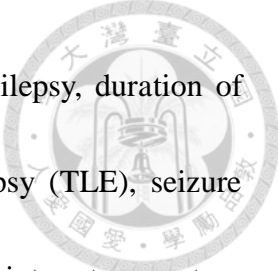


development. The heart begins to beat before the brain is formed. Whether conventional hierarchical central commands sent by the brain to the heart alone explain all the interplay between these two organs should be reconsidered. The heart has been considered the source of emotional experience and wisdom in many cultures throughout the ages. Nevertheless, scientists have been telling a different story which emphasizes the role of the brain as being responsible for those. The heart and the brain are the two most important organs in the body and their electromagnetic dynamics can easily be measured. The connection of the heart and brain is mainly through autonomic pathways by current knowledge. According to previous neuroanatomical and pharmacophysiological findings, various functional units within the central nervous system (CNS) serving either attention, emotion, physiological adaptabilities, and behavioral responses to accommodate fast changing environmental demands were proposed. These units such as the central autonomic network (Benarroch, 1993), the anterior executive region (Devinsky et al. , 1995), the emotion circuit (Damasio, 1998), the frontal-subcortical circuits (Masterman et al. , 1997), and the cardiovascular control circuits during affective behavior (Spyer, 1989) all share many common components and pathways. Thayer has suggested those units may just represent a common central functional network recognized from diverse approaches and proposed the neurovisceral integration model, which included inhibitory GABAergic pathways from the prefrontal



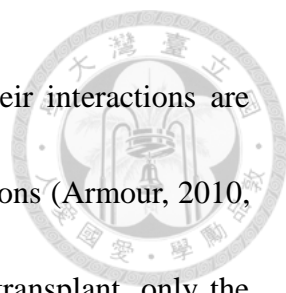
cortex (mainly right side) to the amygdala and another inhibitory pathways between the amygdala and the medullary neurons of sympathoexcitatory and para-sympathoinhibitory output (Thayer et al. , 2009). Cerebral hemispherical dominance with regard to autonomic control was proposed as right predominantly sympathetic and left predominantly parasympathetic (Oppenheimer et al. , 1992).

The heart and the brain have an intimate and underestimated relation (Daemen, 2013). Diseases caused by the disturbance of this relationship can be grouped into three categories: 1) the brain's effects on the heart (i.e., Takotsubo cardiomyopathy (Merli et al. , 2006) and sudden unexpected death in epilepsy (SUDEP) (Dupuis et al. , 2012); 2) neurocardiac syndromes (i.e., hypertrophic cardiomyopathy in Friedreich ataxia); and 3) the heart's effects on the brain (i.e., the cardiac origin of embolic stroke and the cardiovascular contribution to cognitive impairment (Muqtadar et al. , 2012)). Through the studies of SUDEP one may get a quick impression of how powerful the effect of the neurocardiological connection can be. Sudden unexpected death in epilepsy (SUDEP) is the most important direct epilepsy-related cause of death in people with chronic epilepsy. It remains an unknown case in pathophysiology and may share the same mechanism with Takotsubo cardiomyopathy. It has been understood as the effect of autonomic storm, both sympathetic-early and parasympathetic-later impacts mainly through direct nerve terminal but not hormonal pathway (adrenal glands) (Samuels,



2007). The risk factor include age (young male), early onset of epilepsy, duration of epilepsy (long), uncontrolled seizures, mainly temporal lobe epilepsy (TLE), seizure frequency (more), anti-epileptic drugs number (more), and winter temperature (Stollberger et al. , 2004). As stimulation of certain brain areas (subiculum, posterior hypothalamus, ventrolateral thalamus and substantia nigra) has been shown to modify heart function without producing disturbances in the activity of the brain (Delgado, 1960), SUDEP could possibly be related to some focal brain lesion. Epileptic activity originating in the amygdala, cingulated gyrus, insular cortex, frontopolar or frontoorbital regions may induces supraventricular tachycardia, sinus tachycardia, sinus bradycardia, sinus arrest, atrioventricular block and asystole (Devinsky et al. , 1997). Current data (experimental and clinical) support an important role of thalamus on manifestations, initiation and propagation of epileptic seizures (Scorza et al. , 2009).

The heart communicates with the brain in three ways: neurologically, biochemically, and possible energetically (as electromagnetic field). The neurological communication between the heart and the brain is bidirectional. Evidences showed that the intrinsic cardiac ganglia contain sensory and local circuit neurons as well as sympathetic and parasympathetic efferent postganglionic neurons; and the intrathoracic extracardiac ganglia contain not only cardiac sympathetic efferent postganglionic neurons but also cardiac afferent neurons and local circuit neurons. These neurons can operate and



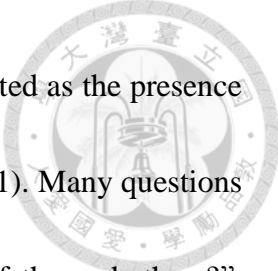
processes information independently of the brain and they and their interactions are under the tonic influence of central (medullary and spinal cord) neurons (Armour, 2010, 2011). This is what allows a heart transplant to work. In a heart transplant, only the intrinsic cardiac nervous system is intact and the connections to other body parts do not reconnect for an extended period of time, if at all; however, the transplanted heart is able to function in its new host. Studies have demonstrated that stimulation of vagus afferents regulate brain structures involved in epilepsy on the hypothesis that vagal afferents have diffuse projections into the central nervous system and that activation of these afferents has a widespread effect on neuronal excitability (Boon et al. , 2001, Beekwilder et al. , 2010). Vagal stimulation is an FDA-approved treatment for epilepsy and is currently under investigation as a therapy for obesity, depression, migraine anxiety and Alzheimer's disease (Beekwilder et al. , 2010).

The body often responds to a future emotionally arousing stimulus 1 to 10 seconds prior to experiencing the stimulus. This process is system-wide as studies reported changes in pupil size and blinking (Radin et al. , 2009) as well as both the heart and brain (Radin, 1997, McCraty et al. , 2004a, b, Mossbridge et al. , 2012, Mossbridge et al. , 2014). And the heart may even response earlier than the brain (McCraty et al. , 2004b). If the heart does percept a future external event before the brain, current knowledge of human body should be extended revised.



1.2 Biological rhythms

Most neuroscientists consider consciousness or even thought is merely an epiphenomenon of the human brain function and its associated neurophysiology. They believe that eventual understanding of these physiological processes through studies such as anatomical structure of the brain for cognition, sensory perception, and language will ultimately reveal the mind's structure and function. It is most hard for me to believe that "thought" simply emerges from the chemical and physical components of neurons following the correct dynamics of the system. However, the secret of life remains extremely concealed. What might be a practical approach is to better understand the emergent properties of the systems once the interactions between their parts are known. Such approach deals with what is called complexity and rhythms. There are all sorts of rhythms in human bodies, like heart beats, brain waves, circadian cycles, menstrual cycles, the repetitive swings of limbs in locomotion, and many other rhythms underlying the release of hormones that regulating metabolism, growth and degeneration, etc. All these rhythms are central to life. The rhythms interact with each other as well as the outside fluctuating, noisy environment under the control of innumerable feedback systems. They provide an orderly function that enables life. Through this aspect, we could say that life is self-organized complexity of various physiological rhythms (Glass, 1988). Applying techniques of engineering to the analysis



of “rhythms” would be able to find long trends which can be interpreted as the presence of memory, an interesting feature in biological systems (Gisiger, 2001). Many questions are waiting to be answered, such as “Where are the pacemakers of these rhythms?”, “Are they running in stochastic or deterministic ways?” etc.

The analysis of such high-level dynamics induced by internal interactions and feedbacks cannot be reduced to analysis of their components. The “whole” is more than the sum of the parts, so the traditional reductionistic modeling is not appropriate. Nevertheless, biomedical signals (biosignals) in their manifold forms which when appropriately processed are rich information sources, including individual dynamics, couplings between varied systems, responses to stresses, interaction with the environment and even disease prediction/diagnosis. According to studies, contradictory to the traditional sense of homeostasis as equilibrium, the best condition of the human body may not be in a steady state, it fluctuates (Goldberger et al. , 2002). Regardless of the mechanism, it is debatable whether this fluctuation is essential to physiological function, and to what extent is the fluctuation acceptable. Furthermore, in most natural as opposed to laboratory settings, the interaction from the environment is continuous, so that separation of dynamics due to intrinsic from extrinsic mechanism is not possible. It is very difficult in dealing with complex physiological rhythms.



1.3 Electroencephalography (EEG)

The wakeful resting EEG represents the stimulus-independent intrinsic activity of the brain, which accounts for a big part of the energy budget of the brain (Raichle, 2006), and its alteration may lead to disorders ranging from Alzheimer's to schizophrenia (Zhang et al. , 2010). The underlying origins of EEG rhythms remain mystery. The network is extremely complicated.

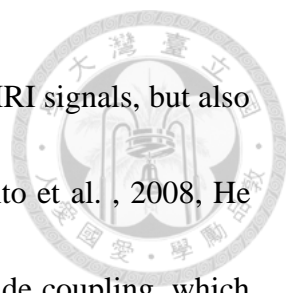
The human head consists of different layers including the scalp, skull, brain, and many other thin layers in between. The skull attenuates the signals approximately one hundred times more than the soft tissue. Only large populations of active neurons can generate enough potential to be recordable using the scalp electrodes. Approximately 10^{11} neurons are developed at birth when the central nervous system (CNS) becomes complete and functional. This makes an average of 10^4 neurons per cubic mm. Neurons are interconnected interwoven through synapses. Adults have approximately 5×10^{14} synapses. The number of synapses per neuron increases with age, whereas the number of neurons decreases with age. Because of the huge attenuation by the skull, EEGs are of tiny amplitudes which would easily be corrupted by noises such as the patient-related or internal artefacts: electromyography (EMG), ECG (and pulsation), electroculograph (EOG), ballistocardiogram, and sweating. The system artefacts include 50/60 Hz power supply interference, impedance fluctuation, cable defects, electrical noise from the

electronic components, and unbalanced impedances of the electrodes.



1.3.1 Components and characteristics of EEG

In neuroscience, the reactions of neurons or neural networks upon particular stimuli can be regarded as impulse responses. Examples are, currents through single ion channels as measured in patch-clamp experiments, receptor potentials, local field potentials, evoked or event-related brain potentials (ERP), and functional magnetic imaging (fMRI) data, in psychophysics and cognitive neuroscience (beim Graben et al. , 2007). The dynamics of EEG is therefore extremely not stationary. Rhythmic oscillations were the very beginning of EEG research. The German neurophysiologist Berger (1929) first observed the dominant oscillations of approximately 10 Hz recorded from the human scalp, which was called alpha waves. The second type of rhythm approximately 12-30 Hz was called beta waves by Berger. Adrian (1942) named oscillations around 40 Hz (more general 30-80 Hz) observed after odor stimulation in the hedgehog as gamma waves. The slow oscillations below 4 Hz was named delta next, and then, the rhythm around 4-8 Hz was named theta after the first letter of their assumed region of origin, the thalamus. Arrhythmic EEG activities were recognized much later. The arrhythmic EEG contains no true rhythms but mainly the slow cortical potential (SCP) (Steriade et al. , 1993), which is scale-free and may better be considered as fluctuations rather than oscillations at the slow end (mainly < 1 Hz, can extend up to



4 Hz) of the field potential. The SCP does not only correlate with fMRI signals, but also seems to modulate the amplitude of higher-frequency activity (Monto et al. , 2008, He et al. , 2009). The mechanism of this cross-frequency phase amplitude coupling, which means that the amplitude of one frequency band is dependent on the phase of the other, is not yet clear.

The brain is an organ with memories so EEG records might be highly autocorrelated and even worse as the time delay is longer than 10 msec since the feedback through synapses might come into play (Xu et al. , 1988). Does a series of data points taken from a segment of one channel of EEG represent an attractor of brain? To answer this question, one need to exclude the data considered as the transient effect than calculate the dimension from the remaining data. The embedding theorem requires that all data points are on the attractor and also an infinite number of clean values, which means a long series of noise-free points. However, in the case of EEG record we do not know where the transient segment is and how rapidly the brain changes its states. Besides, the tendency to see things as results of short-term events undermines our ability to see things on a grander scale. In the other hand, if the EEG data belong to a mixture of different dimensions, then what would be the results as we calculate them as a whole? All these limitations have made EEG analysis difficult in real time status monitoring.



1.3.2 Functional connectivity

The human brain is believed to function on the base of networks of interactivity of neural assemblies, which could be approached through the transient phase couplings (synchronization) of different types between EEG signals from various regions. Balance between synchronization (phase locking between two regions) and desynchronization (phase shifting) is essential for normal brain function and abnormal balance is often associated with diseases (Stam et al. , 2003, Hong et al. , 2004, Pijnenburg et al. , 2004, Garcia Dominguez et al. , 2005, Lackner et al. , 2013). Functional connectivity thus was proposed to be essential for cognitive functions. However, functional MRI (fMRI) studies showed that a direct anatomical link does not necessarily coexist with robust functional connectivity (Koch et al. , 2002) and the within-subject test–retest reliability of functional connectivity as measured was surprisingly low (Honey et al. , 2009).

A study in 1988 reported that in normal opened eyes resting states, the correlation dimensions of EEGs are coincidentally about 3-4, while in closed-eye states, the dimensions are varied between people (Xu et al. , 1988). Is this result related to mental states, free thought or attention states? While in open-eye states, a big part of the input information into brain would be from visual sensation. Would this associate with the attention state which determines the dimension of EEGs?



1.3.3 Amplitude of EEG

The dynamics of EEG rhythm has been proved to provide information related to cognitive functions (Vecchio et al. , 2013). Whether the dynamics of EEG amplitude also correlates to cognitive functions is not often discussed. The EEG amplitude of a normal subject in the wakeful state recorded with the scalp electrodes is 10 μ V to 100 μ V. Higher background amplitudes are associated with lower frequencies in normal EEGs for all age groups (Aurlien et al. , 2004). Symmetrical low voltage and even visually unrecognizable alpha rhythm was not regarded as pathological. The well known and widely-used techniques in amplitude estimates of EEG include the amplitude integrated EEG (aEEG), integrated root mean square voltage (RMS), and the integrated magnitude of the analytic associate of the EEG (mA A) (Stevenson et al. , 2010):

- 1) the amplitude integrated EEG (aEEG)

$$aEEG(t_0) = \frac{1}{L} \int_{t_0-L/2}^{t_0+L/2} |eeg(t)F(eeg(t))| dt ,$$

$$\text{where } F(eeg(t)) = \begin{cases} eeg(t) & |eeg(t)| \leq 10\mu V \\ 10\log_{10}(eeg(t)) & |eeg(t)| > 10\mu V \end{cases}$$

- 2) integrated RMS voltage (RMS)

$$RMS(t_0) = \sqrt{\frac{1}{L} \int_{t_0-L/2}^{t_0+L/2} eeg(t)^2 dt}$$



3) integrated magnitude of the analytic associate of the EEG (mAA A)

$$\text{mAA}(t_0) = \int_{t_0-L/2}^{t_0+L/2} |z(t)| dt$$

$$Z(t) = \text{eeg}(t) + jH\{\text{eeg}(t)\}$$

These methods actually do not represent the real EEG amplitude intuitively sensed by the neurophysiologist. We would expect nonlinear approaches can reveal more of the hidden characteristics of EEG amplitude. The question is how to evaluate the EEG amplitude intuitively and separately from the rhythm.

The scalp EEG mainly records large postsynaptic potentials (Nunez, 1981). One peak of a single-channel EEG contains relatively simultaneous firing electromagnetic activities of a big collection of neurons. The peaks and troughs of a physical wave indicate levels of probability for the occurrence of certain phenomenon. One peak implies a local maximal (in time domain) amount of synchronized active neurons in a localized region. One intuitively expects that the brain works on those synchronized firing. The dynamics of the local peaks of EEG reflects the changing degree of neuronal couplings in the localized brain area. One would suppose these discrete events (local maxima) may provide more focused information in certain dimension of the dynamics. When extracting the peaks from a single-channel EEG, one obtains two sequences, the local-peak voltage sequence and the interpeak interval sequence. The local-peak voltage sequence depicts the amplitude change while the interpeak interval sequence illustrates

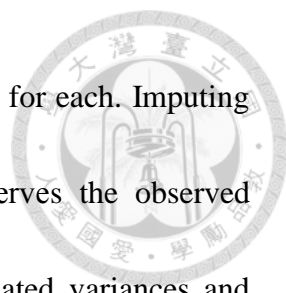
the instantaneous frequency. This is my approach to treating the amplitude and rhythm separately.



1.4 Electrocardiography (ECG)

Signal processing has made ECG a new tool to understand physiology through its dynamic properties as expressed by changes in rhythm and beat morphology. Techniques have been developed that characterize oscillations related to the cardiovascular system and reflected by subtle variations in heart rate. Heart period variability is the result of the following mechanisms: cardiovascular reflexes mediated by vagal and sympathetic afferences, activity of vasomotor and respiratory centers, baroreflex and chemoreflex feedback loops, and vascular autoregulation. All these mechanisms act over similar but not coincident frequencies (below 0.5 Hz) contributing to the complexity of the signal (Guzzetti et al. , 2005). The study of heart rate variability (HRV), namely the variability of RR intervals (RRI), can monitor the autonomic system. The detection of low-level, alternating changes in T wave amplitude comprises another dynamic complexity which can indicate the risk for sudden, life-threatening arrhythmias (Korhonen et al. , 2009).

Ectopic beats either benign or pathological are very common in clinical ECG recordings; they come from pathological origin or conduction, which cannot represent the real heart rate variability. The problem comes to how to replace the ectopic data



when we exclude them. Two commonly used methods have deficits for each. Imputing an observed variable mean for a variable's missing values preserves the observed sample means, but distorts the covariance structure, biasing estimated variances and covariances toward zero. On the other hand imputing predicted values from regression models tends to inflate observed correlations, biasing them away from zero. So both can lead to misleading standard errors and p -values, since they fail to reflect the uncertainty due to the missing data (Everitt, 2005).

1.5 Exploring a system

1.5.1 System thinking

Ever since Descartes, reductionism has led a dominant role in the modern science of this present civilization. Although smaller and smaller parts such as components inside an atom nucleus have been understood, knowledge such as how life emergent from atoms and how does it work remain mysterious. Genetics studies have gained the most attention in medicine during the second half of the last centuries. A considerably large amount of capital has burned without practical achievements in disease control. In the real world, the “whole” is not the sum of the parts. Therefore, people turned to “systems philosophy”, which regards an understanding of a system by examining the linkages, interactions, and feedback loops between the elements that

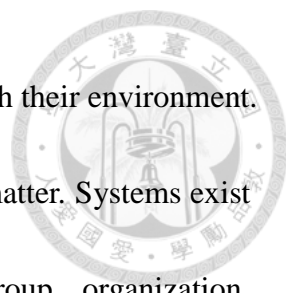
compose the entirety of the system. An important point here is that the interactions of the parts are not "static" and "constant" but "dynamic" processes.



In Schrödinger's "what is life?" published in 1944, he proposed a paradox: According to the second law of thermodynamics, "The entropy of a closed system cannot decrease.", life approaches and maintains a highly ordered state, therefore it seems to violate the second law (Schrödinger, 1944). Entropy is the disorder of an object, and a closed system is a system in which no energy can enter or exit. But life itself is not a closed system since energy can easily enter and leave your body. If a human body were a closed system, then no energy could be taken into or out of the body and thus one would never need to eat. The decrease of order inside an organism would be paid for by an increase in disorder outside this organism.

System theory has provided a view of web, high above the phenomenon. For physiological systems of human body, two concepts would be emphasized first. The first one is "self-regulating system", which means the system is open and can be self-correcting through feedback. The second one is "adaptive system", which means a set of interacting or interdependent entities, real or abstract, forming an integrated whole that together are able to respond to environmental changes or changes in the interacting parts.

In 1978, James Grier Miller has proposed the living system theory. He stated that



living systems are open self-organizing living things that interact with their environment. These systems are maintained by flows of information, energy and matter. Systems exist at eight "nested" hierarchical levels: cell, organ, organism, group, organization, community, society, and supranational system. There are twenty critical subsystems, which process matter–energy or information (Miller et al. , 1992). In the living system theory, it would be difficult to understand if determinism is denied. Thus it still comes to the big problem, how to prove determinism.

1.5.2 System dynamics

System dynamics is an approach to understanding the behavior of complex systems over time. It tries to understand internal feedback loops through the changes of the behavior of the system due to time delays. The use of feedback loops is the weighting point. These loops help describe how even seemingly simple systems display annoying nonlinearity. System dynamics is a methodology and mathematical modeling techniques for framing, understanding, and discussing complex issues and problems. System dynamics is an aspect of systems theory as a method for understanding the dynamic behavior of complex systems. It was developed in the 1950s for helping the understanding of industrial processes (Forrester, 1971). The main part of the method is the recognition of the structure of a system — the many circular, interlocking, sometimes time-delayed relationships among its components.



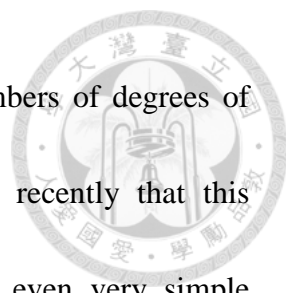
1.5.3 Critical point

A system, no matter it is a laboratory or a mathematical model, is very insensitive to details of its dynamics or structure near critical points. If we can find a parameter which behaves the universality, then we only need to consider the simplest mathematical model possibly conceivable in the same universality class. It will then yield the same critical exponents as the system under study. In other words, for any particular physical system, there may be many scale-dependent parameters and aspects. When we approach the phase transition, the scale-dependent parameters play less and less of an important role, and the scale-invariant parts become dominant. Thus, a simplified, and often solvable, model can be used to approximate the behavior of these systems near the critical point.

1.5.4 Complexity


What is complexity? “When the same action has dramatically different effects in the short run and the long, there is dynamic complexity. When an action has one set of consequences locally and a very different set of consequences in another part of the system, there is dynamic complexity. When obvious interventions produce non-obvious consequences, there is dynamic complexity (Senge, 1990).

For a long time, physics has been able to avoid complex situations and to only work on systems that are comparatively simple. This is because they were only dealing with



few degrees of freedom and when in systems involving large numbers of degrees of freedom one can apply central limit theorems. It became clear recently that this simplification is not sufficient to avoid complex behavior. And even very simple systems with few degrees of freedom can show very complex behavior if they are "chaotic". Confronted with so complex biological systems that might be with large numbers of degrees of freedom, intuitively one best approach would be quantifying this judgment by defining an observable. In serious consideration in physics there are different concepts of complexity, set complexity, algorithmic complexity, true measure complexity, and effective measure complexity. I am not going into details of those; my concerned point is to search for useful variables which are good in prediction of the health condition.

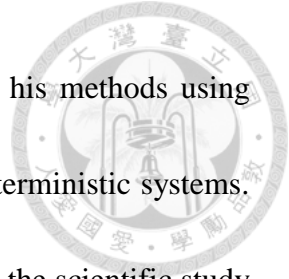
The complexity theory deals with non-equilibrium processes of change. It comes from statistical physics. The real-world processes of change rarely take the form of sudden leaps between equilibrium states. So a general dynamic theory of living systems –the “dynamic-strategy theory” was gradually developed. As it turns out, the construction (rather than the “emergence”) of complex systems is the outcome of a process of “strategic exchange” between the demand and supply sides of dynamic living systems, rather than the outcome of supply-side local interactions between agents (Snooks, 2008). The dynamic model of the strategy process is a way of understanding



how strategic actions occur. Strategic planning is dynamic, that is, strategy-making involves a complex pattern of actions and reactions, which may be involved with deterministic and random parts. This is the breakthrough required in the quest for a general theory of complexity.

There is no such thing as a linear system in the real world. The traditional approach in science is to see complexity and attribute it to randomness, to try to smooth it, and to try to model nonlinearity with successively more complicated approximations to linearity. Through doing this, we might be in a direction away from the reality. To medieval thinkers, the union of mathematics and natural science would have been illicit and barren. Following Aristotle, they held mathematics to be a product of the human mind. For this reason mathematics was not thought to provide true descriptions of reality: useful descriptions – yes – but not true descriptions. Under the thriving computer techniques, mathematics models are much emphasized in life science nowadays. But we should always keep some doubt in mind that the nature does run according to mathematics.

Nevertheless, statistical approaches, typified by fractal statistics, that measure roughness directly, could provide an alternative way of approach. Starting from Poincaré, for example, in the early years of 20th century, recognized this and then promoted a more convenient and "useful" description of the corresponding phenomena.

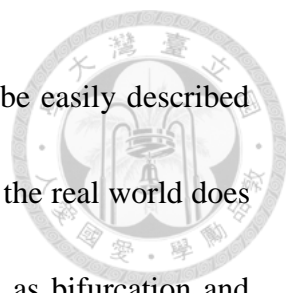


Instead of finding the numerical solution of differential equations, his methods using non-Euclidean geometry opened the door to the study of chaotic deterministic systems.

After a long silence, not until Benoit Mandelbrot's work in 1975 did the scientific study of fractals begin. Besides statistical techniques, other chaotic measures, entropy values, neural networks, genetic algorithms, fuzzy pattern recognition, and machine learning all contribute to the analysis of complexity. The first requirement of physically useful measures of complexity is that they be probabilistic. The second point we should notice is the assumption of ergodicity. In a nonergodic case, the ergodic components are in general enumerable, and we can just study each component by itself (Grassberger, 1986). The third point is then the assumption of stationarity (or translation invariance). The most interesting part is to find the heterogeneity or nontranslational invariance of a system. Through works in last decades, complexity analysis is now commonly performed through the evaluation of entropy (e.g., Shannon entropy) and entropy rate (e.g., approximate entropy, sample entropy, multiscale entropy, or other conditional entropy) with fruitful results in medicine. This would be further discussed in later sections.

1.6 Deterministic dynamics

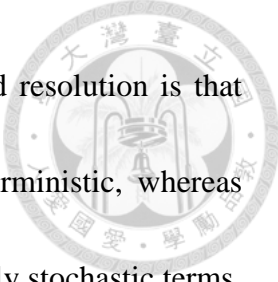
1.6.1 Dynamics observation



Simple observed dynamics such as sinusoidal periodicities can be easily described by traditional tools like Fourier transform. As mentioned before that the real world does not follow linear mathematics at all, more complex dynamics such as bifurcation and chaotic oscillations would be adopted in science. However, those studies of nonlinearity require more sophisticated methods which warrant more considerations for the underlying physics, the signal-to-noise ratio, the sampling rate and the dynamic instrument response.

1.6.2 Randomness and stochasticity

Does God Play Dice? Albert Einstein did not believe that “God plays dice”. He thought the universe is governed by immutable laws of physics and leaves no room for chance. Scientists have reconsidered this after chaos theory showed that the systems obeying precise laws can nevertheless act in a random manner. Perhaps God does play dice, within a cosmic game of complete law and order. In chaotic world, the systems obey simple laws but are neither constant nor predictable. Both chaotic and truly stochastic systems are unpredictable in the long term, but only chaotic systems admit short-term predictability. According to Laplace, randomness is only a measure of our ignorance of the different causes involved in the production of events (Laplace, 1814). The answer to whether the ultimate truth of noise is unknown deterministic chaos of high dimension is in the zone of “God or Gods”, which may be under the category of



“Karma”. Regardless of this extreme question, the general accepted resolution is that simple low dimensional chaotic systems to be recognized as deterministic, whereas complicated, high dimensional systems to be best recognized in purely stochastic terms, using probabilistic prediction at any time scale.

Before understanding “determinism” such as chaotic oscillations we need to sieve out the part as random or stochastic from a system. It is complicated to define the degree of randomness. A discrete random variable is defined in relation to a probability function. For continuous random variables, instead of the probability function, we use the probability density function, which gives the probability of observing a value of the variable within a certain range of possible values. The properties of the probability density function such as variance is then measured to describe the dynamics of a phenomenon or system. A stochastic process is one that evolves over time and for which the evolution at each time step is governed, at least in part, by probability. It could be a random behavior such as ordinary Brownian motion or a behavior that is influenced by both deterministic and random processes. Probability theory is a mathematical model of uncertainty. The real world is full of uncertainty, which is also called noise: bridges design should take account of the vibrations from wind; communication systems are designed to compensate for noise; the power distribution grid carries an unpredictable load; searching for genes is looking for shells among sand; studying heart rate dynamics is looking for the degree

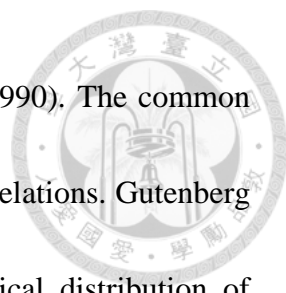
of variation, etc.



1.6.3 Law of nature

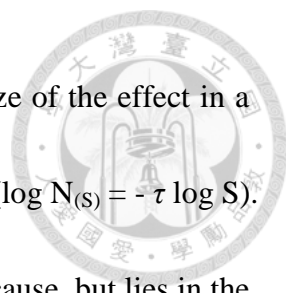
The story begins with the “1/f noise. The 1/f fluctuations were first found in 1925 in an electric current passing a vacuum tube (Johnson, 1925). Many phenomena have been found after, such as frequency fluctuation of cellular membrane potential (Verveen, 1965), conduction of electronic devices, light emission intensity curves in quasars, velocities of underwater sea currents, the flow of sand in an hour glass (Schick et al. , 1974), cyclic insulin needs of diabetics (Campbell et al. , 1972), fluctuation of the alpha brain wave (Suzuki, 1980), the fluctuation of the heartbeat period (Kobayashi et al. , 1982), and highway traffic current fluctuations (Musha, 1976). The 1/f is a rhythm that appears throughout biology, nature, engineering, and elsewhere. The low-frequency power spectra of such systems display a power-law behavior $f^{-\beta}$ over vastly different time scales.

Another puzzle in nature is the empirical observation that many objects, such as coastal lines, mountain landscapes and cosmic strings, appear to be self-similar fractal structures (Mandelbrot, 1983). An important (defining) property of a fractal is self-similarity, which refers to an infinite nesting of structure on all scales. Strict self-similarity refers to a characteristic of a form exhibited when a substructure resembles a superstructure in the same form. Circulatory and bronchial branches in



Human body seem to exhibit fractals as well (Goldberger et al. , 1990). The common features for these systems are the power-law temporal or spatial correlations. Gutenberg and Richter (1954) were the first who found out that the statistical distribution of earthquake sizes follow a power-law (Gutenberg, 1954). Generally, the scale invariant phenomena such as fractals and power laws emerged at the critical point (e.g. between phase transitions).

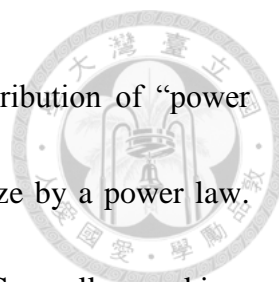
How do physicists explain the power laws? M.E.J. Newman suggests that there are a number of “physical mechanisms” underlying power laws. The chief among them are the “Yule process” (preferential attachment process), often characterized as “the rich get richer”, and theory of self-organised criticality (Newman, 2005). Bak et al. (1987) presented a simple computer-model (Bak-Tang-Wiesenfeld sandpile model, BTW), based on cellular automata, suggested that “self-organized criticality” (SOC) is the common underlying mechanism behind the phenomena of “1/f noise”, “fractal” and “power law”. The definition of SOC is: “*A system exhibits SOC if its phase space contains a strange attractor where events of all sizes occur, and where the size distribution of these events follows a power law.*” They stated: large interacting systems evolve by themselves to a critical state. In this self-organized state disturbances trigger effects the sizes of which correlate negatively with their frequency by a power law ($N_{(S)} = S^{-\tau}$, where $N_{(S)}$ is the number of effects of a given size (or their frequency) and S is



the size of these effects). This means that plotting frequency and size of the effect in a log–log plot results in a straight line, the exponent τ giving its slope ($\log N(s) = -\tau \log S$). Accordingly, the extent of the effect is not due to the strength of its cause, but lies in the intrinsic dynamics of the system (Bak et al. , 1987). This has already been verified and SOC has become a possibility for explaining the behavior of real sand piles, earthquakes, power blackouts and forest fires. SOC could even describe epidemics, biological evolution and financial markets. Although self-organized criticality was able to reproduce $1/f$ noise in sandpile models (Bak et al. , 1987), there are no simple mathematical models to create pink noise. It is usually generated by filtering white noise. Universal theories of $1/f$ noise remain an unresolved problem in current research. SOC is a far-from-equilibrium state, generated by a constant flow of energy from outside the system. In this state, the addition of just a single grain of sand will cause the pile to generate either a single large avalanche or a series of smaller avalanches (Bak et al. , 1989). A critical point of a system needs an exact configuration, so even a tiny change of the variables could destroy the power-law. The puzzle is why so many phenomena follow such a hypothetical critical point, if it is so difficult to reach that state.

1.6.4 Fractals

Fractals are sets defined by the three related principles of self-similarity, scale



invariance, and power law relations. Self-similarity implies a distribution of “power law”. The number of self-similar pieces must be related to their size by a power law.

Therefore the complexity of a fractal pattern can be achieved. Generally speaking, power law distributions are the only scale-invariant distributions. *“The wide applicability of scale invariance provides a rational basis for fractal statistics just as the central limit theorem provides a rational basis for Gaussian statistics.”* (Turcotte, 1997). The essential characteristics of fractal patterns are captured by a statistic called the fractal dimension (Brown, 2010).

power law relations : $f(x) = K x^{-D}$, when the constant K is ignored \rightarrow

$$N = \frac{1}{S^D}, D = - \left(\frac{\log N}{\log S} \right)$$

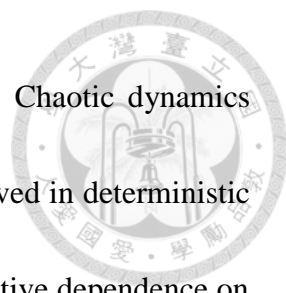
N: the number of self-similar pieces

S: the linear scaling factor (size) of the pieces to the whole

D: the dimension that characterizes the (invariant) relationship between size and number

1.6.5 Deterministic chaos

Being one of the greatest natural science discoveries in the 20th century, chaos theory has been extensively investigated and applied in the broad areas of computer and communication networks, physical and biological networks, as well as social and financial networks. As 1/f and fractals were found, scientists also tried to fit



deterministic chaos (or simply chaos) into one of models for life. Chaotic dynamics describe behaviors that fluctuates irregularly in time, could be observed in deterministic dynamical equations, not a fixed point and not a cycle, and has sensitive dependence on initial conditions (generally referred to as “the butterfly effects”)(Glass, 1986). However, not all behavior that fluctuates irregularly in time represents chaotic behavior.

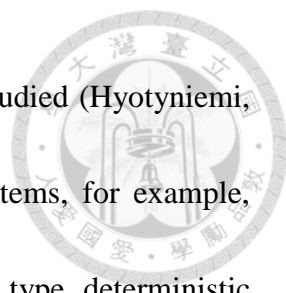
The story may start with whom we have previously mentioned, Henri Poincaré in 1880s. He found that there can be orbits which are nonperiodic, and yet not forever increasing nor approaching a fixed point (Poincaré, 1890). Later in 1898, Jacques Hadamard in his famous “Hadamard’s billiards” studies showed that in chaos all trajectories are unstable in that all particle trajectories diverge exponentially from one another, with a positive Lyapunov exponent. After the appearance of “ergodic theory” and “nonlinear differential equations”, Edward Lorenz in 1961, on the work of weather prediction, with the help of repeated iteration by computers, showed that small changes in initial conditions produced huge changes in the long-term outcome (Lorenz, 1963). In his theory as the famous “Lorenz attractor”, he showed that given detailed modeling long-term predictions were still not possible. The theory of chaos gradually formed under many people’s devotion such as Benoît Mandelbrot (Mandelbrot, 1983), Yoshisuke Ueda, Robert Shaw, Mitchell Feigenbaum, Albert J. Libchaber, and Bak–Tang–Wiesenfeld (whith the work of sandpile) during the second half of last

century. For a dynamical system to be classified as chaotic, it must have the following properties: few variables, trajectories sensible to initial conditions, fractal structure of phase space, being topologically mixing, and dense periodic orbits.



Although the future dynamics are fully defined by the initial conditions, the behavior of chaotic systems seems pretty random. This is because the dynamics manifests itself as an exponential growth of perturbations in the initial conditions. Any minor uncertainty will be amplified so as to render actual knowledge of the state of the system impossible. In a real system (as opposed to an equation) it is always impossible to know the state of a system exactly, since there is always some measure of experimental uncertainty, such as those due to rounding errors in numerical computation. Therefore a long-term prediction is impossible in general.

According to current knowledge, at the lowest level, the elementary particles follow the stochastic model of quantum mechanics with uncertainty. At the atom level, the “billiard balls” model which is deterministic appropriately predicts velocities moments. In a mass of millions of atoms, individual collisions cannot be tracked, and the statistical mechanics again is proper. With increasing numbers of interacting entities and longer time scale, it is deterministic quantities like temperatures, pressures, and entropies that best characterize the system. While regarding convection and turbulence of the temperature distributions, it is statistical model; while in complete turbulence, it

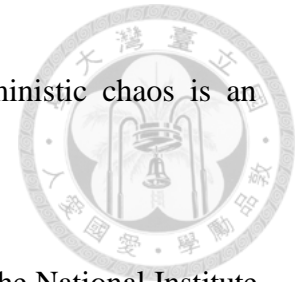


is deterministic model again since only concentrations need to be studied (Hyotyniemi, 2006). This concept is also useful when we regard biological systems, for example, typical cells have of the order of at least 10^3 ionic channels of each type, deterministic equations can be used to model cells even though the underlying mechanism is probably stochastic (DeFelice et al. , 1993). “Science” only provides “appropriate” models for each case, it doesn’t guarantee the truth. There is a bias over here; the methods used to check determinism are based on the assumption of deterministic chaos. However, as mentioned before, regardless of whether the theoretical footstone is strong, rapid developments of nonlinear mathematical methods based on chaos theory have made “rhythms” of the human body being able to connect with some clinical features, and this is where the value is.

1.6.6 Chaos in medicine

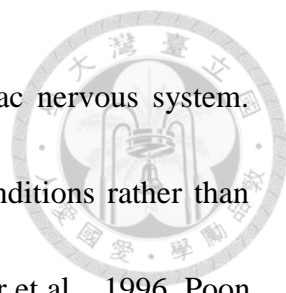
Electrophysiological signals, with electrocardiography (ECG) and electroencephalography (EEG) playing the major roles, are non-linear, non-stationary, and very noisy. For such complex signals, we need to find some suitable models for quantification in order to understand the mechanism governing the dynamics of the system. Major models of complex time series include deterministic chaos, noisy chaos, stochastic oscillations, random $1/f$ processes, random Lévy processes, and complex time series with multiple scaling behaviors (Hu et al. , 2009). Copious works of ECG and

EEG have been especially dedicated to checking whether deterministic chaos is an appropriate model.

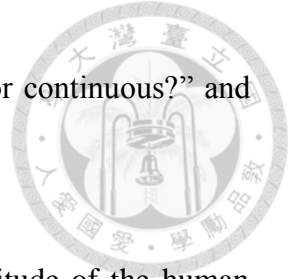


In 1986 the New York Academy of Sciences co-organized with the National Institute of Mental Health and the Office of Naval Research the first important conference on Chaos in biology and medicine. Since then the application of chaos in physiology became popular especially in heart rate dynamics. It is generally accepted that the dynamics of heart rate variability (HRV) are nonlinear, of the $1/f$ fluctuations (Kobayashi et al. , 1982), with fractal noises and motions in time series of presympathetic and sympathetic neural activities (Gebber et al. , 2006), and multifractal (Ivanov et al. , 1999, Sassi et al. , 2009). From a physiological perspective, the detection of robust multifractal scaling in heart rate dynamics is very attractive, because it indicates that the regulation mechanisms might play a part in a system of coupled cascade of feedback loops.

But the issue of whether normal HRV is chaotic or stochastic remains highly controversial. Some authors have claimed the presence of chaos in the HRV or in the whole electrocardiography (ECG) signal of normal subjects (Chaffin et al. , 1991, Baselli et al. , 2002). The heart rate variability (HRV) of cardiac transplant subjects regained the same signature of chaos as that of the HRV for normal subjects 3 months after the transplantations (Khadra et al. , 1997). This may suggest the source of the



chaos characteristic of HRV, if any, is beyond the intrinsic cardiac nervous system. Some authors even showed more chaotic HRV data in healthy conditions rather than diseased states (Babloyantz et al. , 1988, Skinner et al. , 1993, Meyer et al. , 1996, Poon et al. , 1997, Selig et al. , 2011). They generally claimed that there are underlying low dimensional chaos displayed in biological systems. Contradictory evidences also exist as some authors found no evidence for chaos, for example, truly exponential divergence between nearby trajectories in a phase space, however, they still found different nonlinear complexity in HRV between healthy and diseased states (Lefebvre et al. , 1993, Kanters et al. , 1994, Costa et al. , 1999, Hu et al. , 2009). The same situation is seen for EEG, there were evidences of chaotic properties (Babloyantz et al. , 1985, Freeman et al. , 1985, Rapp et al. , 1985, Babloyantz et al. , 1986, Skarda, 1987, Rapp et al. , 1988, Xu et al. , 1988) as well as ones that are not supportive of the presence of deterministic chaos (Korn et al. , 2003). Other than heart beats and brain waves, there are also examples of chaos in biological systems in excitable membrane systems (Chay et al. , 1985, Fan et al. , 1994) and variable determinism was also found in motor system (Riley et al. , 2002). Goldberger has suggested that increased regularity of signals represents a 'decomplexification' characteristic of illness (Goldberger, 1997). We may consider the dynamic patterns of biological signals change with the deterioration of health condition as characterized by loss of complexity and development of stereotypy,

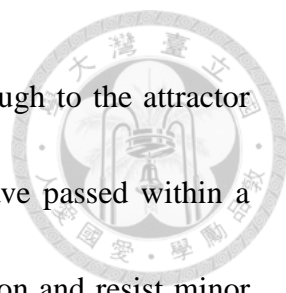


but the questions are “whether this “reordering” process stepwise or continuous?” and “whether this direction is one way and universal?”

Recent studies have shown that sudden transitions in the amplitude of the human electroencephalogram (EEG) are represented by power laws and scale invariance and long-range temporal correlations (Linkenkaer-Hansen et al. , 2001, Freeman, 2003, Parish et al. , 2004, Nikulin et al. , 2005). While the chaos theory widely applied in analysis of EEG during the past 2 to 3 decades, expectation has been too high in unraveling the mystery of mind through the application of chaos models in brain waves. With the less tangible subjective aspects of experience, such as intuition, emotion, or instinct being neglected (Dunne et al. , 2007), the mathematics would not easily resolve the secrets of mind. Nevertheless, mathematical models as fractal, entropy and chaos do provide tools for studying rhythms in human body, especially the interaction between them.


1.6.7 Measures of chaos

Recent developments in the studies of nonlinear problems (Eckmann et al. , 1985) provide some criteria to characterize the chaotic states, such as Kolmogorov entropy, Lyapunov exponents, fractal dimensions, correlation dimensions, etc. The evolution of the system in time defines a trajectory in phase space. When the dynamics of the system exhibits an asymptotic behavior which is almost independent from initial conditions, the



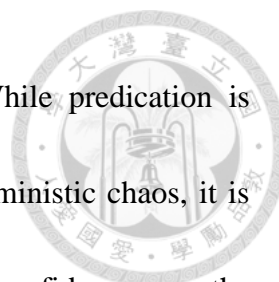
asymptotic trajectory is called "attractor". Points that get close enough to the attractor will be drawn closer to a specific field or point, and after they have passed within a certain distance of the attractor, they will adopt a stable configuration and resist minor disturbances in the system. An attractor can be a point (stable equilibrium), a finite set of points, a curve, a manifold, a limited cycle or even a complicated set with a fractal structure known as a strange attractor. There could be more than one attractor in a system. A strange attractor is a fractal, and its fractal dimension is less than the dimensions of its phase space. An equation that includes a strange attractor must incorporate non-integer dimensional values. Therefore the trajectories of chaos seem to be random and they predict patterns called semi-stable. The dimensionality of strange attractor shows the following properties: 1. the trajectory of a strange attractor cannot intersect with itself; 2. nearby trajectories diverge exponentially. 3. the attractor is bounded to the phase space; 4. the trajectory does not fill the phase space. A chaotic system is deterministic but aperiodic - the trajectory never repeats itself. In conclusion, the infinitely long trajectory occupies only a finite portion of the state space. This leads to the fractal nature of the strange attractor of a chaotic system.

The dimension of an attractor is clearly the first level of knowledge necessary to characterize its properties. There are two groups of methods in determining the fractal dimension (D_F) of a set in a Euclidean space. The first group is called the "metric



dimension” such as capacity, Minkowski-Bouligand dimension (also known as box-counting dimension), and Hausdorff dimension. The other group, frequency (probability) dependent, is called the “dimension of the natural measure” (D_μ), such as information dimension and correlation dimension (D_2) (Farmer et al. , 1983). A box-counting dimension counts how many boxes are required to cover the set lying on an evenly-spaced grid. The dimension is calculated by seeing how this number changes as we make the grid finer by applying a “box-counting” algorithm. The same idea can be used in phase space, as the evolution of the system in time also defines a trajectory in phase space. So with the concept of probability, “dimension of the natural measure” (D_μ) was then appeared. Metric dimension is equal to D_F , and D_μ is less than D_F .

The correlation dimension, D_2 , is widely applied in biological time series to quantify the complexity of the dynamics. D_2 is a lower estimator of the Hausdorff dimension D that measures the occupation of the attractor in phase space ($D_2 < D_F$) (Costa et al. , 1999). A most widely used mathematical method of counting correlation dimension is Grassberger-Procaccia algorithm (Grassberger et al. , 1983, Grassberger, 1986, Shelhamer, 2007). A finite noninteger value of D_2 (deterministic regular dynamics have integer D_2), is consistent with low-dimensional chaotic behavior, but does not necessarily imply the presence of chaos (Osborne et al. , 1989, Rapp et al. , 1993), because correlated stochastic dynamics may give rise to a noninteger D_2 too. So the



correlation dimension is not a definitive diagnostic of chaos. While predication is impossible in the long term for a dynamical system showing deterministic chaos, it is possible to predict the behavior of the system with some degree of confidence over the short term (Farmer et al. , 1991).

The correlation dimension D_2 is defined as:

$$D_2 = \lim_{\epsilon \rightarrow 0} (\log C(\epsilon) / \log (\epsilon)),$$

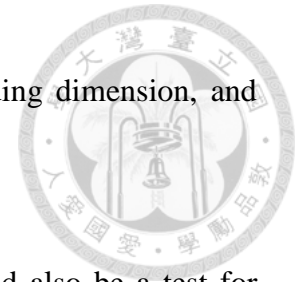
Where $C(\epsilon)$ is called the correlation integral in the form as:

$$C(\epsilon) = (1/N(N-1)) \sum_i \sum_j \theta(\epsilon - |X_i - X_j|) \quad (i \neq j)$$

Where $N(N-1)$ is the number of inter-point pairs of vector X_i and X_j , θ is the Heaviside function.

Chaotic measures such as correlation dimension could be used in physiology under the following hypotheses. At first, the observed signals of physiological data can have been produced by deterministic nonlinear equations with instability, probably spoiled by stochastic noise, that is can follow a low-dimensional chaotic dynamics. Second, the characteristics of such processes can be explored as changing time qualities and give insight into underlying phenomena. Third, abnormal changes in such characteristics can be related to dysfunction or diseases and can be used as monitoring or diagnostic tools. There are of course some problems and limitations over here, such as only finite amount of data could be attained which would not render the real measurements of the


dimension, problems of choice of the time delay and the embedding dimension, and problems distinguishing between signal and noise.



On another side, Lyapunov exponent (Wolf et al. , 1985) could also be a test for determinism as it quantifies the rate of divergence of nearby trajectory paths in the state space, giving a measure of sensitive dependence on initial condition, which is a hallmark of chaos (Binder et al. , 2005). Therefore the Lyapunov exponent quantifies the average stability properties of an orbit on an attractor. For a chaotic system, the distance between two trajectory paths that are initially a distance d_0 apart will increase with time as $d(t) \sim d_0 e^{\lambda t}$, the λ is roughly equal to Lyapunov exponent. Although algorithms were developed, there is difficulty in finding good estimates of the values. In the real world, phase spaces are generically infinitely interwoven patterns of stable and unstable behaviors.

1.6.8 Interpretation of the fractal dimension

Evidences have shown that filtered noise can exhibit a finite correlation dimension, compatible with that from a chaotic system (Rapp et al. , 1993). Besides, purely random processes with power-law frequency spectra (spectra that decay as $f^{-\beta}$) can also yield finite dimensions (Osborne et al. , 1989). Nevertheless, even for those “chaoticity” or dimension not determined by certainty, relative dimension values between different systems can be useful (Rapp et al. , 1993). Instantaneous condition of the dimension of



data evolution could have better dynamic description. Farmer et al. in 1983 proposed the point correlation dimension (Pointwise- D_2 or Pointwise- D_{corr}) (Farmer et al. , 1983), which is not sensitive to changes in frequency or amplitude, could reject bursts of high-dimensional noise in the data (Skinner et al. , 1992). The Pointwise- D_2 has an advantage in that it does not presume stationarity of the data, as the D_2 algorithm must.

There are cases in which signals generated by large and complicated system produced almost disproportionately small dimension, taking EEG as an example, with billions of neurons interconnected in trillions of ways what does it mean for the EEG to have a dimension on the order or 2 to 5 (Rapp et al. , 1993)? Although this question remains unsolved, there are many evidences showing a significant decrease in dimensionality in pathological cases. These might be interpreted as an unhealthy reduction in system flexibility and information-processing capability, reflected in low dimensions. Variation in estimates of correlation dimension may be due to small sample sizes and high embedding dimensions.

Dimension is a critical property because it indicates how many independent state variables are required to reproduce the system dynamics in state space, and this also indicates how many state variables should be included in a mathematical model of the system. The dimension could represent the degree of “complexity” of a system, and tracking any changes in dimension due to pathology, manipulations or other

environmental changes to the system could be a useful diagnostic criterion.



1.6.9 Other fractal measurements

1.6.9.1 Rescaled range analysis (Hurst et al. , 1965, Mandelbrot, 1983)

The rescaled range is a statistical measure of the variability of a time series introduced by the British hydrologist Harold Edwin Hurst (1880-1978). Its purpose is to provide an assessment of how the apparent variability of a series changes with the length of the time-period being considered. The rescaled range is calculated from dividing the range of the values exhibited in a portion of the time series by the standard deviation of the values over the same portion of the time series. For example, consider a time series {2, 5, 3, 7, 8, 12, 4, 2} which has a range, R , of $12 - 2 = 10$. Its standard deviation, S , is 3.69, so the rescaled range is $R/S = 2.71$. In this example, the number of observations, n , of the time series is 8.

If we consider the same time series, but increase the number of observations of it, the rescaled range will generally also increase. The increase of the rescaled range can be characterized by making a plot of the logarithm of R/S vs. the logarithm of n . The slope of this line gives the Hurst exponent, H . If the time series is generated by a random walk it has the value of $H = 1/2$. Many physical phenomena that have a long time series suitable for analysis exhibit a Hurst exponent greater than $1/2$. For example,



observations of the height of the Nile River measured annually over many years gives a value of $H = 0.77$.

The Rescaled Range is calculated for a time series, $X=X_1, X_2, \dots, X_n$, as follows:

Calculate the mean: $m = \frac{1}{n} \sum_{i=1}^n X_i$

Create a mean adjusted series: $Y_t = X_t - m$ for $t=1,2,\dots,n$

Calculate the cumulative deviate series Z : $Z_t = \sum_{i=1}^t Y_i$ for $t=1,2,\dots,n$

Create a range series R : $R_t = \max(Z_1, Z_2, \dots, Z_t) - \min(Z_1, Z_2, \dots, Z_t)$ for $t=1,2,\dots,n$

Create a standard deviation series S : $S_t = \sqrt{1/t \sum_{i=1}^t (X_i - m)^2}$ for $t=1,2,\dots,n$

Calculate the rescaled range series (R/S) : $(R/S)_t = R_t/S_t$ for $t=1,2,\dots,n$

1.6.9.2 Detrended fluctuation analysis (Peng et al. , 1994)

Given a bounded time series $x_t, t \in \mathbb{N}$, first converts this into an unbounded process X_t . X_t is called cumulative sum or profile. This process converts, for example, an independent and identically distributed (i.i.d.) white noise process into a random walk. Then, X_t is divided into time windows Y_j of length L samples, and a local least squares straight-line fit (the local trend) is calculated by minimising the squared error E^2 with respect to the slope and intercept parameters a, b : $E^2 = \sum_{j=1}^L (Y_j - aj - b)^2$. Trends of higher order can be removed by higher order DFA, where the linear function $aj + b$ is replaced by a polynomial of order n . Next, the root-mean-square deviation from the trend, the fluctuation, is calculated over every window at every time scale: $F(L) = [1/L$

$\sum_{j=1}^L (Y_j - a_j - b)^2$, This detrending followed by fluctuation measurement process is repeated over the whole signal at a range of different window sizes L , and a log-log graph of $F(L)$ against L is constructed. A straight line on this log-log graph indicates statistical self-affinity expressed as $F(L) \propto L^\alpha$. The scaling exponent α is calculated as the slope of a straight line fit to the log-log graph of L against $F(L)$ using least-squares. This exponent is a generalization of the Hurst exponent (Hurst, 1951, Hurst et al. , 1965). Because the expected displacement in an uncorrelated random walk of length L grows like \sqrt{L} , an exponent of 1/2 would correspond to uncorrelated white noise. When the exponent is between 0 and 1, the result is fractional Brownian motion, with the precise value giving information about the series self-correlations:

$\alpha < 1/2$: anti-correlated

$\alpha \cong 1/2$: uncorrelated, white noise


$\alpha > 1/2$: correlated

$\alpha \cong 1$: 1/f-noise, pink noise

$\alpha > 1$: non-stationary, random walk like, unbounded

$\alpha \cong 3/2$: Brownian noise

There are different orders of DFA. In the described case, linear fits ($n = 1$) are applied to the profile, thus it is called DFA1. In general, DFA n , uses polynomial fits of order n . Due to the summation (integration) from x_i to X_t , linear trends in the mean of



the profile represent constant trends in the initial sequence, and DFA1 only removes such constant trends (steps) in the x_i . In general DFA of order n removes (polynomial) trends of order $n - 1$. For linear trends in the mean of x_i at least DFA2 is needed. The Hurst R/S analysis removes constants trends in the original sequence and thus, in its detrending it is equivalent to DFA1. Since in the fluctuation function $F(L)$ the square (root) is used, DFA measures the scaling-behavior of the second moment-fluctuations, this means $\alpha = \alpha(2)$. The multifractal generalization uses a variable moment q and provides $\alpha(q)$. Kantelhardt et al. intended this scaling exponent as a generalization of the classical Hurst exponent. The classical Hurst exponent corresponds to the second moment for stationary cases $H = \alpha(2)$ and to the second moment minus 1 for nonstationary cases $H = \alpha(2) - 1$. Generally, we call $\alpha > 0.5$, persistent or correlated and $\alpha < 0.5$, anti-persistent or anti-correlated.

1.6.10 Issues of embedding dimension

Techniques involved in chaos verification have to determine proper values for embedding parameters τ and m (Sauer, 1991). For this purpose, the mutual information (Fraser et al. , 1986) and false nearest neighbour method (Kaplan et al. , 1992) can be used. Selection of embedding dimension m is a major issue. The embedding dimension m should be large enough that the attractor is properly embedded in the topological sense. There should be no trajectory crossings if the system is truly deterministic

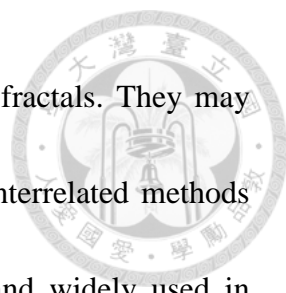
(although all sorts of noise can introduce crossings which can often be safely ignored).

For this purpose, false nearest neighbor method is a good approach. As in false nearest neighbor method, simply to increase the embedding dimension during time-delay reconstruction until there are no false nearest neighbors and no trajectory crossings, and to say that the attractor has the dimension of the least embedding dimension at which this occurs (Shelhamer, 2007).

Although an embedding dimension of at least twice the attractor dimension is required to guarantee a proper embedding, in fact it has been shown that an embedding dimension that is at least equal to the attractor dimension is sufficient for reliable computation of the correlation dimension (Ding et al. , 1993). This holds for large data sets. For shorter data sets of a few thousand points, larger embedding dimensions may be required but not necessarily as large as two times the attractor dimension (Shelhamer, 2007).

1.6.11 Multifractality

A multifractal system is a generalization of a fractal system in which a single exponent (the fractal dimension) is not enough to describe its dynamics; instead, a continuous spectrum of exponents (the so-called singularity spectrum) is needed. The singularity spectrum is a spectrum of related dimensions. In other words, if the dimensions vary but are well-defined power laws, then the phenomenon classifies as



multifractal (Brown, 2010). Multifractals are spatially intertwined fractals. They may have continuous fractal spectra or discrete spectra. Two types of interrelated methods have been developed for modeling the continuous multifractals and widely used in physics and geoscience: the Evertsz-Mandelbrot model has been developed on the basis of the multifractal spectrum and the Schertzer-Lovejoy model on the codimension function $C(y)$ (Cheng, 1997). Multifractals represent the extension of fractal theory from sets to measures. It is a measure incorporates the idea of quantity or magnitude, and addresses not presence/absence questions, but rather quantity, density, concentration, and so forth.

1.6.12 Lacunarity

Lacunarity, meaning “gap” or “lake”, measures the deviation of a geometric object, especially fractals from translational invariance; in other words, how patterns fill space. Patterns having more or larger gaps generally have higher lacunarity. It is important in multifractal analysis. Translational invariance, of course, also can be a property of nonfractal sets. Several works have pointed out that sets with the same fractal dimension may have different lacunarities, only few have emphasized that the lacunarity is highly dependent of dimension (codimension). The properties and characteristics of a fractal set are not completely determined by its fractal dimension D . It is easy to construct a family of fractals that share the same D but differ sharply.



1.6.13 Advantages of chaos in physiology

Chaos theory has helped to resolve some difficult problems in the fields of physics and chemistry, problems such as how to calculate a turbulent event in fluid dynamics and how to quantify the pathway of a molecule during Brownian motion. Biology and medicine also have unresolved problems. Probably the greatest appeal of chaos for physiology is the simple observation that so much physiological activity is highly variable, appearing random or noisy. Application of mathematical tools made a breakthrough for biology that what was thought to be higher-dimensional noise in many of the systems turns out to be low-dimensional chaos (Mayer-Kress et al. , 1988). A chaotic system can appear random as well, but there is an underlying deterministic structure. Even simple nonlinear deterministic systems can exhibit chaotic behavior.

The sensitivity to initial conditions, being one principal characteristic of chaos, can lead two arbitrarily closely points to significant future trajectories. Therefore chaotic complexity could provide biological systems adaptability, flexibility, stability, exploratory and perceptual function, as well as helps in facilitating transitions between behavioral mode (Riley et al. , 2002). The combination of adaptability and stability therefore could provide biological systems “controllability” (Liebovitch, 1998).

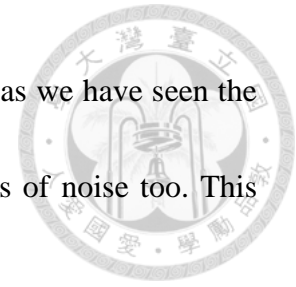
Adaptability makes sure a system can keep on function in an ever-changing or unknown environment. The biological system could be treated as a system with a set of

states and a transition scheme which governing the state to state transitions. The relation between the statistical properties of the biological system and the statistical properties of the environment could reveal something about the ways systems work.

The transition schemes are generally probabilistic. Theoretically, adaptability of the biological system could be due to either intrinsically random processes or completely attributed to deterministic. But if life processes are running according to a random walk without following a certain path or bearing some specific purposes, it would be very hard to explain the extreme rapid processing of neural information, the variability of immunoglobulin molecules produced in very short time when stimulated by stress, and the highly efficient metabolic or hormonal changes which allows organisms to protect their essential dynamical properties in the face of environmental changes by varying less essential dynamical properties.

Genetic variation and population dynamics, as provided by chaos (Emlen et al. , 1998) have made both human bodies and human societies evolve in very efficient ways which should be very difficult to achieve by random process. Another function of chaos is defense, which means that based on a chaotic neural mechanism, the unpredictable manifestation of motor behavior of animals would make the animals more difficult to catch. Finally in the nervous system, with the help of chaotic dynamics the functional independence of different parts could easily be maintained (Conrad, 1986). Chaos looks

random, but there is an underlying deterministic rule. Additionally, as we have seen the function of chaos in physiological systems, there must be functions of noise too. This would be another big issue outside this work.



People argued about whether or not the physiological dynamics reflect real chaos, real as according to the strict definition. People also suspect that chaos is nothing more than a mathematical artefact, a phenomenon non-existing outside the simulations of the computer. It might be much less interesting to clarify those doubts than to elucidate the underlying mechanisms controlling the dynamics (Glass, 2001).

1.6.14 Non-stationarity

Most statistical approaches for time series analysis assume that the observed process is at least locally stationary. It is to say the system's control parameters are constant and external perturbations are minimal. If the observed system is not stationary, that means the parameters of that system change during the time period of data acquisition, the recorded irregular behavior of the dynamics may solely from the nonstationarity but chaos. Biological systems are non-stationary since they all continuously vary in response to the changes of the environment and stress. Another cause of nonstationarity is the noise-contaminated impulse responses, and which can be resolved by ensemble averaging of many realizations as increasing the signal to noise ratio (SNR). Nonstationarity can also occur if the system under study is approaching a bifurcation,

such as an instability threshold.

The usual solution for dealing with potential nonstationarity is to try to limit the data-acquisition process to a relatively short period compared with any slow changes that the system may undergo (Daw et al. , 2003). Methods like Empirical mode decomposition (also known as Hilbert Huang transformation, HHT) (Huang et al. , 1998) and wavelet transformation (Burrus, 1998) would be good choices for non-stationary data.

1.6.15 No guarantee of chaos

The mathematical tools used to explore the dynamics of low dimension of deterministic chaos are themselves based on the assumption that the time series under analysis was indeed generated by a chaotic system. Another issue is that experimental biological time series are necessarily corrupted by noises of endogenous or exogenous origins, even after the most robust noise titration the sufficient condition could still not be achieved (Sassi et al. , 2009). The two main characteristics of chaos to be checked are nonlinearity and determinism.

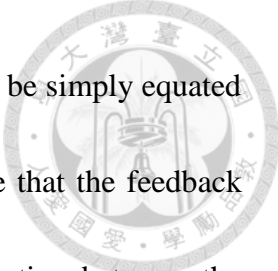
Systems in which the dynamics are governed by a small number of coupled deterministic equations called low-dimensional systems. As mentioned, although a low-dimensional system can behave chaotic dynamics, a low dimension found in a cardiac system by a computer algorithm does not guarantee that the system is chaotic.



Further, although some report low dimensions in normal HRV (Babloyantz et al. , 1988, Bezerianos et al. , 1995), others do not (Kanters et al. , 1994, Costa et al. , 1999).

Although sensitivity to initial conditions is a characteristic in chaotic systems, and it is associated with a positive Lyapunov number, finding a positive Lyapunov number in a cardiac system using a computer algorithm does not necessarily mean that the underlying system displays deterministic chaos. Random systems could also give a positive Lyapunov number. Many papers have mentioned that the subtleties of the computer algorithms that are being used to analyze HRV make them difficult to apply and susceptible to misinterpretation (Glass, 1999).

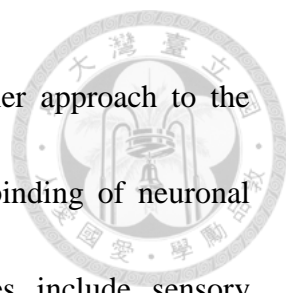
Although physiological and bio-signals can provide physiological meanings. The physiological meanings which are provided by bio-signals could be biased by the acquisition processes as well as the analytic methods of the signals. And the performance of bio-signal classification further depends on the choice of any suitable features, which are called biomarkers or parameters. In a study of COP (center of pressure) dynamics, the result showed that more variability with eye closed was accompanied by less randomness (more determinism), and less variability with eye open was accompanied by more randomness (less determinism). This findings may suggests variability is not equal to randomness (Riley et al. , 1999). In another experiment of COP with suprapostural task, the investigators observed that just as



variability cannot be equated with randomness, controllability cannot be simply equated with determinism (Balasubramaniam et al. , 2000). I would suppose that the feedback from visual inputs to the balance of posture is a process of interaction between the environment and the human bodies. It is much more complicated than the determinism of this system; therefore it is classified as randomness. And this is the problem of standing point. Being deterministic or not depends on the scale of the view point. For example a random part viewing from human body's scale could be explained by some deterministic rule if you examine it from a higher scale's view such as the earth or the universe. Stephen Hawking has alleged the inevitable uncertainty in the universe by the argument that loss of particles and information occurs when a system falls down into black holes which means that the particles that come out from black holes are random. That may be right, but although one could not make any definite predictions, one could calculate probabilities at some scale. The scale is not only about which position is one standing (e.g., inside a cell, inside the body, or inside the earth, etc.), it may also be about how the data together with the noise being collected. Further, since those biological data are discrete what we analyze, the time scale we collected them could also interfere the prediction of "degree of randomness".

1.7 Entropy

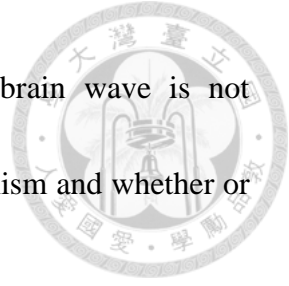
As mentioned above, the search for specific sequences or patterns more frequent



than others which is the basis of information or entropy is another approach to the detection of determinism in a time series. Temporal patterns or binding of neuronal firing are considered as Morse code for neurological activities include sensory awareness (Engel et al. , 2001), motor tasks (Hooper, 1998), or autonomic control (Porta et al. , 1998).

Phase-locked dynamics have been observed in spontaneous oscillators such as cardiac cells (Guevara et al. , 1981) and neurons (Aihara et al. , 1986) when they are stimulated by periodic electrical impulses, and the phase locking phenomenon could be disrupted by changing either the amplitudes or the frequencies of the periodic inputs. Mechanical stimulation through ventilator could also produce such phenomenon to neural cells in the respiratory center (Petrillo et al. , 1984) or sympathetic neurons (Porta et al. , 1996). This kind of coordination may not be rigidly fixed: changes in the coupling ratio (Glass et al. , 1983) and in phase (Porta et al. , 1996) have been detected. These evidences suggested the pattern of regularity in biological signals could be externally manipulated and thus change. Being able to show the regularity of a system, entropy is a useful reflection of the complexity of the deterministic structure of the time series.

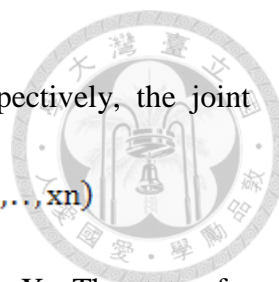
It is important to note that no one measure of overall system complexity has emerged as sufficient. Whether deterministic chaos or stochastic process is suitable to



describe physiological phenomenon as heart rate variability or brain wave is not important for clinicians. What is important is the underlying mechanism and whether or not quantification of the degree of regularity is clinically useful.

1.7.1 Information entropy

In 1964, James Lovelock, who was requested by NASA to make a theoretical life detection system to look for life on Mars, had made the following comment: to find signs of life, one must look for “a reduction or a reversal of entropy”. Most people are familiar with entropy in the thermodynamic sense but not with entropy as information content. The amount of information contained in a message is directly related to the uncertainty or inversely proportional to the probability of its occurrence (Al-Nashash et al. , 2005). In probability theory, entropy quantifies the uncertainty associated to a random process, and is a measure of unpredictability. C.E. Shannon 1948 proposed that in a discrete source of the finite state type, for each possible symbols i , there will be a set of probabilities $p_i(j)$ of producing the various possible symbol j . Thus there is an entropy H_i for each state. The entropy of the source will be defined as the average of these H_i weighted in accordance with the probability of occurrence of the states: information entropy $H = \sum_i P_i H_i = -\sum_i P_i \sum_j P_i(j) \log p_i(j)$, (Shannon, 1948). Entropy is simply the expectation value of the information produced by the experiment. For a time series representing the output of a stochastic process, that is, an indexed sequence of n



random variables, $\{X_1, \dots, X_n\}$, with set of values V_1, \dots, V_n , respectively, the joint entropy is defined as $H_n = - \sum_{x_1 \in V_1} \dots \sum_{x_n \in V_n} p(x_1, \dots, x_n) \log p(x_1, \dots, x_n)$

where $p(x_1, \dots, x_n)$ is the joint probability for the n variables X_1, \dots, X_n . The state of a system at a certain instant, X_n , is partially determined by its history, $X_1; X_2; \dots; X_{n-1}$.

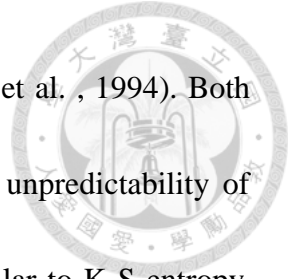
However, each new state carries a certain amount of new information.

The mean rate of creation of information is known as the Kolmogorov-Sinai (KS) entropy. Considering that the phase space of a system with D degrees of freedom is partitioned into hypercubes of content ϵ^D and the state of the system is measured at intervals of time τ , The KS entropy is defined as $H_{ks} = \lim_{\tau \rightarrow 0} \lim_{\epsilon \rightarrow 0} \lim_{n \rightarrow \infty} (H_{n+1} - H_n)$ (Costa et al. , 2002).

1.7.2 Measures of entropy

1.7.2.1 Sample entropy and approximate entropy

Regularity before approximate entropy (ApEn) was originally measured by exact regularity statistics, for which accurate entropy calculation requires vast amounts of data, and the results will be greatly influenced by system noise. Because experimental data are noisy, therefore Steve M. Pincus during analysis of heart beat dynamics developed ApEn to handle these limitations by modifying an exact regularity statistic, Kolmogorov–Sinai (K-S) entropy. Sample entropy (SampEn) (Richman et al. , 2000) is



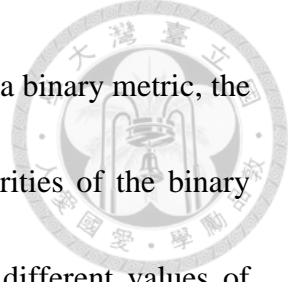
a modification of ApEn (Pincus, 1991, Pincus et al. , 1991, Pincus et al. , 1994). Both are techniques used to quantify the amount of regularity and the unpredictability of fluctuations over time series data; in other words, functionally similar to K-S entropy.

Both SampEn and ApEn serve as the index of entropy rate by measuring the complexity of the dynamical relationship between a pattern and the next datum. They are tools widely applied in biological time series and are suitable for short and noisy experimental time series. Informally, given N points, the family of statistics ApEn (m, r, N) is approximately equal to the negative average natural logarithm of the conditional probability that two sequences that are similar for m points remain similar, that is, within a tolerance r , at the next point. Thus a low value of ApEn reflects a high degree of regularity. How does the ApEn work? Take a simplified example of time series of RRI for understanding the idea, the first step is coding into S_i :

$$S_i = 0, \text{ if } RRI \geq 0,$$

$$1, \text{ if } RRI < 0, (RRI = RR \text{ interval})$$

In ApEn for binary sequences of length 8, the binary sequence 00000000 is more regular than 01100010. ApEn calculates the logarithmic frequency that sequences of length m that are close (within a tolerance r) remain close (within the same tolerance) in sequences of length $m + 1$, ApEn (m, r) depends on the length m and the tolerance r , and it assigns higher numbers to more irregular sequences. For binary sequences, the



tolerance r is set to $r = 1$ because this is the only practical setting for a binary metric, the length m is set to 1. Due to redundancies with respect to irregularities of the binary sequences, the $2^8 = 256$ different sequences are assigned only 17 different values of ApEn (Cysarz et al. , 2007).

ApEn and SampEn were developed for physiological data in view of their robustness to noise and finitude of data sets and they can be applied to stochastic, nonlinear-deterministic and composite processes (Pincus et al. , 1994, Richman et al. , 2000). Beside their original application in HRV, these two entropy have been also successfully applied to EEG analysis in Alzheimer's disease (Abasolo et al. , 2005), seizures (Yum et al. , 2008), anaesthesiology (Jordan et al. , 2008), hypoxia (Papadelis et al. , 2007) and sleep (Burioka et al. , 2005).

When m , r , τ and N , referred to as pattern length, normalized threshold, time delay and signal length respectively, for a time series $[x(j)]$, $j = 1, \dots, N$, the vectors of the length m , $X_m^{(i)}$, and a distance between any two vectors $d_m(X_m^{(i)}, X_m^{(j)})$

$$X_m^{(i)} = [x(i), x(i + \tau), \dots, x(i + (m - 1)\tau)], i = 1, \dots, N - (m - 1)\tau \quad (1)$$

$$d_m(X_m^{(i)}, X_m^{(j)}) = \max_{k=0, \dots, m-1}, [|x(i + k\tau) - x(j + k\tau)|] \quad (2)$$

The probability $C_i^m(r)$ that any vector $X_m^{(j)}$ is within the distance r from the “template” $X_m^{(i)}$ is estimated as

$$C_i^m(r) = B_m^r(i) / (N - (m - 1)\tau) \quad (3)$$



Where $B_m^r(i)$ is a number of vectors for which the distance is below the predefined threshold value r , with $I\{\cdot\}$ denoting an indicator function:

$$B_m^r(i) = \sum_{j=1}^{N-(m-1)\tau} I\{d_m(X_m^{(i)}, X_m^{(j)}) < r\}, i = 1, \dots, N - (m - 1) \tau \quad (4)$$

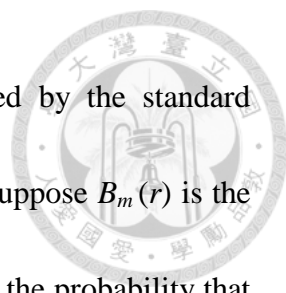
The procedure is then repeated for vectors of the length $m + 1$ and ApEn is defined

$$\text{as ApEn}(m, r, N, \tau) = \frac{1}{N-(m-1)\tau} \sum_{i=1}^{N-(m-1)\tau} \ln(C_i^m(r)) - \frac{1}{N-m\tau} \sum_{i=1}^{N-m\tau} \ln C_i^{m+1}(r) \quad (5)$$

ApEn allows self-matches ($j = i$) in Eq. (3) to avoid logarithm of zero, thus inducing the bias in estimates. SampEn approach eliminates this bias, making the following alternations: (a) self-matches are excluded from $B_m^r(i)$; (b) the number of sliding window comparison for template vectors of length m and $m + 1$ are equalized; (c) summation and logarithm in Eq. (5) exchange the places:

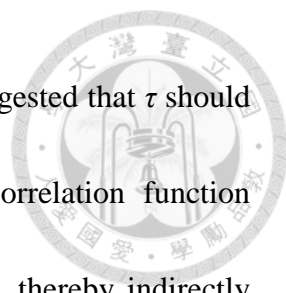
$$\text{SampEn}(m, r, N, \tau) = \ln \sum_{i=1}^{N-m\tau} (B_m^r(i) - 1) - \ln \sum_{i=1}^{N-m\tau} (B_{m+1}^r(i) - 1) \quad (6)$$

To be more clearly, ApEn (m, r, N) is biased and suggests more similarity than is present, and the bias is from self-matching. There are two differences between the modified version, SampEn and ApEn. First, SampEn does not count self-matches thus reduces bias. Discounting self-matches is more reasonable since entropy is conceived as a measure of the rate of information production, therefore comparing data with themselves is meaningless. Second, SampEn does not use a template-wise approach when estimating conditional probabilities. To describe SampEn in short, when m, r and



N , referred to as pattern length, normalized threshold (normalized by the standard deviation of the original sequence), and signal length respectively, suppose $B_m(r)$ is the probability that two sequences will match for m points, and $A_m(r)$ is the probability that two sequences will match for $m + 1$ points. The match is considered within tolerance and with self-matches excluded. The parameter, SampEn, is estimated by the statistic $\text{SampEn}(m, r, N) = -\ln [A_m(r) / B_m(r)]$. In contrast to $\text{ApEn}(m, r, N)$, which calculates probabilities in a template-wise fashion, $\text{SampEn}(m, r, N)$ calculates the negative logarithm of a probability associated with the time series as a whole.


There are no explicit constraints regarding the signal stationarity within the aforementioned definitions of ApEn and SampEn (Boskovic et al. , 2012). The choice of parameters m and r is critical, especially for moderately sized signal lengths N (Pincus et al. , 1994). Parameter m is closely related to data length N and threshold r as many studies (Chen et al. , 2005, Lu et al. , 2008, Chon et al. , 2009) have been shown. The false nearest neighbors approach (Kennel et al. , 1992) is a good method dedicated to a reasonable choice of m . As to the parameter τ (the delay), Govindan et al. firstly raised the issue of suitability of unit delay ($\tau = 1$) for signals with long range linear correlation (Govindan et al. , 2007). If the autocorrelation function is decaying rapidly as most of the physiological data are, unity delay may be sufficient to provide an accurate measure of signal complexity resulting from the nonlinear features in the signal.



If the autocorrelation function is decaying slowly, Kaffashi et al suggested that τ should be chosen as the first minimum or zero crossing of the autocorrelation function (Kaffashi et al. , 2008b). Chen et al. showed that down sampling, thereby indirectly adjusting the time delay parameter in the computation, and reducing the linear correlation between consecutive samples, resulted in higher signal complexity (Chen et al. , 2005). Threshold, r , is defined as a fixed percentage of the standard deviation estimated from the signals, therefore the signal need to be at least wide sense stationary (Boskovic et al. , 2012). Studies especially in neurological signal analysis note that the stationarity is not a prerequisite for ApEn (and SampEn) estimates (Hudetz et al. , 2003, Huang et al. , 2004). Pincus and Goldberger state that ApEn is insensitive to artifacts (outliers) if they are not frequent. (Pincus et al. , 1994). Nevertheless, an analysis of RRI recordings on ApEn showed that outlying points which inflate standard deviation of the time series could reduced entropy values (Lake De Fau - Richman et al. , 2002). In order to decrease the non-stationarity of EEG in SampEn measurement, nonlinear filters such as empirical mode decomposition (EMD) could supplied good results of data detrending and increased the group differentiating power of SampEn in dementia (Tsai et al. , 2012).

1.7.2.2 Multiscale entropy (MSE)

MSE was introduced in 2002 by Costa and colleagues for the purpose of analysis of



HRV (Costa et al. , 2002, 2005). It is an extension of SampEn into multiple time scales, based on the assumption that dynamical complexity of biological signals may operate across a range of temporal scales. Since interactions due to both local dense interconnectivity and sparse long-range excitatory projections give rise to the outputs of neuronal networks (Friston et al. , 1995), the resulting dynamics could be expected to operate at multiple scales. MSE approaches have been fruitfully applied in medical fields. It compared different physiological conditions in HRV like aging, disease, and pregnancy (Costa et al. , 2005, Baumert et al. , 2012). It provided novel insight into physiological mechanisms in neuronal spiking patterns in human (Bhattacharya et al. , 2005). It empowered the role of postural sway time series in rehabilitation (Costa et al. , 2007). It analyzed EEG of aging (McIntosh et al. , 2008, Takahashi et al. , 2009) and dementia (Escudero et al. , 2006). It identified abnormal dynamics of the EEG in schizophrenia and that abnormality was normalized selectively in fronto-central areas after antipsychotic treatment (Takahashi et al. , 2010). This has suggested quite promising contributions in clinical monitoring by MSE.

This method consists of two parts, coarse graining procedure and SampEn. The method of MSE analysis inspects signals at different time scales by performing the coarse-graining procedure. The process of coarse-graining in MSE is: given a one-dimensional discrete time series, $\{X_1, \dots, X_i, \dots, X_N\}$, construct consecutive

coarse-grained time series, $\{y^{(\tau)}\}$, determined by the scale factor, τ , according to the equation: $y^{(\tau)}_j = \frac{1}{\tau} \sum_{i=(j-1)\tau+1}^{j\tau} X_i$, $1 \leq j \leq \frac{N}{\tau}$. For scale one, the time series $\{y^{(1)}\}$ is simply the original time series. The length of each coarse-grained time series is N/τ .

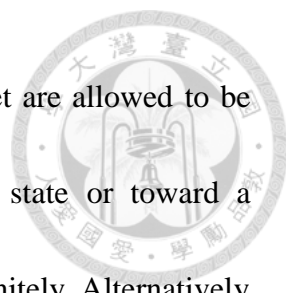
The sample entropy (SampEn) for each coarse grained time series is measured and plotted as a function of the scale factor.

1.7.3 Network theory

The macromolecules in living cells are connected to each other, and the different cell types of an organ connected to each other. How do we model biological networks?

There are three possible types of network, regular, random and scale free. The number of connections per node for both the regular and random networks will have a roughly normal distribution with an average value that gives a characteristic “scale” to the network. In the third type, ranging from a very few highly connected nodes to a large number of weakly connected nodes, the number of molecules (N) with a given number of connections (k) falls off as a power law: $N(k) \sim k^{-g}$, where g is between 2 and 3.

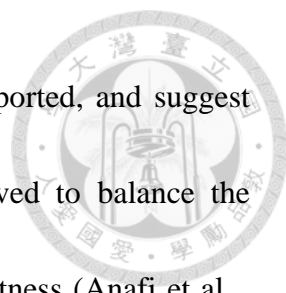
Because $N(k)$ does not show a characteristic peak value, this type of network is often referred to as “scale free” (Bray, 2003). The most well-studied re-entrant artificial neural network is the Hopfield net (Hopfield 1984) in which every neuron is connected to every other neuron. It is a recurrent neural network having synaptic connection pattern such that there is an underlying Lyapunov function for the activity dynamics



(Hopfield, 1982, 1984). If the synaptic strengths of the Hopfield net are allowed to be asymmetrical, the network can converge toward a single stable state or toward a repeating pattern of two or more states that it cycles between indefinitely. Alternatively it may move chaotically between different states without converging. For biological system, the asymptotic dynamic behavior of a network can also depend on its initial conditions (Bates, 2006).

1.7.4 Multiple attractors or single attractor

Almost all diseases, no matter simple as common cold, complicated as cancer, chronic as hypertension, acute as stroke, strange as autoimmune diseases, or mysterious as degenerative brain diseases, are all found to be of multi-factorial etiologies, widely varying prognoses, and frequently unclear therapeutic options. This brought up the thought that multiple attractors exist in biological networks, and that makes a disease state the entrapment in a non-normal attractor (Segel, 1998, Bates, 2006). Whether biological networks fit in this or even work in mathematical law, the theory of networks has been as applied to the immune system (Detours, 1996). A Hopfield-type theory with multiple attractors was used to explain the effects of vaccination on immunological status (Segel, 1998). And the attractors of the network of gene interactions were used to explain cellular phenotypes (Kauffman, 1971, Ribeiro et al. , 2007, Kim et al. , 2011). There were evidences showing that there is a critical degree of

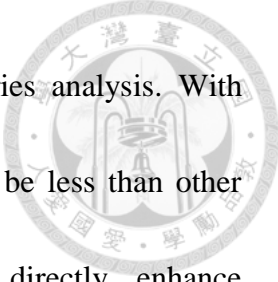


network connectivity beyond which multiple attractors can be supported, and suggest that the connectivity of real biological networks may have evolved to balance the dangers of multiple attractors against the need for agility and robustness (Anafi et al. , 2010). A disease called idiopathic pulmonary fibrosis, which manifests as inappropriate persistence in processes of repairing for tissue injury, could be explained by an entrapment in a abnormal attractor (Agostini et al. , 2006).

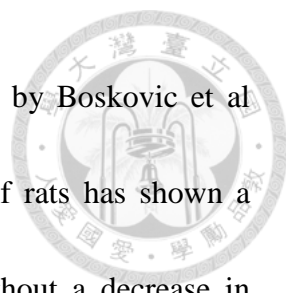
1.8 Symbolic dynamics

1.8.1 Symbolization or symbolic time-series analysis

Symbolic dynamics is based on a way of coarse graining or reduction of description. The phase space is divided into a finite number of partitions which are labeled with a symbol. In the study of biological signals, we sample points along the trajectories of a continuous flow. In other analytical methods like those time series analyses, infinite sequences of numbers are used to represent the trajectories. In symbolic dynamics, one watches the alternation of symbols of those partitions. At first, the data are transformed into a pattern which is composed of only a few symbols. Then only the dynamics of the symbol sequences is studied. Although losing a great amount of detailed information, some of the invariant, robust properties of the dynamics may be kept, e.g. periodicity, symmetry, or chaotic nature of an orbit (Bai-lin, 1991).

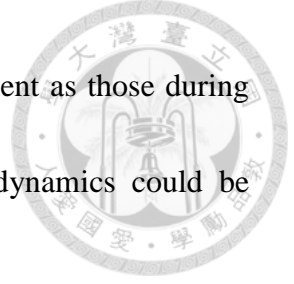


There are some merits of symbolization or symbolic time-series analysis. With careful partitioning process, the effects of noise interference could be less than other methods, as beim Graben showed that symbolization can directly enhance signal-to-noise ratios (beim Graben et al. , 2007). Therefore it can sometimes be accomplished by low-resolution (even “disposable”) sensors as long as an appropriate analysis is used. Good applications of symbolic methods could be favored in situations when cost, speed, or noise is seriously considered. Noise can either enhance or distort the information content. Cuellar and Binder found that by adding a small amount of uncorrelated noise before discretization limited the increase of the average error and improved the estimation of Lyapunov exponents (Cuellar et al. , 2001). Tang et al. has shown the method of symbol sequences statistics is quite good in the problem of reconstruction of chaotic dynamics from short and/or noisy data sets even in the presence of observational and dynamic noise (Tang et al. , 1995). The partition process acts just like down-sampling, through which the entropy can increase since the statistical dependence of consecutive samples decreases (Chen et al. , 2005, Kaffashi et al. , 2008a). Evidence could be provided in the work of Chen et al (Chen et al. , 2005) of ApEn and SampEn showing that down sampling the respiratory time series increased its complexity. The partition process in symbolic analysis is similar to using large values of r in the sense of down sampling. As one may intuitively think that large values of r is



too coarse to enable pronounced process distinction, yet the work by Boskovic et al (Boskovic et al. , 2012) in estimating entropy of HRV in stress of rats has shown a stable entropy difference between different clinical situations, without a decrease in sensitivity.

After the symbolic series being constructed, measures of entropy or entropy rate are generally adopted to explore the dynamics. The following treatments were shown in literature for HRV analysis: 1) the calculation of Shannon entropy (SE) of the distribution of patterns lasting three beats; 2) the calculation of a regularity index based on an entropy rate (i.e., the conditional entropy); 3) the classification of frequent deterministic patterns (FDPs) lasting three beats (Porta et al. , 2001, Guzzetti et al. , 2005). With the symbolization method, two studies enriched HRV in clinical role, one showed that in congestive heart failure, the heart is largely decreased the influence from the autonomic nervous system (Cysarz et al. , 2007); whereas the other one showed the neural pathophysiological mechanisms occurring during the short periods that precede acute cardiac events (Guzzetti et al. , 2005). Symbolic dynamics may well detect the phase transitions in EEG signal analyses. It provided especial good reflection of the state changes in epileptic EEGs (Staniek et al. , 2008, 2009, Schindler et al. , 2012, Zhao et al. , 2012, Paternoster et al. , 2013). It was successfully applied with neural network models in EEG dynamics during mental tasks (Dimitriadis et al. , 2012). Phase



changes in wakeful resting EEG in dementia may not be as prominent as those during epileptic bursts and mental tasks, but the degree of change of dynamics could be compared.

1.8.2 Procedure of symbolization (Porta et al. , 2001)

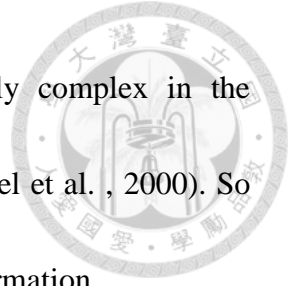
Each sample of the series $X = \{X_i, i = 1, \dots, N\}$ is first normalized by subtracting the mean and, then, divided by the standard deviation, thus obtaining the series $x = \{x_i, i = 1, \dots, N\}$. Next, through coarse-graining, the full range of a series $x = \{x_i, i = 1, \dots, N\}$ was uniformly spread on ζ levels (from 0 to $\zeta-1$) and transformed into a series of symbols $x^\zeta = \{x_i^\zeta, i = 1, \dots, N\}$ from the limited alphabet of symbols $\{0, 1, \dots, \zeta-1\}$. From the symbolic series x^ζ , patterns of L delayed samples were constructed as $x_{3,i}^\zeta = (x_i^\zeta, x_{i-1}^\zeta, x_{i-2}^\zeta)$. The overlapping delayed symbol $x_{3,i}^\zeta$ was codified in decimal format as $(x_i^\zeta, x_{i-1}^\zeta, x_{i-2}^\zeta)_{\text{decimal}} = x_i^\zeta * \zeta^{L-1} + x_{i-1}^\zeta * \zeta^{L-2} + x_{i-2}^\zeta * \zeta^{L-3} = w_i$, $w = \{w_i, i = 1, \dots, N-L+1\}$ with w_i ranging from zero to $N_p = (\zeta-1) \sum_{i=0}^{L-1} \zeta^i$.

An important condition should be noticed is that the number of detected pattern $N-L+1$ should be larger than the number of possible patterns N_p+1 in order to allow patterns to be found several times (Porta et al. , 2001).

1.8.3 Forbidden words

A high number of forbidden words (same as missing pattern) stands for a rather

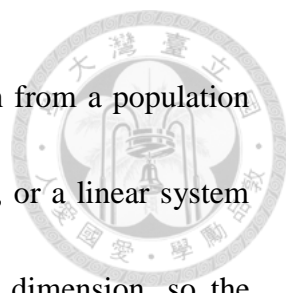
regular behavior in the time series. If the time series is highly complex in the Shannonian sense, only a few forbidden words can be found (Wessel et al. , 2000). So the number or the pattern of forbidden words may also embrace information.



1.9 Surrogate data

For a data driven analysis, the application of nonlinear time series methods has to be justified by establishing nonlinearity in the time series in order to represent a fair account of the structures that are present in the data. For example, in epileptic EEG, strong fluctuations could be from a large collection of neurons intermittently synchronizing to give rise to the burst episodes. However, the spikiness could come from a distortion by the measurement procedure and the serial correlations are due to linear stochastic dynamics (Schreiber et al. , 2000).

Surrogate data sets are generally created under a null single hypothesis. Different surrogates can be generated by randomizing some aspect of the data, and this randomization can be carried many times with different results each time, but all based on the same null hypothesis. Then the particular values of some properties would be taken from those surrogate data. For example, the correlation dimension of each surrogate data are calculated, thereby the distribution of dimensions under that particular null hypothesis is determined. Finally the correlation dimension from the original data is compared to the distribution of dimensions under the null hypothesis.



The simplest null hypothesis is that the data are random and drawn from a population with a given set of values. Other null hypotheses include Gaussian, or a linear system with a particular autocorrelation function. Pure noise has infinite dimension, so the surrogates should have dimensions that are greater than that of the original. In short, determinism (non-randomness) could be tested by random shuffling and non-linearity by phase randomization of the surrogate data provided. Three classes of surrogates are now commonly in use: random-shuffle surrogates, random-phase surrogates (i.e. Fourier Transform), and Gaussian-scaled random-phase surrogates (e.g. amplitude adjusted Fourier transform (AAFT) (Theiler et al. , 1992) and iterated amplitude adjusted Fourier transform (IAAFT) (Schreiber et al. , 1996)). The AAFT algorithm can yield an incorrect test since it introduces a bias towards a slightly flatter spectrum and leads to spurious detection of nonlinearity partitioning (Rapp et al. , 1994). An IAAFT surrogate time series is random, matches the original power spectrum, and preserves the exact original marginal distribution. The linear structure of the IAAFT surrogate time series may differ only slightly from the original linear structure, favoring rejection of the test. There are other surrogate data methods, some based on wavelet transform (Breakspear et al. , 2003, Keylock, 2007) and some capable of dealing with some types of non-stationary data (Nakamura et al. , 2006, Lucio et al. , 2012). Finally, the number of detected patterns should be larger than the number of possible patterns in order to



allow patterns to be found several times (Porta et al. , 2001).

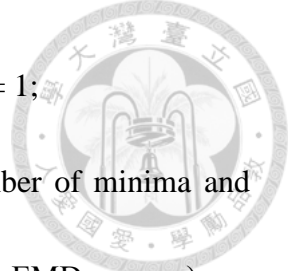
1.10 Empirical mode decomposition (EMD)

Empirical mode decomposition (EMD) (Huang et al. , 1998) is based on nonlinear theories and was designed to extract dynamic information from nonstationary signals at different time scales. It makes no assumptions a priori about the composition of the signal. The advantages of EMD over traditional Fourier-based methods have been appreciated in many studies of different physiological systems such as blood pressure hemodynamics, cerebral autoregulation, cardiac dynamics, respiratory dynamics, and electroencephalographic activities (Lo et al. , 2009).

The decomposition is based on the simple assumption that any data consists of a finite number of intrinsic modes of oscillations. For a time series $x(t)$ with at least 2 extremes, the EMD applies a sifting procedure to extract intrinsic mode functions (IMFs) one by one from a smallest to the largest time scale.

$$\begin{aligned}x(t) &= c_1(t) + r_1(t) \\ &= c_1(t) + c_2(t) + r_2(t) \\ &\vdots \\ &= c_1(t) + c_2(t) + \dots + c_n(t)\end{aligned}$$

where $c_k(t)$ is the k th IMF and $r_k(t) = x(t) - \sum_{i=1}^k c_i(t)$ is the residual after extracting the first k IMFs. The steps of sifting process to extract the k th IMF (Thuraisingham, 2006):

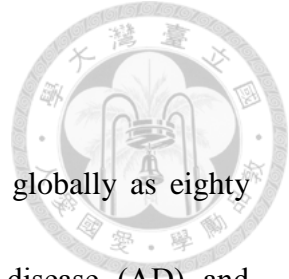


- (1) Initialize $h_0(t) = h_{i-1}(t) = r_{k-1}(t)$ (if $k = 1$, $h_0(t) = x(t)$), where $i = 1$;
- (2) Extract local minima and maxima of $h_{i-1}(t)$ (if the total number of minima and maxima is less than 2, $c_k(t) = h_{i-1}(t)$ and it's the end of the whole EMD process);
- (3) Obtain upper envelope, $u(t)$, and lower envelope, $l(t)$, by the cubic spline interpolation for local minima and maxima of $h_{i-1}(t)$, respectively;
- (4) Calculate the $h_i(t) = h_{i-1}(t) - \text{mean of } (u(t) + l(t))$;
- (5) Calculate the standard deviation (SD) of the mean of $(u(t) + l(t))$;
- (6) To determine a criterion for the sifting process to stop, calculate the limiting size of standard deviation to guarantee that the IMF components retain enough physical sense of both amplitude and frequency modulations.

$$SD_{\max} = \sum_{t=0}^T [|(h_{i-1}(t) - h_i(t))|^2 / h_{i-1}^2(t)] \text{ (typically between 0.2 and 0.3) (Hu et al. , 2008)}$$

- (7) When $SD < SD_{\max}$, the k th IMF is assigned as $c_k(t) = h_i(t)$ and $r_k(t) = r_{k-1}(t) - c_k(t)$;
otherwise repeat steps (2) to (5) for $i + 1$ until $SD < SD_{\max}$.

By definition, an IMF is any function with the same number of extrema and zero crossings, whose envelopes are symmetric with respect to zero. This definition guarantees a well-behaved Hilbert transform of the IMF. Each IMF represents a certain frequency–amplitude modulation at a specific time scale, and therefore it can be used to analyze temporal or phase associations with comparable IMFs from other signals.



1.11 Dementia

The load of care for demented patients is increasing very fast globally as eighty million demented population is expected in 2040. Alzheimer's disease (AD) and vascular dementia (VD) are the two major causes of dementia. Since all current therapies for dementia depend on early diagnosis, risk and predicative factors for dementia are crucial. AD and VD share common risk factors as aging and vascular risks such as diabetes, hypertension, metabolic syndrome, homocystinemia, atrial fibrillation, and smoking. There are bidirectional connections between the heart and the brain. A neurovisceral integration model with laterality on the right prefrontal cortex was proposed to describe the pathways.

The cholinergic deficits in the brain of dementia may affect the central autonomic network. Yet the HRV changes in dementia in previous reports were not congruent. A higher risk of dementia was shown in people with obstructive sleep apnea, which could be indicated by some newly developed methods of HRV analysis.

Traditional EEG records hardly help the diagnosis or treatment of dementia, although the decline in mentality does slow down the brain waves. Using new mathematical techniques with computers' help, scientists hope to find some characteristics to help in early diagnosis or treatment monitoring.

Chapter 2 Experiments



2.1 Hypotheses

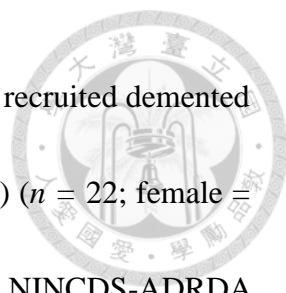
1. Correlations between the heart and brain can be found in signal complexity.
2. Higher complexity does not guarantee more health.
3. Discrete events can provide more direct information than continuous waveforms.
4. Pathological condition is continuous rather than stepwise.
5. Regularity based study is good for the study of biological rhythms.

* The experiments were published (Lin et al. , 2014, Lin et al. , 2015)

2.2 Material and Methods


2.2.1. Study population

The final study population included 89 geriatric outpatients, who were free of previously diagnosed neurologic and cardiovascular diseases (except mild hypertension), and found to have varied cognitive abilities (female = 43; age = 79.3 ± 6.4 years, mean \pm standard deviation (SD), range 65.3–93.7 years). Sixty (female = 30; 81.1 ± 5.7 years) newly diagnosed cases of dementia presented on the first visit with a chief complaint of memory or cognitive decline, corroborated by informants, and had a Chinese version of the mini-mental state examination, the mini-mental state examination of Taiwan, version 1 (MMSE-T1) score with illiteracy adjustment less than



or equal to 26. After laboratory tests and brain-imaging referrals, the recruited demented patients included only two types: probable Alzheimer's disease (AD) ($n = 22$; female = 7; age = 81.9 ± 6.6 years; MMSE-T1 = 22.2 ± 5.8) according to NINCDS-ADRDA (McKhann et al. , 1984) and vascular dementia (VD) ($n = 38$; female = 23; age = 80.6 ± 5.1 years; MMSE-T1 = 18.4 ± 7.2) of subcortical arteriosclerotic encephalopathy according to NINDS-AIREN (Roman et al. , 1993). The control group consisted of Twenty-nine (female = 13; age = 75.5 ± 6.2 years; MMSE-T1 = 28.4 ± 0.9) ambulatory geriatric patients with only mild hypertension and/or mild diabetes. The original MMSE-T1 scores were adjusted for illiteracy by multiplying 30/27 (3 points for reading or writing Chinese characters). Exclusion criteria included mixed dementia, heart failure, atrial fibrillation, frequent atrial premature complex or ventricular premature complex, major systemic diseases, infection, hypothyroidism, vitamin B12 or folic acid deficiency, psychosis, previous stroke, major head injury, epilepsy, normal pressure hydrocephalus, subdural effusion or hemorrhage, and exposure to sympatholytic agents (including beta blockers), acetyl cholinesterase inhibitors, tranquilizers, or antidepressants. The ethics committee on human research of Tainan Hospital approved the study. All participants or their surrogates gave written informed consent. The investigation conformed to the principles of the Declaration of Helsinki.

2.2.2 Data collection



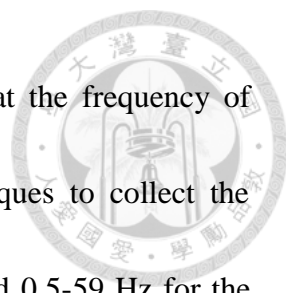
All subjects underwent routine EEG recordings with determination of arousal reaction to eye opening and references at ear electrodes. The routine multichannel EEG includes two parts: the 30-minute wakeful resting recording and the 2.5-minute recording under intermittent photic stimulation. The surface EEG was collected by a digital EEG recorder (Harmonie version 3.1 digital EEG Stellate Systems, Canada) at 200Hz from the 19 electrodes of the international standard 10/20 system (Figure 1). The raw data, contaminated with artifacts such as eye movements, blinks, muscle activities and others, were saved in text files for off-line analysis on a personal computer. I chose three 80-second segments from each file: one visually-censored (by an experienced neurologist) artifact-free eye-closed wakeful resting recording, one photic-simulated recording at frequencies 1, 3, 6 and 9 Hz (slowPS, duration 10 seconds and interval 10 seconds) and one photic-simulated recording at frequencies 12, 15, 18 and 24 Hz (fastPS, duration 10 seconds and interval 10 seconds). The ECGs simultaneously recorded with the EEGs were also obtained. R-peak detection and the beat annotations were performed by an automated arrhythmia detection algorithm and verified by visual inspection. The series of interbeat interval between successive R-peaks, that is the R-R interval (RRI, figure 1), served as the basis for the calculations. Occasional ectopic beats were identified and replaced with linearly interpolated RRI data. Those subjects

with more than 1% ectopic beats were excluded from the final analysis. All the data from EEG would be applied in the analysis of MSE and symbolic dynamics.

All subjects underwent electrocardiography (ECG) monitoring for 24 hours by a standard ambulatory ECG recorder (MyECG E3-80 Portable Recorder, Microstar, Taiwan) at 250 Hz. Two epochs of 2-hour ECG recorded during 9-11am (wakeful) and 1-3 am (sleep) were obtained from each subject. Another 7-minute ECG recording was extracted from the wakeful resting EEG for each subject (Figure 1). The R-peak detection was performed by an automated arrhythmia detection algorithm and corrected by visual inspection. Occasional ectopic beats were identified and replaced with linearly interpolated RRI data. Those people with a rate of ectopic beats higher than 1 % were excluded from the final analysis. Four people having too many ectopic beats only during sleep were included in the final analysis only with the awake RRI data. The three RRI time series were linearly re-sampled at 2 Hz. Because of insufficient data points for the 7-minute RRI, only the two 2-hour RRI time series proceeded to the MSE analysis. One 80-second RRI recorded simultaneously with the EEG from each subject was extracted to be applied in the symbolic analysis. They were not re-sampled.

2.2.3 Data analysis

2.2.3.1 *Filtering and detrending of EEG*



The EEG recordings were firstly processed by a notch filter at the frequency of current 60 Hz. They were further processed by the EMD techniques to collect the components of frequency around 1-58 Hz for the MSE analysis and 0.5-59 Hz for the symbolic analysis. The broader band used in the symbolic analysis was aimed to preserve the components of slow cortical potential, to which the relationship of the simultaneous RRI dynamics would be explored.

2.2.3.2 LF/HF ratio

The low-to-high frequency power (LF/HF) ratio of RRI was calculated to represent sympatho-vagal balance.

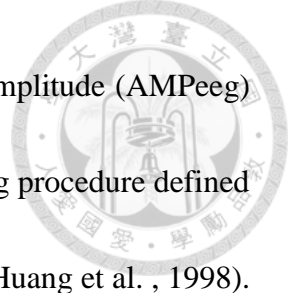
2.2.3.3 Multiscale entropy

Multiscale entropy (MSE) analysis was applied to three epochs (wakeful resting, fastPS and slowPS) of EEG in the 1-58 Hz frequency range, and three (2-hour awake, 2-hour sleep, 7-minute from EEG recordings) epochs of RRIs.

2.2.3.4 Symbolic dynamics

2.2.3.4.1 Four sequences derived from EEG

I detected the local peaks (points from which all paths are downhill) along the EEG waveform and made two sequences from them: the local-peak voltage and interpeak interval sequences (figure 2a). I then calculated the difference between the respective



envelopes of the peaks and troughs to acquire the EEG excursion amplitude (AMPeeg) (Stevenson et al. , 2010) using a method based on the envelope fitting procedure defined in the sifting process of the empirical mode decomposition (EMD) (Huang et al. , 1998).

The local peaks of the AMPeeg were also detected to form another two sequences: the local-peak voltage and interpeak interval of the AMPeeg. Details of the procedure are described below. Then peak detection was performed for each channel of the EEG according to the EMD method:

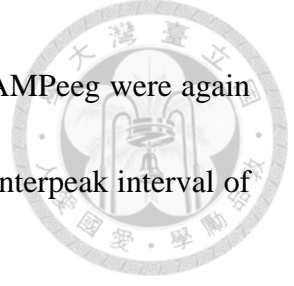
$$\text{maxima}(n) = \begin{cases} 1 & x(n+1) - x(n) \leq 0 \ \& \ x(n) - x(n-1) > 0 \\ 0 & \text{otherwise} \end{cases}$$

$$\text{minima}(n) = \begin{cases} 1 & x(n+1) - x(n) \geq 0 \ \& \ x(n) - x(n-1) < 0 \\ 0 & \text{otherwise} \end{cases}$$

$$n_{\text{max}} = n, \text{ when } \text{maxima}(n) = 1; \ n_{\text{min}} = n \text{ when } \text{minima}(n) = 1;$$

where $x(n)$ is the filtered EEG signal, $n = \{0,1,2,\dots, N - 1\}$ and N is the signal length.

With the local peaks of the filtered EEG, I made two sequences, the local-peak voltage ($x(n_{\text{max}})$) and interpeak interval (difference (n_{max})) sequences (Fig. 2a). Next, natural cubic splines were applied to the maximal (n_{max} , $x(n_{\text{max}})$) and minimal (n_{min} , $x(n_{\text{min}})$) points respectively according to the sifting procedure of the EMD. Thus the upper EEG envelope ($\text{EEG}_{\text{env}}^u$) and the lower EEG envelop ($\text{EEG}_{\text{env}}^l$) were formed from the maximal points and minimal points, respectively. The EEG excursion amplitude (AMPeeg) was defined as the difference between the upper and lower envelopes,



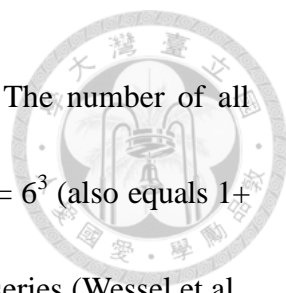
AMPeeg (n) = EEG_{env}^u - EEG_{env}^l (figure 2b). The local peaks of the AMPeeg were again detected to form another two sequences, the local-peak voltage and interpeak interval of the AMPeeg (figure 2c).

2.2.3.4.2 Construction of symbolic sequences

I followed the method developed and validated by Porta et al. (Porta et al. , 2001). Each sample of the series $X = \{X_i, i = 1, \dots, N\}$ (either a RRI, a filtered single-channel EEG whole tracing, or any of the four sequences derived from each single-channel EEG) is first normalized by subtracting the mean and, then, divided by the standard deviation, thus obtaining the series $x = \{x_i, i = 1, \dots, N\}$. Next, through coarse-graining, the full range of a series $x = \{x_i, i = 1, \dots, N\}$ was uniformly spread on 6 levels (from 0 to 5) and transformed into a series of symbols $x^6 = \{x^6_i, i = 1, \dots, N\}$ from the limited alphabet of symbols $\{0, 1, \dots, 5\}$ (figure 2d, 3b). From the symbolic series x^6 , patterns of 3 delayed samples ($L = 3$) were constructed as $x^6_{3, i} = (x^6_i, x^6_{i-1}, x^6_{i-2})$. The overlapping triplet symbol $x^6_{3, i}$ was codified in decimal format as $(x^6_i, x^6_{i-1}, x^6_{i-2})_{\text{decimal}} = x^6_i * 6^{3-1} + x^6_{i-1} * 6^{3-2} + x^6_{i-2} * 6^{3-3} = w_i$, $w = \{w_i, i = 1, \dots, N-L+1\}$ with w_i ranging from zero to $N_p = (6-1) \sum_{i=0}^{3-1} 6^i$ (figure 3c).

2.2.3.4.3 Number of forbidden words and surrogate data

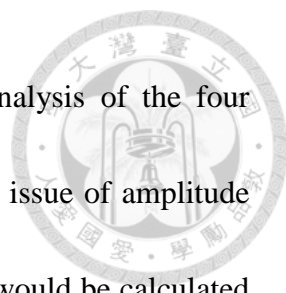
I counted the number of forbidden words (NumFW) of the overlapping triplet



symbols $x_{3,i}^6$ - that is the number of patterns which never occur. The number of all possible patterns of the overlapping triplet symbols $x_{3,i}^6$ equals $216 = 6^3$ (also equals $1 + N_p$). A high NumFW stands for a rather regular behavior in the time series (Wessel et al. , 2000). The sample length of the of the overlapping triplet symbols $x_{3,i}^6$ would be checked to ensure that all patterns (ie. 216) could be found several times. To test the presence of deterministic structures in a sequence, I carried out a surrogate data analysis using Gaussian-scaled random-phase surrogates by iterated amplitude adjusted Fourier transform (IAAFT). (Schreiber et al. , 1996) An IAAFT surrogate time series is random, matches the original power spectrum and preserves the exact original marginal distribution.

2.2.3.4.4 Steps and others

At first, five methods were applied to the symbolic analysis of each RRI and filtered single-channel EEG whole tracing. Sample entropy (SampEn) (Richman et al. , 2000), Shannon entropy (Shannon, 1948), alpha (1) for detrended fluctuation analysis (DFA) (Peng et al. , 1994) and Hurst exponent for rescaled range analysis (RS) (Hurst, 1951) were calculated for each decimalized symbolic sequence, w , of the RRIs and EEG whole tracings. Number of forbidden words (NumFW) was calculated for each sequence of the overlapping triplet symbols, $x_{3,i}^6$, of the RRIs and EEG whole tracings. Methods that showed no significant between group differences by multivariate analysis

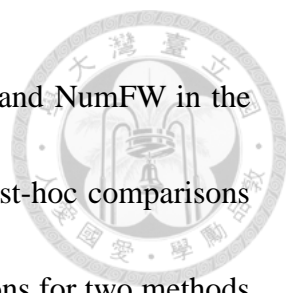


of variance (MANOVA) statistics would not be applied in the analysis of the four EEG-derived sequences. The second step was aimed to explore the issue of amplitude versus instantaneous frequency. Methods chosen from the first step would be calculated for the symbolic sequences of the four EEG-derived sequences (the local-peak voltage, interpeak interval, local-peak voltage of the AMPeeg and interpeak interval of the AMPeeg).

For the SampEn, I chose $m = 2$ and $r = 0.2$. For the algorithms for other calculations, please refer to the references. The SampEn, alpha (1) for DFA and Hurst exponent for RS of the EEG whole tracings without the symbolization procedure were also calculated for comparison.

2.2.3.5 Statistical analysis

All statistical analyses were performed using R 2.11.0 at a 0.05 alpha level. For the symbolic dynamic study, I performed MANOVA to test for significant differences between means. For the symbolic analysis in the first step, I performed a one-way Multivariate analysis of variance (MANOVA) for significant differences between means. In post-hoc analyses, I used Tukey's Honestly Significant Difference (HSD) test to correct for multiple comparisons of 19 electrode sites in three conditions. And the Tukey's p values were further adjusted by Bonferroni corrections for five methods (by multiplication with five). SampEn and NumFW were chosen from the first step. In



the second step, I also performed MANOVA to examine SampEn and NumFW in the symbolic analysis of the four EEG-derived sequences. And the post-hoc comparisons using Tukey's HSD test were also followed by Bonferroni corrections for two methods and four sequences (by multiplication with eight). Paired-t tests with Bonferroni corrections (19 electrode sites) were used to compare the very much correlated data in three EEG conditions. For the analysis of MSE, I performed Student's t-tests to evaluate group differences, and age- and gender-adjusted Pearson's partial correlation coefficients to evaluate correlations between any two variables. And I used Bonferroni corrections to adjust p -values by multiplying the number of the EEG channels (19 channels). I used Student's t-tests to evaluate group differences, and age- and gender-adjusted Pearson's partial correlation coefficients to evaluate correlations between any two variables. The correlations among the three EEGs or three RRIs were calculated using paired t-tests. Kolmogorov-Smirnov and Levene tests were used to assess the normality of distribution and homoscedasticity, respectively.

Chapter 3 Results




3.1 MSE analysis (non-simultaneous EEG and RRI) (Lin et al., 2014)

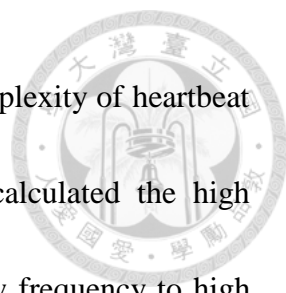
3.1.1 Linear correlations between the MSE of EEG and RRI

I performed a visual inspection of the obtained MSE curves which represent the SampEn values of each coarse-grained sequence versus the scale. Most of the MSE curves had a pattern of an initial increase (from scale 1 to 5 for EEG and from scale 1 to 10 for RRI) before a plateau or a fall. If the SampEn increases initially because of decorrelation before it begins to decrease because of averaging process, the presence of complex long time correlations is expected (Thuraisingham, 2006) (Figure 4). I also analyzed regression coefficients for the MSE slopes over τ of 1-5, 6-10, 11-15 and 16-20, and found no significant differences between groups. The MSE profiles of either the RRIs or EEGs showed no preference to evolve into a plateau or a fall in either the VD, AD or control subjects. Nevertheless the plateau on the MSE profiles of the EEGs seemed to be higher in the control than in the two demented groups.

In all patients, I found significant and very consistent inverse linear correlations between any of the MSE values of the wakeful RRIs on the scale from 11 to 20 (after the initial rising) and any of the MSE values of the EEGs in many channels on the scale

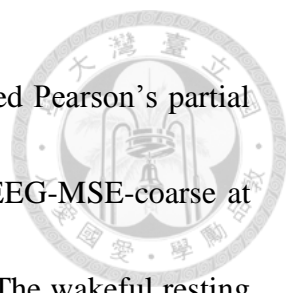


from 6 to 20 (after the initial rising). Therefore I summed up the MSE values on 10 scales (11-20) for the RRIs and on 15 scales (6-20) for the EEGs to facilitate statistical analyses. Using Pearson's partial correlation tests with adjustment for age and gender, in all patients, I found significant inverse associations between the summed MSE values on the scales 11-20 of the RRI (RRI-MSE-coarse) during the wakeful state and the summed MSE values on the scales 6-20 of the EEG (EEG-MSE-coarse) during the resting-wakeful state after Bonferroni corrections at electrodes Fp2 ($r = -0.363$, $p = 0.012$), C4 ($r = -0.344$, $p = 0.024$), T6 ($r = -0.332$, $p = 0.036$) and T4 ($r = -0.325$, $p = 0.046$) (Figure 5). The inverse associations were present in all three patient groups individually, but failed to reach the alpha level after stringent Bonferroni corrections. The RRI-MSE-coarse of the RRI during sleep was not correlated with the EEG-MSE-coarse of the wakeful resting EEG at any channel. The EEG-MSE-coarse of the fast-PS EEG was also inversely correlated to the wakeful RRI-MSE-coarse after Bonferroni corrections at electrodes O1 ($r = -0.336$, $p = 0.011$), O2 ($r = -0.357$, $p = 0.015$) and C4 ($r = -0.327$, $p = 0.042$) (Figure 6), but not to the sleep RRI-MSE-coarse. In contrast, the EEG-MSE-coarse of the slow-PS EEG was significantly inversely correlated to the sleep RRI-MSE-coarse after Bonferroni corrections at electrode Fp2 ($N = 83$, $r = -0.332$, $p = 0.049$), but not to the wakeful RRI-MSE-coarse.



In order to examine whether these associations between the complexity of heartbeat and brainwaves come from the autonomic nervous network, I calculated the high frequency power (HF), low frequency power (LF), and ratio of low frequency to high frequency power (LF/HF ratio) for all the three RRI time series. I found that the LF/HF ratio and RRI-MSE-coarse of the wakeful RRI had a positive age- and gender-adjusted Pearson's partial correlation coefficient ($r = 0.307$, $p = 0.004$) between each other. Nevertheless, the inverse association between the LF/HF ratio of the wakeful RRI and the wakeful resting EEG-MSE-coarse at any channel was not strong enough to exist after Bonferroni corrections. In contrast, the LF/HF ratio and any of the MSE value on the fine scales (scales 1-3) of the wakeful RRI were inversely correlated to each other (age- and gender-adjusted Pearson's partial correlation coefficients $r = -0.420$ to -0.337 , p -values all < 0.0001). The LF/HF ratio of the sleep RRI was not correlated to the sleep RRI-MSE-coarse or any of the EEG-MSE-coarse. Additionally, I found that both the RRI-MSE-coarse and LF/HF ratio of the wakeful RRI were negatively correlated to age using gender-adjusted Pearson's partial correlation tests ($r = -0.301$, $p = 0.005$ and $r = -0.214$, $p = 0.047$, respectively).

Results of Student's t-tests with Bonferroni corrections revealed that the wakeful resting EEG-MSE-coarse at electrode F8 ($p = 0.036$) and the fast-PS EEG-MSE-coarse at electrode Cz ($p = 0.019$) were significantly decreased in the VD group compared to



the control group. I also found a significant age- and gender-adjusted Pearson's partial correlation between the MMSE-T1 score and the wakeful resting EEG-MSE-coarse at electrode F8 ($r = 0.332$, $p = 0.036$) after the Bonferroni correction. The wakeful resting EEG-MSE-coarse was not correlated to age or gender. None of the two sets of RRI-MSE-coarse showed group differences among the three patient groups using student's t-tests after Bonferroni corrections.

3.1.2 Correlated data

The Fourier-based spectra of all three RRI time series were significantly similar to each other in spectral distribution. For the LF, HF and LF/HF ratio between the 2-hour sleep and 2-hour wakeful RRIs, the p -values for Pearson's correlation coefficients were all below 10^{-6} . For the LF and HF between the 7-minute and either of the 2-hour RRIs (wakeful or sleep), the p -values for Pearson's correlation coefficients were all significantly below 0.001. Of the sleep RRI, the LF and LF/HF ratio ($N = 83$, $p = 0.003$ and 0.019 respectively) were significantly lower in the VD group compared to the control group using Student's t-tests. In contrast to previous evidence which showed either lower wakeful LF and LF/HF ratio in AD (Murakami et al. , 2002) or no HRV change in AD and VD (Allan et al. , 2005), our patients with VD other than AD had more prominent autonomic cardiac involvement. Finally, the paired-t test also showed that the EEG-MSE-coarse of the fast-PS EEG was much smaller than the

EEG-MSE-coarse of either the wakeful resting EEG or slow-PS EEG (p -values < 0.0001 at all electrode sites).



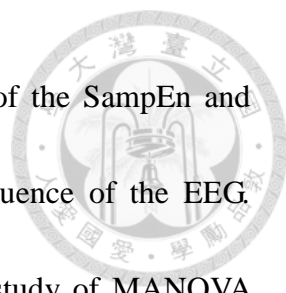
3.2 Symbolic dynamics (simultaneous EEG and RRI) (Lin et al. , 2015)

3.2.1 Discriminative power found only after the symbolization procedure

In the symbolic analysis of the EEG whole tracings: no alpha (1) for DFA or Hurst exponent for RS demonstrated significant differences among groups; Shannon entropy shared nearly the same findings with SampEn in the MANOVA and the post-hoc tests, only with larger p -values; NumFW revealed highest discriminative power. We chose SampEn and NumFW for the second step. For comparison, analyses of the EEG whole tracings without the symbolization procedure were performed with all methods except NumFW (not applicable). Findings without the symbolization procedure did not reveal any significant difference among groups.

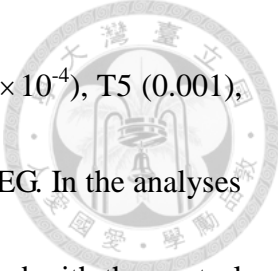
3.2.2 The local-peak voltage sequence of EEG shows the same dynamics in the EEG whole tracing

Among patient groups, consistent relative values of SampEn of the decimalized symbolic sequence (Control = AD < VD) and NumFW of the overlapping triplet symbols (Control = AD > VD) were presented in the symbolic analyses of both the EEG whole tracing and the local-peak voltage sequence. Table 1 shows the means and standard deviations of the SampEn and NumFW of the symbolic dynamics of the EEG

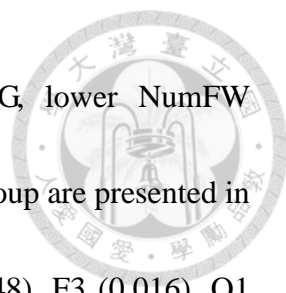


whole tracing. Table 2 shows the means and standard deviations of the SampEn and NumFW of the symbolic dynamics of the local-peak voltage sequence of the EEG. Significant discriminative brain regions revealed by the post-hoc study of MANOVA were denoted by the star signs as “*” for corrected p value < 0.05 and “**” for corrected p value < 0.01 . The symbolic dynamics of the other three sequences derived from EEGs (the interpeak interval sequence of the local peaks of the EEG, the interpeak interval sequence of the local peaks of the AMPeeg, and the local-peak voltage sequence of the AMPeeg) or any RRI sequence did not show discriminative ability. In conclusion, the symbolic dynamics in the EEG whole tracing were only found again in the local-peak voltage sequence of the EEG.

The discriminative brain regions for the SampEn are presented as topographic maps in figure 7 and figure 8. In the analyses of the EEG whole tracings, lower NumFW (NumFW_EEGwhole) values in the VD compared with the control group are presented in figure 3 (a1- a3) at Fp2 (corrected p -value: 0.025), F4 (0.025), F8 (4×10^{-4}), C4 (5×10^{-5}), T4 (0.002), P4 (5×10^{-4}), T6 (2×10^{-4}), O2 (0.005), Fp1 (0.030), F3 (0.010), F7 (0.040), C3 (0.015), P3 (7×10^{-4}), Fz (0.001), Cz (0.005) and Pz (6×10^{-4}) with the wakeful resting EEG; at C4 (0.030), T4 (0.010), T6 (0.020), F7 (0.005), C3 (0.001), T3 (0.002), P3 (2×10^{-4}), T5 (0.005), O1 (0.005) and Pz (0.005) with the slowPS EEG; and at F4 (0.030), F8 (0.010), C4 (0.005), T4 (0.020), P4 (0.035), T6 (0.005), O2 (0.001),

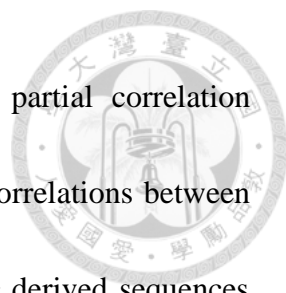


Fp1 (0.005), F3 (0.010), F7 (0.030), C3 (8×10^{-4}), T3 (4×10^{-4}), P3 (8×10^{-4}), T5 (0.001), O1 (2×10^{-4}), Fz (0.015), Cz (0.020) and Pz (0.002) with the fastPS EEG. In the analyses of the EEG whole tracings, higher SampEn values in the VD compared with the control group are presented in figure 3 (b1- b3) at C4 (2×10^{-4}), P4 (0.015), T6 (0.010), Fz (0.010), Cz (0.012) and Pz (0.002) with the wakeful resting EEG; at F7 (0.025), P3 (0.015) and T5 (0.005) with the slowPS EEG; and at P4 (0.03), T6 (0.035), O2 (0.010), F3 (0.040), F7 (0.015), C3 (0.010), T3 (0.005), P3 (0.010), T5 (0.010), and Pz (0.005) with the fastPS EEG. In the analyses of the EEG whole tracings, lower NumFW_EEGwhole values in the VD compared with the AD group are presented in figure 3 (c1- c3) at F8 (0.028), C4 (0.049), T4 (0.002), P4 (8×10^{-4}), T6 (2×10^{-4}), O2 (7×10^{-4}), T5 (0.040), Fz (0.035) and Pz (0.005) with the wakeful resting EEG; at C4 (0.005), T6 (0.030), C3 (0.020), T3 (0.035), T5 (0.005), O1 (0.015), Cz (0.030) and Pz (0.005) with the slowPS EEG; and at F4 (0.005), C4 (0.005), T4 (0.005), P4 (0.020), T6 (0.001), O2 (0.001), F3 (0.020), C3 (0.020), T3 (0.005), P3 (0.005), T5 (0.005), O1 (0.025), Fz (0.005), Cz (0.005) and Pz (0.002) with the fastPS EEG. In the analyses of the EEG whole tracings, higher SampEn values in the VD compared with the AD group are presented in figure 3 (d1- d3) at T6 with the wakeful resting EEG; at T6 (0.040) with the slowPS EEG; and at C4 (0.025), T4 (0.005), P4 (0.010), T6 (0.010), O2 (0.005) and Cz (0.045) with the fastPS EEG.



In the analyses of the local-peak voltage sequence of EEG, lower NumFW (NumFW_EEGpeak) values in the VD compared with the control group are presented in figure 4 (a1- a3) at Fp2 (0.048), C4 (0.032), P4 (0.048), Fp1 (0.048), F3 (0.016), O1 (0.048), Fz (0.003), Cz (0.016) and Pz (10^{-4}) with the wakeful resting EEG; at Fp2 (0.008), C4 (0.048), Fp1 (0.008), F3 (0.002), F7 (0.016), C3 (7×10^{-4}), P3 (6×10^{-4}), T5 (0.002), O1 (0.032), Fz (0.016) and Pz (0.008) with the slowPS EEG; and at F4 (0.032), C4 (8×10^{-4}), T4 (0.048), O2 (0.048), F3 (0.008), C3 (0.016), T3 (0.040), P3 (0.008), T5 (0.032), O1 (0.003), Fz (0.016), Cz (0.016) and Pz (0.024) with the fastPS EEG. In the analyses of the local-peak voltage sequence of EEG, higher SampEn values in the VD compared with the control group are presented in figure 4 (b1- b3) at C4 (0.003), T4 (0.032), P4 (0.008), Fz (0.008), Cz (0.008) and Pz (2×10^{-4}) with the wakeful resting EEG; at F3 (0.040), P3 (0.016) and T5 (0.032) with the slowPS EEG; and at C4 (0.16), F3 (0.016), O1 (0.024) and Pz (0.040) with the fastPS EEG. In the analyses of the local-peak voltage sequence of EEG, lower NumFW_EEGpeak values in the VD compare In conclusion, symbolic entropy of the amplitude rather than the instantaneous frequency of EEG varies in dementia. The lower NumFW and higher SampEn of either the whole EEG tracings or the local-peak voltage sequences in the VD group implied a loss of regularity.

The linear correlations between the NumFWwhole and NumFW_EEGpeak in all



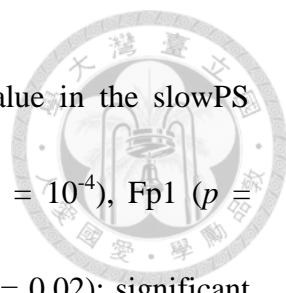
three conditions were very high (the age- and gender-adjusted partial correlation coefficients $r = 0.52$ to 0.85 , $p = 10^{-7}$ to 10^{-25}). I did not find any correlations between the NumFWwhole and the NumFW of any of the other three EEG derived sequences (the interpeak interval sequence of the local peaks of the EEG, the local-peak voltage sequence of the AMPeeg and the interpeak interval sequence of the local peaks of the AMPeeg.). The MMSE-T1 score decreased linearly with age (gender-adjusted Pearson's partial correlation coefficient $r = -0.337$, $p = 0.001$). Using ANOVA test, the MMSE-T1 score was significantly lower in the VD compared with in the control ($p = 3 \times 10^{-10}$) and AD ($p = 0.04$) groups.

3.2.3 No correlations between simultaneous EEG and RRI

I failed to find any correlation between the parameters from the symbolic analysis of the simultaneous RRIs and EEGs.

3.2.4 Correlated data

The NumFW_EEGpeak values in the EEGs of all three conditions were highly correlated with one another (all the p -values for Pearson's correlation coefficients < 0.001). Using paired-t tests with Bonferroni corrections, I found that: significant lower NumFW_EEG_whole value in the slowPS compared with the wakeful resting state at F1 ($p = 6 \times 10^{-6}$), Fz ($p = 6 \times 10^{-5}$), F2 ($p = 4 \times 10^{-4}$), F3 ($p = 0.003$), F4 ($p = 0.009$), Cz (p

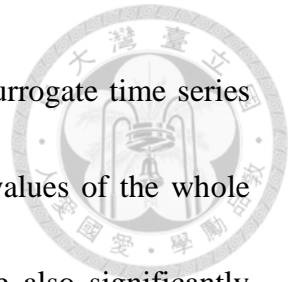


= 0.030) and F8 (0.040); significant lower NumFW_EEGpeak value in the slowPS compared with the wakeful resting state at Fz ($p = 10^{-5}$), Fp2 ($p = 10^{-4}$), Fp1 ($p = 7 \times 10^{-4}$), F8 ($p = 0.007$), Cz ($p = 0.008$), F3 ($p = 0.003$) and F4 ($p = 0.02$); significant lower NumFW_EEGwhole value in the fastPS compared with the wakeful resting state at Fz ($p = 10^{-4}$), Fp1 ($p = 2 \times 10^{-4}$), Fp2 ($p = 0.004$), F3 ($p = 0.007$) and F8 ($p = 0.01$); significant lower NumFW_EEGpeak value in the fastPS compared with the wakeful resting state at F4 ($p = 6 \times 10^{-6}$), F1, F8, F3 and Fp2 (all p -values = 0.01). Both the NumFW_EEGwhole and NumFW_EEGpeak did not significantly differ between the slowPS and fastPS conditions. The NumFW values of the RRIs in all three conditions (wakeful resting, slowPS, and fastPS) were highly correlated to each other (Pearson's correlation, p -values < 0.0001) but not different in their means (paired-t tests). High correlations were also seen with the SampEn

3.2.5 The number N of words used for estimation of the number of forbidden words

The sample length of the EEG whole tracing signal was originally 16,000 (80 seconds, 200Hz). After the symbolic pattern construction of 3 delayed samples, the number N of words used for estimation of the number of forbidden words (N) became 15998. The N of the local-peak derived sequences was around 1300-3000, and of the AMPeeg-derived sequence was around 400-1000. They were also large enough to allow

patterns (i.e., 216) to be found several times. I also used IAAFT surrogate time series for comparison. I found that in all three conditions, the NumFW values of the whole EEG tracings or their derived sequences (around 30 to 200) were also significantly much higher than those of their surrogate data (close to 0). Non-randomness and non-linearity in our data were justified.



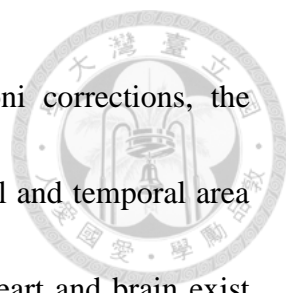
Chapter 4 Discussion



4.1 Inverse correlations between the signal complexity of cardiac and cerebral activities (Lin et al., 2014)

The MSE analyses of non-simultaneous EEGs and RRIs displayed inverse correlations between the signal complexity of cardiac and cerebral activities. And these could not be fully explained by the central autonomic pathways. The wakeful resting EEG was associated to the wakeful RRI time series in the right frontopolar, central and temporal area, the fast-PS EEG was also associated to the wakeful RRI time series in the bilateral occipital and right central area, whereas the slow-PS EEG was associated to the sleep RRI time series in the right frontopolar region. These results may imply a strong correlation between the dynamics of heartbeat and brainwaves; and the correlation could be manipulated by photic stimulation, and affected by the sleep-wake cycle.

Although I adopted a stringent statistical criterion by using Bonferroni adjustments to enlarge the p -values by 19 times based on the interdependence between the EEGs of 19 electrode sites, I understand that the likelihood of type II error is also increased, so that truly important differences are deemed non-significant (Perneger, 1998). Before Bonferroni corrections, the significant sites showing the heart-brain connection

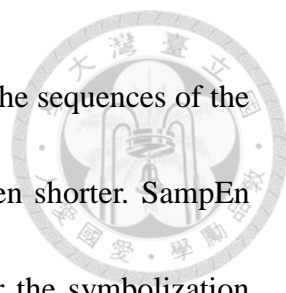


distributed widely over the whole head, whereas after Bonferroni corrections, the heart-brain connection only appeared in the right frontopolar, central and temporal area during the wakeful state. Whether these correlations between the heart and brain exist globally and favor the right brain, and whether they could be fully explained by the central autonomic pathways are unknown. These correlations seemed to exist in all three aging groups, but whether they exist in younger populations as well is also questionable. According to previous neuroanatomical and pharmacophysiological findings, the prefrontal cortex plays the leading role in the central autonomic network. The connection between the heart and brain in signal complexity is beyond the anatomical evidence of the central autonomic network.

The results correspond with the cholinergic hypothesis (Pakaski et al. , 2008) which states that cognitive decline (a lower EEG-MSE-coarse) is related to central cholinergic neuronal dysfunction and a consequent decrease in vagal cardiac modulation (a higher LF/HF and a higher RRI-MSE-coarse). In addition, because of the similarity between all three RRI data, HRV is stable and therefore characteristic of an individual (Sinnreich et al. , 1998). Finally, conforming to previous evidence, both the MMSE-T1 score and HRV in our study decreased linearly with age.

4.2 The merits of symbolization (Lin et al. , 2015)


A continuous visually clean EEG recording could only be acquired in a very limited



period because of copious artifacts from muscles or environments. The sequences of the amplitude and interpeak interval of the local peaks of EEG are even shorter. SampEn showed discriminative ability on the EEG whole tracing only after the symbolization techniques. This has clearly showed the merit of the symbolization technique. The NumFW, also known as missing patterns, outperformed SampEn in group differentiation. True missing patterns are robust against noise and they have the potential ability for distinguishing deterministic behavior from randomness in finite time series contaminated with observational white noise (Amigó et al. , 2007, Carpi et al. , 2010). In conclusion, the symbolization technique amplified the discriminative power in EEG. It is due to better sigal-noise ratio after the symbolization technique.

4.3 Study of the discrete events (Lin et al. , 2015)

The dynamics of heartbeat is studied through its discrete events, namely RRI. However, the study of the dynamics of EEG is generally not through the discrete events except the evoked potential. Detecting the local peaks, I approached the background of resting EEG through the aspect of discrete events. The human brain is believed to function on the base of networks of interactivity of neural assemblies, which could be approached through the transient phase couplings of EEG signals from various regions. A balanced dynamical pattern that switches between synchronization (phase coupling between two regions) and desynchronization (phase shifting) is crucial to proper brain



function (Stam et al. , 2003, Hong et al. , 2004, Pijnenburg et al. , 2004, Garcia Dominguez et al. , 2005, Lackner et al. , 2013). The scalp EEG mainly records large postsynaptic potentials (Nunez, 1981). Only large populations of active neurons can generate enough potential to be recordable using the scalp electrodes. The peaks and troughs of a physical wave indicate levels of probability for the occurrence of certain phenomenon. One peak of a single-channel EEG implies a local maximal (in time domain) amount of synchronized active neurons in a localized region. Therefore, the dynamics of the local maxima of a single-channel EEG reflects the changing degree of neuronal couplings in the localized brain area. I supposed that discrete events can provide more focused information in certain dimension of the dynamics. The EEG whole tracing revealed slightly more discriminative brain regions compared with the local-peak voltage sequence. This was due to that the Bonferroni corrections were more rigorous in the analyses of the local-peak voltage sequences according the study design. Whether the discrete events provide more focused information was not answered. But we can say that they provide no less information than the continuous EEG recordings.

Using symbolic analysis, the differences between the VD and control groups in the dynamics of the EEG whole tracings could only be found in its local-peak voltage but not interpeak interval sequences. This may imply that the dynamics of the amount (local-peak voltage) of but not the interval (interpeak interval) between each

synchronous firing of adjacent cerebral neurons are relevant to clinical conditions.

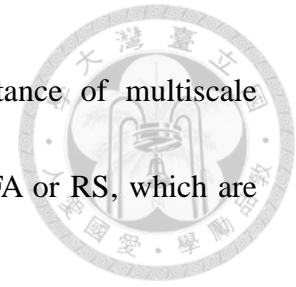


4.4 Regularity based complexity study

It is still under debate whether chaos is present in the biological rhythms. In practice, this issue is not as interesting as one might think in clinical application. Actually, very few of the time series considered for a nonlinear treatment pass even a simple test for Gaussianity. Since both deterministic regularity and irregularity are present in the biological rhythms, regularity based complexity study should well explore the system dynamics.

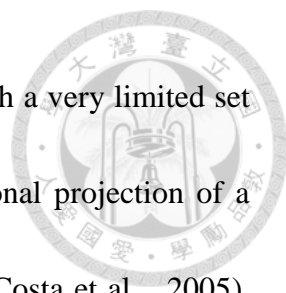
Biological systems are complex at multiple levels of temporal and spatial scales and consist of interconnected feedback loops. The Fourier-based spectral analysis averages the signals, so it can not sufficiently display the nonlinear and non-stationary properties of complex biological systems. The science of complex systems is closely related to variability analysis which detects and characterizes nonlinear dynamics (Stam, 2005). Heart rate variability (HRV) and signal variability of resting-state brain activity convey important information about network dynamics (Deco et al. , 2011). I found the entropy measurement techniques, which compute the regularity patterns of a time series, best suit our data and the entropy values can provide quantitative connotations to facilitate comparisons and correlations between two systems and between individual subjects. I also successfully used MSE to demonstrate the correlation between the

non-simultaneous EEGs and RRIs. This has proven the importance of multiscale approaches. In contrast, we found no discriminative abilities in DFA or RS, which are fractal based analyses.



4.5 The issue of more or less complexity (Lin et al. , 2014, Lin et al. , 2015)

Living organisms are generally believed to behave in a manner of high complexity in order to respond to a broad range of stimuli (Peng et al. , 2009). With the deterioration of health conditions, the change in dynamic patterns of biological signals is characterized by loss of complexity and development of stereotypy such as Cheyne-Stokes respiration, Parkinsonian gait, cardiac rhythms in heart failure (Goldberger, 1997) and dementia (Jeong, 2004). Nevertheless, an increase of entropy (ApEn) was noted in the hormone release patterns in Cushing's disease (van den Berg et al. , 1997) and acromegaly (Hartman et al. , 1994). Previous EEG studies showed more regularity in AD using approximate entropy (Abasolo et al. , 2007) and SampEn (Park et al. , 2007). Various analytic methods may have explored different scales or dimensions. For example, multiscale entropy analysis revealed different results across fine- or coarse-time scales in AD, higher or less regularity, respectively (Escudero et al. , 2006, Yang et al. , 2013). With multifractal biological signals, Vaillancourt and Newell made a point that no one direction fits all results (Thaler, 2002). Any physiological phenomenon plays only one part in the complex networks of a human body. While

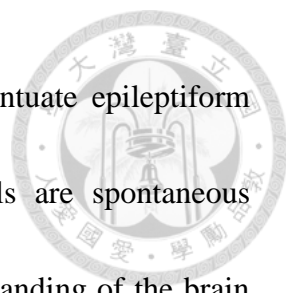


exploring the dynamics of highly complex physiological signals with a very limited set of signals as state variables, one actually observes a low-dimensional projection of a trajectory embedded in the much higher dimension of state space (Costa et al. , 2005).

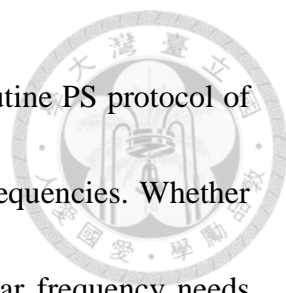
Riley et al. also revealed that more variability does not mean more randomness, and more controllability does not mean more deterministic characteristics (Riley et al. , 2002).

I found a consistent decrease of regularity in the symbolic dynamics of EEG but an increase of regularity in the coarse-scaled MSE in VD. This discrepancy may be caused by the multifractal characteristic of EEG signals and the limitations of the analytic methods. The symbolic analysis of the discrete events and the MSE analysis depict different scales of the EEG dynamics. In addition, the correlations between the LF/HF ratio and MSE values of the wakeful RRI being positive on the coarse scales and negative on the fine scales of MSE. This has advocated the importance of a multiscale approach to biological signals. In conclusion, the direction of complexity change does not guarantee a better or worse physiological condition. But a consistent inverse correlation most likely indicates a certain physiological connection between the two systems.

4.6 Photic stimulation amplified differences between groups (Lin et al. , 2014, Lin et al. , 2015)



Photic stimulation (PS) is a procedure meant to elicit or accentuate epileptiform discharges during a routine EEG. Both cardiac and neuron cells are spontaneous oscillators. Despite the widespread utilization, the complete understanding of the brain response to PS is still an open problem. Photic stimulation (PS) of either slow or fast frequencies significantly interrupted the EEG dynamics with both the whole tracing and the local-peak voltage sequence. The PS procedure widely affects the EEG dynamics over the whole head in the MSE study. The symbolic dynamics under PS was significantly less regular (lower NumFW) in the frontal regions but not the occipital regions. Intuitively, any changes in cortical activity that occur during the PS procedure are attributed to the visual stress, which logically should mainly affect the occipital regions. In all our brain images, the frontal regions either are scattered with ischemic lesions or show age- or disease-related atrophy, whereas the occipital regions are relatively intact. Therefore I can attribute the changes in the frontal regions by the PS procedure to the vulnerability of the frontal regions. The PS procedure amplified the group differences, especially in fast frequencies. One can find more discriminative brain regions in the fastPS condition compared with the wakeful resting condition in both the EEG whole tracing and the local-peak voltage sequence from the topographic maps (figure 7, figure 8). The visual cortices were brightened up by the PS in fast frequencies. The PS procedure should have exerted a strong influence on the brain and consequently




provokes varied effects on different defective brain regions. The routine PS protocol of our laboratory uses a combination of short segments of different frequencies. Whether the symbolic dynamics can also be changed by PS at any particular frequency needs further research.

A study of EEG under PS found no significant difference between the power spectra of the EEG under PS of frequencies 11 and 20 Hz (Kikuchi et al. , 2002). I found different MSE or symbolic entropy values between the EEGs under different PS frequencies. The fast-PS procedure changed the EEG dynamics and shifted the heart-brain associations topographically into the occipital lobes, the visual cortex. The slow-PS procedure, although not causing any obvious change in the MSE of EEG, also changed the EEG dynamics and shifted the heart-brain associations from wakeful state into sleep. I assume that the stimulation of fast-PS is very strong that highlights the connection between the heart and brain in the visual cortex, whereas the stimulation of slow-PS is weak and only blocks the background activity in the visual cortex just like what happens during sleep, being eye-closed. Sleep is a state of arousable “loss of consciousness” with slowed heartbeats and brainwaves, and the mechanism of sleep remains unknown.

4.7 Nonlinear and non-stationary filters

I used linear filter to remove power line because the current oscillations are

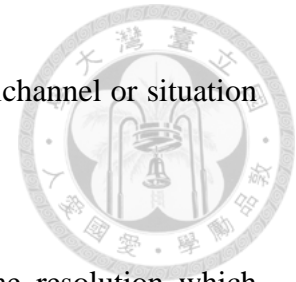


sinusoidal periodicities and used nonlinear and non-stationary filter to remove nonlinear trending or mixed non-stationarities from artifacts such as eye and muscle movements. I have compared nonlinear decomposing techniques such as independent component analysis (ICA) (Comon, 1994), a stochastic approach, and empirical mode decomposition (EMD) (Huang et al. , 1998), a deterministic approach. Both techniques can detect and separate the contamination from wide variability of artificial sources in EEG recordings. ICA is suitable in eye-artifact elimination (Plochl et al. , 2012), whereas EMD works well for eliminating both eye- and muscle-artifact in EEG (Tsai et al. , 2012). EMD outperformed ICA for the denoising of data highly contaminated by muscular activity (Safieddine et al. , 2012). In this study, I chose the cleanest segments from long raw data by an experienced neurologist, eliminated the 60 Hz noise by notch filter, and eliminated the remained non-stationarities by EMD.

4.8 Single or multi-channelled EEG

Some studies have successfully approached the brain dynamics in a holistic way, namely multichannel, either through neural network models (Dimitriadis et al. , 2012) or through many other bivariate or multivariate synchronization models (Jalili et al. , 2013). The scalp EEG signals of one single-channel already contain information shifting between synchronization and desynchronization of a certain network at a microscopic aspect. I took single-channel approach also because I intended to compare the

topographical results with those from fMRI studies. However, multichannel or situation under mental tasks would be considered in my future study.



EEG possesses a remarkable advantage with its excellent time resolution which gives us a unique window on the dynamics of brain functions. When neuronal activity is measured by fMRI, a direct anatomical link does not necessarily coexist with robust functional connectivity (Koch et al. , 2002) and the within-subject test–retest reliability of functional connectivity as measured was surprisingly low (Honey et al. , 2009). Studies of EEG dynamics remains worthwhile until the questions between the brain and consciousness are fully answered.

4.9 Wide band or narrow band

Changes in the EEG dynamics of AD or amnesic mild cognitive impairment were reported in varied frequency ranges such as alpha1 (8–10.5 Hz) (Babiloni et al. , Adler et al. , 2003), theta (Adler et al. , 2003, Garn et al. , 2014), delta (Laskaris et al. , 2013) and all frequencies (Koenig et al. , 2005). Disturbed phase relations in vascular dementia revealed changes in all bands except delta (van Straaten et al. , 2014). Different methods may just explore different aspects or dimensions. Studies of approximate entropy (Abasolo et al. , 2007), SampEn (Park et al. , 2007) and multiscale entropy (Escudero et al. , 2006, Park et al. , 2007, Yang et al. , 2013) in dementia using wide-band EEG successfully showed eminent discriminative ability. Therefore I chose

wide-band EEG without *a priori* assumptions of the contribution of any frequency band.

I have repeated the analyses in separated conventional bands with the symbolic analyses,

but the discriminative ability in any conventional band was not as prominent as in the

wide-band EEG. In addition, the amplitude fluctuation, which is crucial in my study

design, would be reduced by the operation of extracting certain frequency band.

4.10 Limitations

Many recruited subjects were excluded due to varied reasons such as poor cooperation during the EEG procedure, poor EEG qualities, and too many ectopic

heartbeats. A visually clean continuous EEG could only be acquired in a very limited

period because of copious artifacts from eye movements, muscles or environments. The

electromagnetic activity of the brain works at an extremely fast speed, and the

quasi-stationary epochs of EEG are, in general, short lasting, in the order of tens of

seconds (Fingelkurts, 2010). Therefore the simultaneous EEG and ECG data were not

long enough for MSE, which warrants long series for better probability estimation.

Using the symbolization techniques, I still found no correlation between the

simultaneous EEG and RRI data. It is due to that the length of the RRI data in this study,

even under the symbolization procedure, was too short to be characteristic of an

individual. To achieve constant heart rate variability, it is generally recommended to

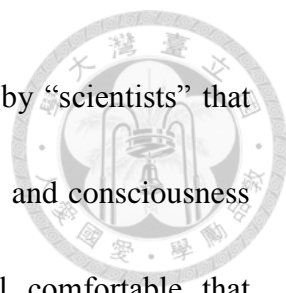
obtain a minimum 5-minute ECG recording (Sinnreich et al. , 1998).

Chapter 5 Conclusion



Answers to the hypotheses:

1. Correlations between the heart and brain can be found in signal complexity. → Yes, the correlations were found in the MSE analyses of non-simultaneous EEG and RRI data.
2. Higher complexity does not guarantee more health. → True, at first, it depends on the method and the scale or dimension that the method evaluates. Secondly, in the EEG dynamics for healthy brain conditions, homeostasis (less complexity) remains necessary in certain dimensions of the symbolic dynamics, whereas variability (more complexity) is found in the coarse scales of the MSE.
3. Discrete events can provide more direct information than continuous waveforms. → I only proved the discrete events can show no less information than the continuous waveforms of EEG. Further studies are warranted to answer this hypothesis.
4. Pathological condition is continuous rather than stepwise. → Yes, at least in dementia as the EEG-MSE-coarse at F8 was proportional to the score of cognitive test (MMSE-T1) in dementia.
5. Regularity based study is good for the study of biological rhythms → Yes. I found the regularity based analyses perform much better than the fractal based analyses.



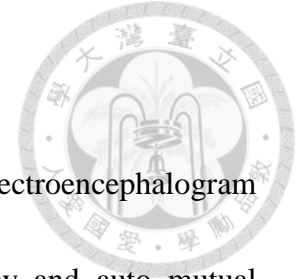
In lecture Halls of modern western medicine, I was persuaded by “scientists” that life is but an “integrative level” emerging on non-living substances, and consciousness emerging on electromagnetic activities of neurons. I don’t feel comfortable that consciousness is only some emergent phenomenon. I am puzzled by the mysterious meaning of the correlations between the signal complexity of the heart and brain that I found. We can’t consciously control any of the rhythms in our own bodies: heart rates, brain waves, circadian cycles, menstrual cycles, etc. But they do interact with each other and operate with an automatic way in a “subconscious” level. We don’t really understand the conscious mind, not to say the subconscious one.

Humans have been very good in inventing new terms whenever a mystery is encountered and then leave the unknown untouched ever since. The biggest example is possibly the God or Gods. A trendy term is called *psi* which denotes anomalous processes of information or energy transfer that are currently unexplained in terms of known physical or biological mechanisms. Modern scientists do not want to leave it untouched any more, but to do more experiments and to make models. Phenomena such as near death experiences (Charland-Verville et al. , 2014, Palmieri et al. , 2014), phantom pain (Lotze et al. , 2001) and personality change after organ transplantation (Bunzel et al. , 1992) could be very difficult to be explained by current scientific knowledge. Quantum physics informs us that a system exists in all possible states —

until we observe that it is only in one specific state (Rovelli, 1996, Aspect, 2007). What is reality? What is life?



Reference



Abasolo D, Hornero R, Espino P, Escudero J, Gomez C. Electroencephalogram background activity characterization with approximate entropy and auto mutual information in Alzheimer's disease patients. *Conf Proc IEEE Eng Med Biol Soc.* 2007;2007:6192-5.

Abasolo D, Hornero R, Espino P, Poza J, Sanchez CI, de la Rosa R. Analysis of regularity in the EEG background activity of Alzheimer's disease patients with Approximate Entropy. *Clin Neurophysiol.* 2005;116:1826-34.

Adler G, Brassens S, Jajcevic A. EEG coherence in Alzheimer's dementia. *J Neural Transm.* 2003;110:1051-8.

Agostini C, Gurrieri C. Chemokine/cytokine cocktail in idiopathic pulmonary fibrosis. *Proc Am Thorac Soc.* 2006;3:357-63.

Aihara K, Numajiri T, Matsumoto G, Kotani M. Structures of attractors in periodically forced neural oscillators. *Physics Letters A.* 1986;116:313-7.

Al-Nashash HA, Thakor NV. Monitoring of global cerebral ischemia using wavelet entropy rate of change. *IEEE Trans Biomed Eng.* 2005;52:2119-22.

Allan LM, Kerr SR, Ballard CG, Allen J, Murray A, McLaren AT, et al. Autonomic function assessed by heart rate variability is normal in Alzheimer's disease and vascular dementia. *Dement Geriatr Cogn Disord.* 2005;19:140-4.

Amigó JM, Zambrano S, Sanjuán MAF. True and false forbidden patterns in deterministic and random dynamics. *EPL (Europhysics Letters)*. 2007;79:50001.

Anafi RC, Bates JHT. Balancing robustness against the dangers of multiple attractors in a Hopfield-type model of biological attractors. *PLoS ONE*. 2010;5:e14413.

Armour JA. Functional anatomy of intrathoracic neurons innervating the atria and ventricles. *Heart Rhythm*. 2010;7:994-6.

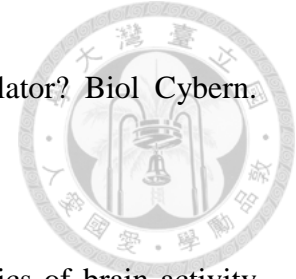
Armour JA. Physiology of the intrinsic cardiac nervous system. *Heart Rhythm*. 2011;8:739.

Aspect A. Quantum mechanics: To be or not to be local. *Nature*. 2007;446:866-7.

Aurlien H, Gjerde IO, Aarseth JH, Eldøen G, Karlsen B, Skeidsvoll H, et al. EEG background activity described by a large computerized database. *Clinical neurophysiology : official journal of the International Federation of Clinical Neurophysiology*. 2004;115:665-73.

Babiloni C, Frisoni GB, Vecchio F, Pievani M, Geroldi C, De Carli C, et al. Global functional coupling of resting EEG rhythms is related to white-matter lesions along the cholinergic tracts in subjects with amnesic mild cognitive impairment. *J Alzheimers Dis*. 19:859-71.

Babloyantz A, Destexhe A. Low-dimensional chaos in an instance of epilepsy. *Proc Natl Acad Sci U S A*. 1986;83:3513-7.



Babloyantz A, Destexhe A. Is the normal heart a periodic oscillator? *Biol Cybern.* 1988;58:203-11.

Babloyantz A, Salazar JM, Nicolis C. Evidence of chaotic dynamics of brain activity during the sleep cycle. *Physics Letters A.* 1985;111:152-6.

Bai-lin H. Symbolic dynamics and characterization of complexity. *Physica D: Nonlinear Phenomena.* 1991;51:161-76.

Bak P, Chen K. Self-organized criticality in the 'Game of Life.'. *Nature.* 1989;342:780.

Bak P, Tang C, Wiesenfeld K. Self-organized criticality: An explanation of the $1/f$ noise. *Phys Rev Lett.* 1987;59:381-4.

Balasubramaniam R, Riley MA, Turvey MT. Specificity of postural sway to the demands of a precision task. *Gait & Posture.* 2000;11:12-24.

Baselli G, Cerutti S, Porta A, Signorini MG. Short and long term non-linear analysis of RR variability series. *Med Eng Phys.* 2002;24:21-32.

Bates J. Nonlinear network theory of complex disease. In: Bar-Yam Y, ed 2006; Boston, MA: New England Complex Systems Institute, 28. 2006.

Baumert M, Javorka M, Seeck A, Faber R, Sanders P, Voss A. Multiscale entropy and detrended fluctuation analysis of QT interval and heart rate variability during normal pregnancy. *Comput Biol Med.* 2012;42:347-52.

Beekwilder JP, Beems T. Overview of the clinical applications of vagus nerve



- stimulation. *J Clin Neurophysiol.* 2010;27:130-8.
- beim Graben P, Drenhaus H, Brehm E, Rhode B, Saddy D, Frisch S. Enhancing dominant modes in nonstationary time series by means of the symbolic resonance analysis. *Chaos.* 2007;17:043106.
- Benarroch EE. The central autonomic network: functional organization, dysfunction, and perspective. *Mayo Clin Proc.* 1993;68:988-1001.
- Bezerianos A, Bountis T, Papaioannou G, Polydoropoulos P. Nonlinear time series analysis of electrocardiograms. *Chaos.* 1995;5:95-101.
- Bhattacharya J, Edwards J, Mamelak AN, Schuman EM. Long-range temporal correlations in the spontaneous spiking of neurons in the hippocampal-amygdala complex of humans. *Neuroscience.* 2005;131:547-55.
- Binder PM, Igarashi R, Seymour W, Takeishi C. Determinism test for very short time series. *Physical Review E.* 2005;71:036219.
- Boon P, Vonck K, Van Walleghem P, D'Have M, Goossens L, Vandekerckhove T, et al. Programmed and magnet-induced vagus nerve stimulation for refractory epilepsy. *J Clin Neurophysiol.* 2001;18:402-7.
- Boskovic A, Loncar-Turukalo T, Sarenac O, Japundzic-Zigon N, Bajic D. Unbiased entropy estimates in stress: A parameter study. *Comput Biol Med.* 2012;42:667-79.
- Bray D. Molecular Networks: The Top-Down View. *Science.* 2003;301:1864-5.



Breakspear M, Brammer M, Robinson PA. Construction of multivariate surrogate sets from nonlinear data using the wavelet transform. *Physica D: Nonlinear Phenomena*. 2003;182:1-22.

Brown CT, Liebovitch Larry. *Fractal analysis*. Los Angeles: SAGE Publications; 2010.

Bunzel B, Schmidl-Mohl B, Grundbock A, Wollenek G. Does changing the heart mean changing personality? A retrospective inquiry on 47 heart transplant patients. *Quality of life research : an international journal of quality of life aspects of treatment, care and rehabilitation*. 1992;1:251-6.

Burioka N, Miyata M, Cornelissen G, Halberg F, Takeshima T, Kaplan DT, et al. Approximate entropy in the electroencephalogram during wake and sleep. *Clin EEG Neurosci*. 2005;36:21-4.

Burrus CS, Gopinath, R.H., Guo, H. . *Introduction to Wavelets and Wavelet Transforms, A Primer*. NJ.: Prentice-Hall, Englewood Cliffs, ; 1998.

Campbell MJ, Jones BW. Cyclic Changes in Insulin Needs of an Unstable Diabetic. *Science*. 1972;177:889-91.

Carpi LC, Saco PM, Rosso OA. Missing ordinal patterns in correlated noises. *Physica A: Statistical Mechanics and its Applications*. 2010;389:2020-9.

Chaffin DG, Goldberg CC, Reed KL. The dimension of chaos in the fetal heart rate. *Am J Obstet Gynecol*. 1991;165:1425-9.



Charland-Verville V, Jourdan JP, Thonnard M, Ledoux D, Donneau AF, Quertemont E, et al. Near-death experiences in non-life-threatening events and coma of different etiologies. *Frontiers in human neuroscience*. 2014;8:203.

Chay TR, Rinzel J. Bursting, beating, and chaos in an excitable membrane model. *Biophys J*. 1985;47:357-66.

Chen X, Solomon I, Chon K. Comparison of the use of approximate entropy and sample entropy: applications to neural respiratory signal. *Conf Proc IEEE Eng Med Biol Soc*. 2005;4:4212-5.

Cheng Q. Multifractal Modeling and Lacunarity Analysis. *Mathematical Geology*. 1997;29:919-32.

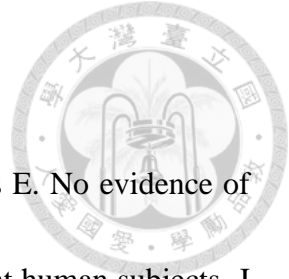
Chon K, Scully CG, Lu S. Approximate entropy for all signals. *IEEE Eng Med Biol Mag*. 2009;28:18-23.

Comon P. Independent component analysis, A new concept? *Signal Processing*. 1994;36:287-314.

Conrad M. what is the use of chaos? In: AV Holden (ed) *Chaos*: Princeton University Press; 1986.

Costa M, Goldberger AL, Peng CK. Multiscale entropy analysis of complex physiologic time series. *Phys Rev Lett*. 2002;89:068102.

Costa M, Goldberger AL, Peng CK. Multiscale entropy analysis of biological signals.



Phys Rev E Stat Nonlin Soft Matter Phys. 2005;71:021906.

Costa M, Pimentel IR, Santiago T, Sarreira P, Melo J, Ducla-Soares E. No evidence of chaos in the heart rate variability of normal and cardiac transplant human subjects. J Cardiovasc Electrophysiol. 1999;10:1350-7.

Costa M, Priplata AA, Lipsitz LA, Wu Z, Huang NE, Goldberger AL, et al. Noise and poise: Enhancement of postural complexity in the elderly with a stochastic-resonance-based therapy. Europhys Lett. 2007;77:68008.

Cuellar MC, Binder PM. Reducing noise in discretized time series. Phys Rev E Stat Nonlin Soft Matter Phys. 2001;64:046211.

Cysarz D, Lange S, Matthiessen PF, Leeuwen P. Regular heartbeat dynamics are associated with cardiac health. Am J Physiol Regul Integr Comp Physiol. 2007;292:R368-72.

Daemen MJ. The heart and the brain: an intimate and underestimated relation. Netherlands heart journal : monthly journal of the Netherlands Society of Cardiology and the Netherlands Heart Foundation. 2013;21:53-4.

Damasio AR. Emotion in the perspective of an integrated nervous system. Brain Res Brain Res Rev. 1998;26:83-6.

Daw CS, Finney CEA, Tracy ER. A review of symbolic analysis of experimental data. Review of Scientific Instruments. 2003;74:915-30.

Deco G, Jirsa VK, McIntosh AR. Emerging concepts for the dynamical organization of resting-state activity in the brain. *Nature reviews Neuroscience*. 2011;12:43-56.

DeFelice LJ, Isaac A. Chaotic states in a random world: Relationship between the nonlinear differential equations of excitability and the stochastic properties of ion channels. 1993:339-54.

Delgado JM. Circulatory effects of cortical stimulation. *Physiol Rev Suppl*. 1960;4:146-78.

Detours V, Sulzer, B., Perelson, AS. Size and connectivity of the idiotypic network are independent of the discreteness of the affinity distribution. *Journal of Theoretical Biology*. 1996;183:409-16.

Devinsky O, Morrell MJ, Vogt BA. Contributions of anterior cingulate cortex to behaviour. *Brain*. 1995;118 (Pt 1):279-306.

Devinsky O, Pacia S, Tatambhotla G. Bradycardia and asystole induced by partial seizures: a case report and literature review. *Neurology*. 1997;48:1712-4.

Dimitriadis SI, Laskaris NA, Tsirka V, Erimaki S, Vourkas M, Micheloyannis S, et al. A novel symbolization scheme for multichannel recordings with emphasis on phase information and its application to differentiate EEG activity from different mental tasks. *Cognitive neurodynamics*. 2012;6:107-13.

Ding M, Grebogi C, Ott E, Sauer T, Yorke JA. Plateau onset for correlation dimension:



When does it occur? *Phys Rev Lett.* 1993;70:3872-5.

Dunne BJ, Jahn RG. Consciousness, Information, and Living Systems. *Explore: The Journal of Science and Healing.* 2007;3:235-43.

Dupuis M, van Rijckevorsel K, Evrard F, Dubuisson N, Dupuis F, Van Robays P. Takotsubo syndrome (TKS): a possible mechanism of sudden unexplained death in epilepsy (SUDEP). *Seizure : the journal of the British Epilepsy Association.* 2012;21:51-4.

Eckmann JP, Ruelle D. Ergodic theory of chaos and strange attractors. *Reviews of Modern Physics.* 1985;57:617.

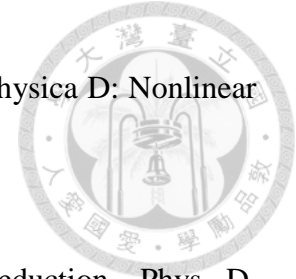
Emlen JM, Freeman DC, Mills A, Graham JH. How organisms do the right thing: The attractor hypothesis. *Chaos.* 1998;8:717-26.

Engel AK, Singer W. Temporal binding and the neural correlates of sensory awareness. *Trends Cogn Sci.* 2001;5:16-25.

Escudero J, Abasolo D, Hornero R, Espino P, Lopez M. Analysis of electroencephalograms in Alzheimer's disease patients with multiscale entropy. *Physiol Meas.* 2006;27:1091-106.

Everitt BS. *An R and S-Plus® Companion to Multivariate Analysis.* Springer; 2005.

Fan YS, Chay TR. Generation of periodic and chaotic bursting in an excitable cell model. *Biol Cybern.* 1994;71:417-31.



Farmer JD, Ott E, Yorke JA. The dimension of chaotic attractors. *Physica D: Nonlinear Phenomena*. 1983;7:153-80.

Farmer JD, Sidorowich JJ. Optimal shadowing and noise reduction. *Phys D*. 1991;47:373-92.

Fingelkurts AA. Short-term EEG spectral pattern as a single event in EEG phenomenology. *Open Neuroimag J*. 2010;4:130-56.

Forrester J. Counterintuitive behavior of social systems. *Technology Review*. 1971;73:52-68.


Fraser AM, Swinney HL. Independent coordinates for strange attractors from mutual information. *Physical Review A*. 1986;33:1134-40.

Freeman WJ. Evidence from human scalp electroencephalograms of global chaotic itinerancy. *Chaos*. 2003;13:1067-77.

Freeman WJ, Skarda CA. Spatial EEG patterns, non-linear dynamics and perception: the neo-Sherringtonian view. *Brain Res*. 1985;357:147-75.

Friston KJ, Tononi G, Sporns O, Edelman GM. Characterising the complexity of neuronal interactions. *Human Brain Mapping*. 1995;3:302-14.

Garcia Dominguez L, Wennberg RA, Gaetz W, Cheyne D, Snead OC, 3rd, Perez Velazquez JL. Enhanced synchrony in epileptiform activity? Local versus distant phase synchronization in generalized seizures. *The Journal of neuroscience : the*

- 
- official journal of the Society for Neuroscience. 2005;25:8077-84.
- Garn H, Waser M, Deistler M, Benke T, Dal-Bianco P, Ransmayr G, et al. Quantitative EEG markers relate to Alzheimer's disease severity in the Prospective Dementia Registry Austria (PRODEM). *Clin Neurophysiol*. 2014.
- Gebber GL, Orer HS, Barman SM. Fractal noises and motions in time series of presympathetic and sympathetic neural activities. *J Neurophysiol*. 2006;95:1176-84.
- Gisiger T. Scale invariance in biology: coincidence or footprint of a universal mechanism? *Biol Rev Camb Philos Soc*. 2001;76:161-209.
- Glass L. Chaos and Heart Rate Variability. *Journal of Cardiovascular Electrophysiology*. 1999;10:1358-60.
- Glass L. Synchronization and rhythmic processes in physiology. *Nature*. 2001;410:277-84.
- Glass L, Guevara MR, Shrier A, Perez R. Bifurcation and chaos in a periodically stimulated cardiac oscillator. *Physica D: Nonlinear Phenomena*. 1983;7:89-101.
- Glass L, Shrier, A., and Bélair. J. . Chaotic cardiac rhythms. In: Holden AV, editor. *Chaos*. Princeton, NJ,: Princeton University Press; 1986.
- Glass LM, M.C. *From Clocks to Chaos: The Rhythms of Life.*: Princeton University Press; 1988.
- Goldberger AL. Fractal variability versus pathologic periodicity: complexity loss and

stereotypy in disease. *Perspect Biol Med.* 1997;40:543-61.

Goldberger AL, Amaral LA, Hausdorff JM, Ivanov P, Peng CK, Stanley HE. Fractal dynamics in physiology: alterations with disease and aging. *Proc Natl Acad Sci U S A.* 2002;99 Suppl 1:2466-72.

Goldberger AL, Rigney DR, West BJ. Chaos and fractals in human physiology. *Sci Am.* 1990;262:42-9.

Govindan RB, Wilson JD, Eswaran H, Lowery CL, Preißl H. Revisiting sample entropy analysis. *Physica A: Statistical Mechanics and its Applications.* 2007;376:158-64.

Grassberger P. Toward a quantitative theory of self-generated complexity. *International journal of theoretical physics.* 1986;25(9):907-38.

Grassberger P, Procaccia I. Measuring the strangeness of strange attractors. *Physica D: Nonlinear Phenomena.* 1983;9:189-208.

Guevara M, Glass L, Shrier A. Phase locking, period-doubling bifurcations, and irregular dynamics in periodically stimulated cardiac cells. *Science.* 1981;214:1350-3.

Gutenberg BaR, C. F. Seismicity of the earth and associated phenomenon. 2nd ed. Princeton: Princeton University Press; 1954.

Guzzetti S, Borroni E, Garbelli PE, Ceriani E, Della Bella P, Montano N, et al. Symbolic dynamics of heart rate variability: a probe to investigate cardiac



autonomic modulation. *Circulation*. 2005;112:465-70.

Hartman ML, Pincus SM, Johnson ML, Matthews DH, Faunt LM, Vance ML, et al.

Enhanced basal and disorderly growth hormone secretion distinguish acromegalic from normal pulsatile growth hormone release. *The Journal of clinical investigation*.

1994;94:1277-88.

He BJ, Raichle ME. The fMRI signal, slow cortical potential and consciousness. *Trends*

Cogn Sci. 2009;13:302-9.

Honey CJ, Sporns O, Cammoun L, Gigandet X, Thiran JP, Meuli R, et al. Predicting

human resting-state functional connectivity from structural connectivity. *Proc Natl*

Acad Sci U S A. 2009;106:2035-40.

Hong LE, Summerfelt A, McMahon R, Adami H, Francis G, Elliott A, et al. Evoked

gamma band synchronization and the liability for schizophrenia. *Schizophrenia*

research. 2004;70:293-302.

Hooper SL. Transduction of temporal patterns by single neurons. *Nat Neurosci*.

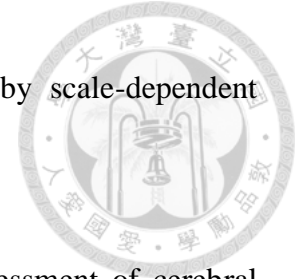
1998;1:720-6.

Hopfield JJ. Neural networks and physical systems with emergent collective

computational abilities. *Proc Natl Acad Sci U S A*. 1982;79:2554-8.

Hopfield JJ. Neurons with graded response have collective computational properties

like those of two-state neurons. *Proc Natl Acad Sci U S A*. 1984;81:3088-92.



Hu J, Gao J, Tung WW. Characterizing heart rate variability by scale-dependent Lyapunov exponent. *Chaos*. 2009;19:028506.

Hu K, Peng CK, Czosnyka M, Zhao P, Novak V. Nonlinear assessment of cerebral autoregulation from spontaneous blood pressure and cerebral blood flow fluctuations. *Cardiovasc Eng*. 2008;8:60-71.

Huang L, Wang Y, Liu J, Wang J. Approximate entropy of EEG as a measure of cerebral ischemic injury. *Conf Proc IEEE Eng Med Biol Soc*. 2004;6:4537-9.

Huang NE, Shen Z, Long SR, Wu MC, Shih HH, Zheng Q, et al. The Empirical Mode Decomposition and the Hilbert Spectrum for Nonlinear and Non-Stationary Time Series Analysis. *Proceedings: Mathematical, Physical and Engineering Sciences*. 1998;454:903-95.

Hudetz AG, Wood JD, Kampine JP. Cholinergic reversal of isoflurane anesthesia in rats as measured by cross-approximate entropy of the electroencephalogram. *Anesthesiology*. 2003;99:1125-31.

Hurst HE. Long term storage capacity of reservoirs *Trans Am Soc Eng*. 1951;116:770-99.

Hurst HE, Black RP, Simaika YM. Long-term storage : an experimental study / by H.E. Hurst, R.P. Black, Y.M. Simaika. London :: Constable; 1965.

Hyotyniemi H. *Neocybernetics in Biological Systems*. Helsinki University of



Technology, Control Engineering Laboratory; 2006.

Ivanov PC, Amaral LA, Goldberger AL, Havlin S, Rosenblum MG, Struzik ZR, et al.

Multifractality in human heartbeat dynamics. *Nature*. 1999;399:461-5.

Jalili M, Barzegharan E, Knyazeva M. inverted question mark Synchronization of EEG:

Bivariate and Multivariate Measures. *IEEE transactions on neural systems and*

rehabilitation engineering : a publication of the IEEE Engineering in Medicine and

Biology Society. 2013.

Jeong J. EEG dynamics in patients with Alzheimer's disease. *Clin Neurophysiol*.

2004;115:1490-505.

Johnson JB. The Schottky Effect in Low Frequency Circuits. *Physical Review*.

1925;26:71-85.

Jordan D, Stockmanns G, Kochs EF, Pilge S, Schneider G. Electroencephalographic

order pattern analysis for the separation of consciousness and unconsciousness: an

analysis of approximate entropy, permutation entropy, recurrence rate, and phase

coupling of order recurrence plots. *Anesthesiology*. 2008;109:1014-22.

Kaffashi F, Foglyano R, Wilson C, Loparo K. The effect of time delay on Approximate

& Sample Entropy calculations. *Physica D: Nonlinear Phenomena*.

2008a;237:3069-74.

Kaffashi F, Foglyano R, Wilson CG, Loparo KA. The effect of time delay on



- Approximate & Sample Entropy calculations. *Physica D: Nonlinear Phenomena*. 2008b;237:3069-74.
- Kanters JK, Holstein-Rathlou NH, Agner E. Lack of evidence for low-dimensional chaos in heart rate variability. *J Cardiovasc Electrophysiol*. 1994;5:591-601.
- Kaplan DT, Glass L. Direct test for determinism in a time series. *Physical Review Letters*. 1992;68:427-30.
- Kauffman S. Differentiation of malignant to benign cells. *Journal of Theoretical Biology*. 1971;31:429-51.
- Kennel MB, Brown R, Abarbanel HD. Determining embedding dimension for phase-space reconstruction using a geometrical construction. *Phys Rev A*. 1992;45:3403-11.
- Keylock CJ. A wavelet-based method for surrogate data generation. *Physica D: Nonlinear Phenomena*. 2007;225:219-28.
- Khadra LM, Maayah TJ, Dickhaus H. Detecting chaos in HRV signals in human cardiac transplant recipients. *Comput Biomed Res*. 1997;30:188-99.
- Kikuchi M, Wada Y, Takeda T, Oe H, Hashimoto T, Koshino Y. EEG harmonic responses to photic stimulation in normal aging and Alzheimer's disease: differences in interhemispheric coherence. *Clin Neurophysiol*. 2002;113:1045-51.
- Kim TK, Sul JY, Peterenko NB, Lee JH, Lee M, Patel VV, et al. Transcriptome transfer



- provides a model for understanding the phenotype of cardiomyocytes. *Proc Natl Acad Sci U S A.* 2011;108:11918-23.
- Kobayashi M, Musha T. 1/f fluctuation of heartbeat period. *IEEE Trans Biomed Eng.* 1982;29:456-7.
- Koch MA, Norris DG, Hund-Georgiadis M. An investigation of functional and anatomical connectivity using magnetic resonance imaging. *Neuroimage.* 2002;16:241-50.
- Koenig T, Prichep L, Dierks T, Hubl D, Wahlund LO, John ER, et al. Decreased EEG synchronization in Alzheimer's disease and mild cognitive impairment. *Neurobiology of Aging.* 2005;26:165-71.
- Korhonen P, Husa T, Konttila T, Tierala I, Makijarvi M, Vaananen H, et al. Complex T-wave morphology in body surface potential mapping in prediction of arrhythmic events in patients with acute myocardial infarction and cardiac dysfunction. *Europace.* 2009;11:514-20.
- Korn H, Faure P. Is there chaos in the brain? II. Experimental evidence and related models. *Comptes rendus biologiques.* 2003;326:787-840.
- Lackner CL, Marshall WJ, Santesso DL, Dywan J, Wade T, Segalowitz SJ. Adolescent anxiety and aggression can be differentially predicted by electrocortical phase reset variables. *Brain and cognition.* 2013.



Lake De Fau - Richman JS, Richman Js Fau - Griffin MP, Griffin Mp Fau - Moorman

JR, Moorman JR. Sample entropy analysis of neonatal heart rate variability. 2002.

Laplace P. Essai Philosophique sur les Probabilités. 1814.

Laskaris NA, Tarnanas I, Tsolaki MN, Vlaikidis N, Karlovasitou AK. Improved detection of amnesic MCI by means of discriminative vector quantization of single-trial cognitive ERP responses. *J Neurosci Methods*. 2013;212:344-54.

Lefebvre JH, Goodings DA. Predictability of normal heart rhythms and deterministic chaos. *Chaos*. 1993;3:267.

Liebovitch LS. *Fractals and chaos simplified for the life sciences*. New York: Oxford University Press; 1998.

Lin PF, Lo MT, Tsao J, Chang YC, Lin C, Ho YL. Correlations between the Signal Complexity of Cerebral and Cardiac Electrical Activity: A Multiscale Entropy Analysis. *PLoS One*. 2014;9:e87798.

Lin PF, Tsao J, Lo MT, Lin C, Chang YC. Symbolic entropy of the amplitude rather than the instantaneous frequency of EEG varies in dementia. *Entropy*. 2015 accepted.

Linkenkaer-Hansen K, Nikouline VV, Palva JM, Ilmoniemi RJ. Long-range temporal correlations and scaling behavior in human brain oscillations. *The Journal of neuroscience : the official journal of the Society for Neuroscience*. 2001;21:1370-7.

Lo M-T, Tsai P-H, Lin P-F, Lin C, Hsin YL. THE NONLINEAR AND



NONSTATIONARY PROPERTIES IN EEG SIGNALS: PROBING THE
COMPLEX FLUCTUATIONS BY HILBERT–HUANG TRANSFORM. *Advances*

in *Adaptive Data Analysis*. 2009;01:461-82.

Lorenz EN. Deterministic nonperiodic flow. *Journal of the Atmospheric Sciences*.

1963;20:130-41.

Lotze M, Flor H, Grodd W, Larbig W, Birbaumer N. Phantom movements and pain. An

fMRI study in upper limb amputees. *Brain*. 2001;124:2268-77.

Lu S, Chen X, Kanters JK, Solomon IC, Chon KH. Automatic selection of the threshold

value R for approximate entropy. *IEEE Trans Biomed Eng*. 2008;55:1966-72.

Lucio JH, Valdes R, Rodriguez LR. Improvements to surrogate data methods for

nonstationary time series. *Phys Rev E Stat Nonlin Soft Matter Phys*.

2012;85:056202.

Mandelbrot BB. *The fractal geometry of nature* / Benoit B. Mandelbrot. New York W.H.

Freeman; 1983.

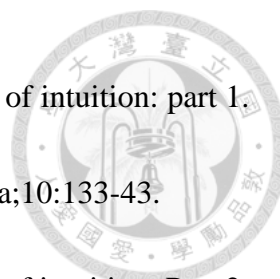
Masterman DL, Cummings JL. Frontal-subcortical circuits: the anatomic basis of

executive, social and motivated behaviors. *J Psychopharmacol*. 1997;11:107-14.

Mayer-Kress G, Yates FE, Benton L, Keidel M, Tirsch W, Pöppel SJ, et al. Dimensional

analysis of nonlinear oscillations in brain, heart, and muscle. *Mathematical*

Biosciences. 1988;90:155-82.



McCraty R, Atkinson M, Bradley RT. Electrophysiological evidence of intuition: part 1.

The surprising role of the heart. *J Altern Complement Med.* 2004a;10:133-43.

McCraty R, Atkinson M, Bradley RT. Electrophysiological evidence of intuition: Part 2.

A system-wide process? *J Altern Complement Med.* 2004b;10:325-36.

McIntosh AR, Kovacevic N, Itier RJ. Increased Brain Signal Variability Accompanies

Lower Behavioral Variability in Development. *PLoS Comput Biol.*

2008;4:e1000106.

McKhann G, Drachman D, Folstein M, Katzman R, Price D, Stadlan EM. Clinical

diagnosis of Alzheimer's disease: report of the NINCDS-ADRDA Work Group

under the auspices of Department of Health and Human Services Task Force on

Alzheimer's Disease. *Neurology.* 1984;34:939-44.

Merli E, Sutcliffe S, Gori M, Sutherland GG. Tako-Tsubo cardiomyopathy: new insights

into the possible underlying pathophysiology. *European journal of*

echocardiography : the journal of the Working Group on Echocardiography of the

European Society of Cardiology. 2006;7:53-61.

Meyer M, Marconi C, Ferretti G, Fiocchi R, Cerretelli P, Skinner JE. Heart rate

variability in the human transplanted heart: nonlinear dynamics and QT vs RR-QT

alterations during exercise suggest a return of neurocardiac regulation in long-term

recovery. *Integr Physiol Behav Sci.* 1996;31:289-305.



Miller JL, Miller JG. Greater than the sum of its parts, I: subsystems which process both matter-energy and information. Behav Sci. 1992;37:1-38.

Monto S, Palva S, Voipio J, Palva JM. Very slow EEG fluctuations predict the dynamics of stimulus detection and oscillation amplitudes in humans. The Journal of neuroscience : the official journal of the Society for Neuroscience. 2008;28:8268-72.

Mossbridge J, Tressoldi P, Utts J. Predictive physiological anticipation preceding seemingly unpredictable stimuli: a meta-analysis. Frontiers in psychology. 2012;3:390.

Mossbridge JA, Tressoldi P, Utts J, Ives JA, Radin D, Jonas WB. Predicting the unpredictable: critical analysis and practical implications of predictive anticipatory activity. Frontiers in human neuroscience. 2014;8:146.

Muqtadar H, Testai FD, Gorelick PB. The dementia of cardiac disease. Current cardiology reports. 2012;14:732-40.

Murakami S, Yamanaka T, Kubo Y, Wada T, Yano S, Nishimura Y, et al. [Heart rate variability analysis and neurobehavioral function in community-dwelling older people aged 75 or older]. Nippon Ronen Igakkai Zasshi. 2002;39:520-6.

Musha TaH, H. . The 1/f Fluctuation of a Traffic Current on an Expressway. Japanese Journal of Applied Physics. 1976;15:1271- 5.



Nakamura T, Small M, Hirata Y. Testing for nonlinearity in irregular fluctuations with long-term trends. *Phys Rev E Stat Nonlin Soft Matter Phys.* 2006;74:026205.

Newman MEJ. Power laws, Pareto distributions and Zipf's law. *Contemporary Physics.* 2005;46:323-51.

Nikulin VV, Brismar T. Long-range temporal correlations in electroencephalographic oscillations: Relation to topography, frequency band, age and gender. *Neuroscience.* 2005;130:549-58.

Nunez P. *Electric fields of the brain: the neurophysics of EEG.* 1st ed. New York: Oxford University Press; 1981.

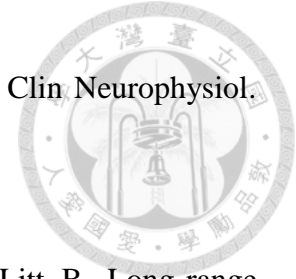
Oppenheimer SM, Gelb A, Girvin JP, Hachinski VC. Cardiovascular effects of human insular cortex stimulation. *Neurology.* 1992;42:1727-32.

Osborne AR, Provenzale A. Finite correlation dimension for stochastic systems with power-law spectra. *Physica D: Nonlinear Phenomena.* 1989;35:357-81.

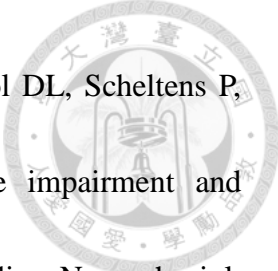
Pakaski M, Kalman J. Interactions between the amyloid and cholinergic mechanisms in Alzheimer's disease. *Neurochem Int.* 2008;53:103-11.

Palmieri A, Calvo V, Kleinbub JR, Meconi F, Marangoni M, Barilaro P, et al. "Reality" of near-death-experience memories: evidence from a psychodynamic and electrophysiological integrated study. *Frontiers in human neuroscience.* 2014;8:429.

Papadelis C, Kourtidou-Papadeli C, Bamidis PD, Maglaveras N, Pappas K. The effect



- of hypobaric hypoxia on multichannel EEG signal complexity. *Clin Neurophysiol.* 2007;118:31-52.
- Parish LM, Worrell GA, Cranstoun SD, Stead SM, Pennell P, Litt B. Long-range temporal correlations in epileptogenic and non-epileptogenic human hippocampus. *Neuroscience.* 2004;125:1069-76.
- Park JH, Kim S, Kim CH, Cichocki A, Kim K. Multiscale entropy analysis of EEG from patients under different pathological conditions. *Fractals.* 2007;15:399-404.
- Paternoster L, Vallverdu M, Melia U, Claria F, Voss A, Caminal P. Analysis of epileptic EEG signals in children by symbolic dynamics. *Conf Proc IEEE Eng Med Biol Soc.* 2013;2013:4362-5.
- Peng CK, Buldyrev SV, Havlin S, Simons M, Stanley HE, Goldberger AL. Mosaic organization of DNA nucleotides. *Phys Rev E Stat Phys Plasmas Fluids Relat Interdiscip Topics.* 1994;49:1685-9.
- Peng CK, Costa M, Goldberger AL. Adaptive data analysis of complex fluctuations in physiologic time series. *Adv Adapt Data Anal.* 2009;1:61-70.
- Perneger TV. What's wrong with Bonferroni adjustments. *BMJ (Clinical research ed).* 1998;316:1236-8.
- Petrillo GA, Glass L. A theory for phase locking of respiration in cats to a mechanical ventilator. *Am J Physiol.* 1984;246:R311-20.



Pijnenburg YA, v d Made Y, van Cappellen van Walsum AM, Knol DL, Scheltens P, Stam CJ. EEG synchronization likelihood in mild cognitive impairment and Alzheimer's disease during a working memory task. *Clin Neurophysiol.* 2004;115:1332-9.

Pincus SM. Approximate entropy as a measure of system complexity. *Proc Natl Acad Sci U S A.* 1991;88:2297-301.

Pincus SM, Gladstone IM, Ehrenkranz RA. A regularity statistic for medical data analysis. *J Clin Monit.* 1991;7:335-45.

Pincus SM, Goldberger AL. Physiological time-series analysis: what does regularity quantify? *Am J Physiol.* 1994;266:H1643-56.

Plochl M, Ossandon JP, Konig P. Combining EEG and eye tracking: identification, characterization, and correction of eye movement artifacts in electroencephalographic data. *Frontiers in human neuroscience.* 2012;6:278.

Poincaré JH. Sur le problème des trois corps et les équations de la dynamique. Divergence des séries de M. Lindstedt. *Acta Mathematica.* 1890;13:1-270.

Poon CS, Merrill CK. Decrease of cardiac chaos in congestive heart failure. *Nature.* 1997;389:492-5.

Porta A, Baselli G, Liberati D, Montano N, Cogliati C, Gneccchi-Ruscione T, et al. Measuring regularity by means of a corrected conditional entropy in sympathetic



outflow. *Biol Cybern.* 1998;78:71-8.

Porta A, Baselli G, Montano N, Gnecci-Ruscione T, Lombardi F, Malliani A, et al.

Classification of coupling patterns among spontaneous rhythms and ventilation in the sympathetic discharge of decerebrate cats. *Biol Cybern.* 1996;75:163-72.

Porta A, Guzzetti S, Montano N, Furlan R, Pagani M, Malliani A, et al. Entropy, entropy

rate, and pattern classification as tools to typify complexity in short heart period variability series. *IEEE Trans Biomed Eng.* 2001;48:1282-91.

Radin D. Unconscious perception of future emotions. *Journal of science exploration* 1997;11:18.

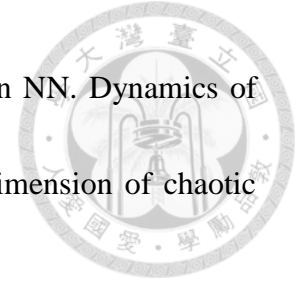
Radin D, Borges A. Intuition through time: what does the seer see? *Explore (NY)*. 2009;5:200-11.

Raichle ME. Neuroscience. The brain's dark energy. *Science.* 2006;314:1249-50.

Rapp PE, Albano AM, Schmah TI, Farwell LA. Filtered noise can mimic low-dimensional chaotic attractors. *Physical Review E.* 1993;47:2289-97.

Rapp PE, Albano AM, Zimmerman ID, Jiménez-Montaña MA. Phase-randomized surrogates can produce spurious identifications of non-random structure. *Physics Letters A.* 1994;192:27-33.

Rapp PE, Latta RA, Mees AI. Parameter-dependent transitions and the optimal control of dynamical diseases. *Bull Math Biol.* 1988;50:227-53.



Rapp PE, Zimmerman ID, Albano AM, Deguzman GC, Greenbaun NN. Dynamics of spontaneous neural activity in the simian motor cortex: The dimension of chaotic neurons. *Physics Letters A*. 1985;110:335-8.

Ribeiro AS, Kauffman SA. Noisy attractors and ergodic sets in models of gene regulatory networks. *Journal of Theoretical Biology*. 2007;247:743-55.

Richman JS, Moorman JR. Physiological time-series analysis using approximate entropy and sample entropy. *Am J Physiol Heart Circ Physiol*. 2000;278:H2039-49.

Riley MA, Balasubramaniam R, Turvey MT. Recurrence quantification analysis of postural fluctuations. *Gait Posture*. 1999;9:65-78.

Riley MA, Turvey MT. Variability of determinism in motor behavior. *J Mot Behav*. 2002;34:99-125.

Roman GC, Tatemichi TK, Erkinjuntti T, Cummings JL, Masdeu JC, Garcia JH, et al. Vascular dementia: diagnostic criteria for research studies. Report of the NINDS-AIREN International Workshop. *Neurology*. 1993;43:250-60.

Rovelli C. Relational quantum mechanics. *Int J Theor Phys*. 1996;35:1637-78.

Safieddine D, Kachenoura A, Albera L, Birot G, Karfoul A, Pasnicu A, et al. Removal of muscle artifact from EEG data: comparison between stochastic (ICA and CCA) and deterministic (EMD and wavelet-based) approaches. *EURASIP J Adv Signal Process*. 2012;2012:1-15.

Samuels MA. The brain-heart connection. *Circulation*. 2007;116:77-84.

Sassi R, Signorini MG, Cerutti S. Multifractality and heart rate variability. *Chaos*. 2009;19:028507.

Sauer T, Yorke, J A and Casdagli, M Embedology. *J Stat Phys*. 1991;65:579–616.

Schick KL, Verveen AA. 1/f noise with a low frequency white noise limit. *Nature*. 1974;251:599-601.

Schindler K, Gast H, Goodfellow M, Rummel C. On seeing the trees and the forest: single-signal and multisignal analysis of periictal intracranial EEG. *Epilepsia*. 2012;53:1658-68.

Schrödinger E. *What is Life – the Physical Aspect of the Living Cell*. : Cambridge University Press. ; 1944.

Schreiber T, Schmitz A. Improved Surrogate Data for Nonlinearity Tests. *Phys Rev Lett*. 1996;77:635-8.

Schreiber T, Schmitz A. Surrogate time series. *Physica D: Nonlinear Phenomena*. 2000;142:346-82.

Scorza FA, Calderazzo L, de Albuquerque M, Arida RM, de Almeida AC, Cavalheiro EA. Could sudden cardiac death in epilepsy be related to the occurrence of thalamic dysfunction or anatomic change? *Arq Neuropsiquiatr*. 2009;67:139-43.

Segel LA. Multiple attractors in immunology: theory and experiment. *Biophys Chem*.



1998;72:223-30.

Selig FA, Tonolli ER, Silva EV, Godoy MF. Heart rate variability in preterm and term neonates. *Arq Bras Cardiol.* 2011;96:443-9.

Senge P. *The Fifth Discipline: The Art and Practice of the Learning Organization.* 1990.

Shannon C. *A Mathematical Theory of Communication.* Bell System Technical Journal. 1948;27:379-423.

Shelhamer M. *nonlinear dynamics in physiology, a state-space approach: world scientific publishing Co. Pte.Ltd.; 2007.*

Sinnreich R, Kark J, Friedlander Y, Sapoznikov D, Luria M. Five minute recordings of heart rate variability for population studies: repeatability and age-sex characteristics. *Heart.* 1998;80:156-62.

Skarda CAaFWJ, , pp *How brains make chaos in order to make sense of the world. . Behavioral and Brain Sciences.* 1987;10:161-73.

Skinner J, Molnar M, Vybiral T, Mitra M. Application of chaos theory to biology and medicine. 1992:39-53.

Skinner JE, Pratt CM, Vybiral T. A reduction in the correlation dimension of heartbeat intervals precedes imminent ventricular fibrillation in human subjects. *Am Heart J.* 1993;125:731-43.

Snooks GD. *A general theory of complex living systems: Exploring the demand side of*



- dynamics. *Complex*. 2008;13:12-20.
- Spyer KM. Neural mechanisms involved in cardiovascular control during affective behaviour. *Trends Neurosci*. 1989;12:506-13.
- Stam CJ. Nonlinear dynamical analysis of EEG and MEG: review of an emerging field. *Clin Neurophysiol*. 2005;116:2266-301.
- Stam CJ, van der Made Y, Pijnenburg YA, Scheltens P. EEG synchronization in mild cognitive impairment and Alzheimer's disease. *Acta neurologica Scandinavica*. 2003;108:90-6.
- Staniek M, Lehnertz K. Symbolic transfer entropy. *Phys Rev Lett*. 2008;100:158101.
- Staniek M, Lehnertz K. Symbolic transfer entropy: inferring directionality in biosignals. *Biomedizinische Technik Biomedical engineering*. 2009;54:323-8.
- Steriade M, Nunez A, Amzica F. A novel slow (< 1 Hz) oscillation of neocortical neurons in vivo: depolarizing and hyperpolarizing components. *The Journal of neuroscience : the official journal of the Society for Neuroscience*. 1993;13:3252-65.
- Stevenson NJ, Korotchikova I, Boylan GB. An estimate of newborn EEG amplitude with limited frequency content. *Information Sciences Signal Processing and their Applications (ISSPA), 2010 10th International Conference 2010*. p. 288-91.
- Stollberger C, Finsterer J. Cardiorespiratory findings in sudden unexplained/unexpected



death in epilepsy (SUDEP). *Epilepsy Res.* 2004;59:51-60.

Suzuki M, Odaka, T. , Kosugi, Y., Ikebe, J., Matsuoka, K., and Takakura, K., .

Frequency fluctuation of human EEG and quantitative analysis of relief of pain. *Rep*

Tech Res Group IECE Japan. 1980;vol. MBE 80-59:33-40.

Takahashi T, Cho RY, Mizuno T, Kikuchi M, Murata T, Takahashi K, et al.

Antipsychotics reverse abnormal EEG complexity in drug-naive schizophrenia: A

multiscale entropy analysis. *Neuroimage.* 2010.

Takahashi T, Cho RY, Murata T, Mizuno T, Kikuchi M, Mizukami K, et al. Age-related

variation in EEG complexity to photic stimulation: a multiscale entropy analysis.

Clin Neurophysiol. 2009;120:476-83.

Tang XZ, Tracy ER, Boozer AD, deBrauw A, Brown R. Symbol sequence statistics in

noisy chaotic signal reconstruction. *Phys Rev E Stat Phys Plasmas Fluids Relat*

Interdiscip Topics. 1995;51:3871-89.

Thaler DS. Design for an aging brain. *Neurobiology of Aging.* 2002;23:13-5.

Thayer JF, Lane RD. Claude Bernard and the heart-brain connection: further elaboration

of a model of neurovisceral integration. *Neurosci Biobehav Rev.* 2009;33:81-8.

Theiler J, Eubank S, Longtin A, Galdrikian B, Doynne Farmer J. Testing for nonlinearity

in time series: the method of surrogate data. *Physica D: Nonlinear Phenomena.*

1992;58:77-94.



Thuraisingham RG, G. On multiscale entropy analysis for physiological data. . Physica

A: Statistical Mechanics and its Applications. 2006; 366:323-32

Tsai PH, Lin C, Tsao J, Lin PF, Wang PC, Huang NE, et al. Empirical mode

decomposition based detrended sample entropy in electroencephalography for

Alzheimer's disease. J Neurosci Methods. 2012;210:230-7.

Turcotte DL. Fractals and Chaos in Geology and Geophysics. 2nd ed. Cambridge:

Cambridge University Press; 1997.

van den Berg G, Pincus SM, Veldhuis JD, Frolich M, Roelfsema F. Greater

disorderliness of ACTH and cortisol release accompanies pituitary-dependent

Cushing's disease. European journal of endocrinology / European Federation of

Endocrine Societies. 1997;136:394-400.

van Straaten EC, den Haan J, de Waal H, van der Flier WM, Barkhof F, Prins ND, et al.

Disturbed phase relations in white matter hyperintensity based vascular dementia:

An EEG directed connectivity study. Clin Neurophysiol. 2014.

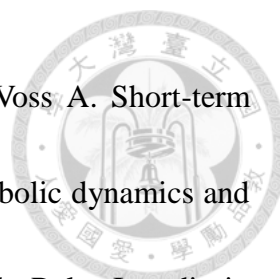
Vecchio F, Babiloni C, Lizio R, Fallani Fde V, Blinowska K, Verrienti G, et al. Resting

state cortical EEG rhythms in Alzheimer's disease: toward EEG markers for clinical

applications: a review. Supplements to Clinical neurophysiology. 2013;62:223-36.

Verveen AAaD, H. E. Fluctuations in membrane potential of axons and the problem of

coding. Kybernetik. 1965;2:152-60.



Wessel N, Ziehmann C, Kurths J, Meyerfeldt U, Schirdewan A, Voss A. Short-term forecasting of life-threatening cardiac arrhythmias based on symbolic dynamics and finite-time growth rates. *Phys Rev E Stat Phys Plasmas Fluids Relat Interdiscip Topics*. 2000;61:733-9.

Wolf A, Swift J, Swinney H. Determining Lyapunov exponents form a time series. *Phys D*. 1985;16:285-317.

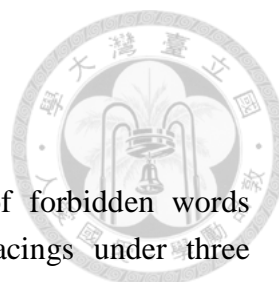
Xu N, Xu JH. The fractal dimension of EEG as a physical measure of conscious human brain activities. *Bull Math Biol*. 1988;50:559-65.

Yang AC, Wang SJ, Lai KL, Tsai CF, Yang CH, Hwang JP, et al. Cognitive and neuropsychiatric correlates of EEG dynamic complexity in patients with Alzheimer's disease. *Progress in neuro-psychopharmacology & biological psychiatry*. 2013;47:52-61.

Yum MK, Jung KY, Kang HC, Kim HD, Shon YM, Kang JK, et al. Effect of a ketogenic diet on EEG: analysis of sample entropy. *Seizure*. 2008;17:561-6.

Zhang D, Raichle ME. Disease and the brain's dark energy. *Nature reviews Neurology*. 2010;6:15-28.

Zhao Y, Hong W. Symbolic dynamics analysis of epileptic EEG signals of the rat. *Shengwu yixue gongcheng xue za zhi = Journal of biomedical engineering = Shengwuyixue gongchengxue zazhi*. 2012;29:760-3.



Tables

Table 1. The sample entropy (SampEn, $m = 2$) and number of forbidden words (NumFW) values (mean \pm SD) of the filtered EEG whole tracings under three conditions (wakeful resting, slow photic stimulation, and fast photic stimulation). In post-hoc analyses one-way multivariate analysis of variance (MANOVA), I used Tukey's Honestly Significant Difference (HSD) test to correct for multiple comparisons of 19 electrode sites in three conditions. And the Tukey's p values were further adjusted by Bonferroni corrections for five methods. (* corrected $p < 0.05$, ** corrected $p < 0.01$, CON: control, AD: Alzheimer's disease, VD: vascular dementia)

EEG sites	wakeful resting		Slow Photic Stimulation		Fast Photic Stimulation	
	SampEn	NumFW	SampEn	NumFW	SampEn	NumFW
	CON (mean \pm SD)	CON (mean \pm SD)	CON (mean \pm SD)	CON (mean \pm SD)	CON (mean \pm SD)	CON (mean \pm SD)
	AD (mean \pm SD)	AD (mean \pm SD)	AD (mean \pm SD)	AD (mean \pm SD)	AD (mean \pm SD)	AD (mean \pm SD)
	VD (mean \pm SD)	VD (mean \pm SD)	VD (mean \pm SD)	VD (mean \pm SD)	VD (mean \pm SD)	VD (mean \pm SD)
Fp2	0.430 \pm 0.27	159.1 \pm 23*	0.616 \pm 0.31	139.6 \pm 32	0.604 \pm 0.32	140.2 \pm 28
	0.570 \pm 0.24	151.6 \pm 26	0.720 \pm 0.28	134.0 \pm 37	0.689 \pm 0.22	143.6 \pm 28
	0.620 \pm 0.32	136.9 \pm 32*	0.768 \pm 0.34	116.9 \pm 44	0.768 \pm 0.33	119.4 \pm 45
F4	0.722 \pm 0.28	123.7 \pm 29*	0.823 \pm 0.27	112.0 \pm 33	0.834 \pm 0.24	111.3 \pm 32*
	0.773 \pm 0.21	122.2 \pm 27	0.872 \pm 0.15	107.5 \pm 24	0.812 \pm 0.15	118.7 \pm 31**
	0.872 \pm 0.26	97.7 \pm 37*	0.987 \pm 0.27	86.0 \pm 42	0.993 \pm 0.29	82.5 \pm 42**
F8	0.633 \pm 0.27	135.5 \pm 33**	0.781 \pm 0.29	113.8 \pm 36	0.773 \pm 0.29	116.9 \pm 32*
	0.705 \pm 0.23	126.7 \pm 29*	0.810 \pm 0.22	115.6 \pm 34	0.781 \pm 0.19	113.9 \pm 33
	0.831 \pm 0.27	98.4 \pm 37**	0.888 \pm 0.29	91.7 \pm 40	0.933 \pm 0.24	86.2 \pm 39*
C4	0.740 \pm 0.31**	115.3 \pm 37**	0.902 \pm 0.22*	100.6 \pm 32*	0.864 \pm 0.26	105.9 \pm 32**
	0.851 \pm 0.13	109.7 \pm 30**	0.891 \pm 0.14	108.2 \pm 23**	0.830 \pm 0.24	111.0 \pm 31**
	0.998 \pm 0.19**	77.1 \pm 31**	1.002 \pm 0.32	72.0 \pm 45**	1.045 \pm 0.25	72.7 \pm 43**
T4	0.849 \pm 0.23	104.9 \pm 34**	0.740 \pm 0.31	115.3 \pm 37*	0.858 \pm 0.26	102.0 \pm 35*
	0.805 \pm 0.16	107.9 \pm 27**	0.851 \pm 0.13	109.7 \pm 30	0.788 \pm 0.18**	108.3 \pm 39**
	0.977 \pm 0.24	73.2 \pm 32**	0.998 \pm 0.19	77.1 \pm 31*	1.021 \pm 0.24**	70.3 \pm 42**
P4	0.820 \pm 0.25*	112.4 \pm 33**	0.903 \pm 0.18	98.6 \pm 22	0.871 \pm 0.22*	101.6 \pm 27*
	0.818 \pm 0.15	117.1 \pm 23**	0.862 \pm 0.17	104.4 \pm 30	0.839 \pm 0.22*	105.6 \pm 32*
	0.991 \pm 0.20*	79.6 \pm 33**	0.999 \pm 0.30	77.5 \pm 45	1.044 \pm 0.23*	74.8 \pm 41*
T6	0.818 \pm 0.24*	108.1 \pm 31**	0.857 \pm 0.23	104.7 \pm 30*	0.857 \pm 0.24*	100.8 \pm 32**
	0.807 \pm 0.19	111.3 \pm 27**	0.794 \pm 0.23*	106.3 \pm 31*	0.809 \pm 0.24*	117.5 \pm 35**
	1.010 \pm 0.21*	74.1 \pm 31**	1.011 \pm 0.29*	74.6 \pm 44*	1.048 \pm 0.26*	67.8 \pm 39**

O2	0.827±0.23	108.9±30**	0.857±0.20	115.3±37	0.864±0.21*	101.2±28**
	0.810±0.16	115.0±24**	0.817±0.23	109.7±30	0.838±0.21**	108.6±31**
	0.986±0.22	80.7±32**	0.988±0.32	77.1±31	1.051±0.23**	72.0±38**
Fp1	0.416±0.23	165.3±18*	0.554±0.30	147.0±29	0.540±0.27	151.2±25**
	0.458±0.283	157.8±26	0.736±0.27	131.1±38	0.657±0.23	141.9±28
	0.589±0.34	142.4±37*	0.762±0.33	122.5±43	0.763±0.36	119.2±42**
F3	0.702±0.25	131.8±27*	0.789±0.30	116.0±35	0.770±0.31*	119.6±35*
	0.738±0.25	124.3±33	0.845±0.23	113.3±37	0.822±0.24	112.7±33
	0.820±0.29	103.8±35*	0.951±0.28	87.5±43	0.973±0.25*	87.2±42*
F7	0.589±0.26	137.1±27*	0.664±0.24*	130.9±32**	0.661±0.30*	126.3±36*
	0.679±0.28	129.0±33	0.767±0.23	117.5±34	0.750±0.24	119.0±38
	0.771±0.29	112.0±37*	0.881±0.31*	95.5±46**	0.898±0.29*	94.7±45*
C3	0.766±0.29	116.7±33*	0.850±0.20	109.3±26**	0.821±0.25*	112.3±33**
	0.837±0.25	109.7±34	0.874±0.22	103.9±34*	0.900±0.18	106.7±33*
	0.932±0.28	86.9±38*	1.008±0.27	73.3±40**	1.022±0.24*	74.9±39**
T3	0.784±0.28	109.4±36	0.828±0.26	105.3±36**	0.802±0.27**	107.4±37**
	0.834±0.24	106.7±35	0.919±0.20	99.0±30*	0.889±0.21	104.2±33**
	0.933±0.27	83.0±39	0.998±0.30	67.9±42**	1.025±0.25**	67.3±39**
P3	0.746±0.27	122.4±30**	0.770±0.23*	117.8±29**	0.830±0.22*	108.8±31**
	0.856±0.22	108.8±33	0.894±0.17	103.7±29	0.887±0.19	106.7±33**
	0.933±0.26	87.4±35**	0.973±0.28*	79.0±41**	1.026±0.24*	72.3±39**
T5	0.787±0.25	110.7±37	0.747±0.20**	113.8±24**	0.777±0.26*	107.1±35**
	0.806±0.20	117.0±33*	0.906±0.14	102.7±26**	0.855±0.25	105.8±31**
	0.887±0.26	86.9±37*	0.968±0.29**	70.7±41**	0.996±0.26*	71.1±38**
O1	0.777±0.25	117.4±31	0.784±0.23	112.0±29**	0.785±0.22	114.3±31**
	0.823±0.23	113.0±31	0.841±0.20	110.3±28*	0.871±0.22	105.2±31*
	0.905±0.30	94.1±33	0.972±0.27	80.5±38**	1.018±0.26	75.4±38**
Fz	0.655±0.31*	137.7±28**	0.839±0.23	117.1±28	0.818±0.25	118.5±34*
	0.725±0.18	132.1±25*	0.854±0.14	118.4±19	0.805±0.19	123.8±24**
	0.865±0.26*	106.7±34.5**	0.945±0.32	94.5±43	1.000±0.31	87.2±44**
Cz	0.790±0.26*	120.1±30**	0.901±0.18	104.3±28	0.879±0.21	107.4±28*
	0.855±0.15	113.8±25	0.882±0.12	110.1±19*	0.842±0.20*	115.5±30**
	0.974±0.23*	91.2±35**	0.997±0.32	82.2±41*	1.042±0.29*	79.0±42**
Pz	0.788±0.24**	117.3±35**	0.840±0.22	109.2±28**	0.827±0.25**	110.4±30**
	0.833±0.16	117.0±24**	0.853±0.16	112.3±26**	0.872±0.16	112.2±30**
	1.004±0.23**	82.5±35**	1.008±0.31	77.3±43**	1.053±0.28**	73.7±41**

Table 2. The sample entropy (SampEn, $m = 2$) and number of forbidden words (NumFW) values (mean \pm SD) of the local peak voltage sequences of the filtered EEG under three conditions (wakeful resting, slow photic stimulation, and fast photic stimulation). In post-hoc analyses of one-way multivariate analysis of variance (MANOVA), I used Tukey's Honestly Significant Difference (HSD) test to correct for multiple comparisons of 19 electrode sites in three conditions. And the Tukey's p values were further adjusted by Bonferroni corrections for two methods and four sequences (by multiplication with eight). (* corrected $p < 0.05$, ** corrected $p < 0.01$, CON: control, AD: Alzheimer's disease, VD: vascular dementia)

EEG sites	wakeful resting		Slow Photic Stimulation		Fast Photic Stimulation	
	SampEn	NumFW	SampEn	NumFW	SampEn	NumFW
	CON (mean \pm SD)	CON (mean \pm SD)	CON (mean \pm SD)	CON (mean \pm SD)	CON (mean \pm SD)	CON (mean \pm SD)
	AD (mean \pm SD)	AD (mean \pm SD)	AD (mean \pm SD)	AD (mean \pm SD)	AD (mean \pm SD)	AD (mean \pm SD)
	VD (mean \pm SD)	VD (mean \pm SD)	VD (mean \pm SD)	VD (mean \pm SD)	VD (mean \pm SD)	VD (mean \pm SD)
Fp2	0.391 \pm 0.25	162.1 \pm 24*	0.574 \pm 0.28	148.2 \pm 22**	0.543 \pm 0.28	146.2 \pm 22
	0.519 \pm 0.26	155.0 \pm 25	0.659 \pm 0.27	143.1 \pm 25	0.611 \pm 0.26	150.5 \pm 25
	0.587 \pm 0.34	139.0 \pm 30*	0.736 \pm 0.33	123.6 \pm 30**	0.731 \pm 0.31	127.9 \pm 34
F4	0.680 \pm 0.27	136.2 \pm 26	0.823 \pm 0.21	124.3 \pm 24	0.817 \pm 0.24	124.8 \pm 26*
	0.813 \pm 0.23	125.8 \pm 31	0.903 \pm 0.18	120.7 \pm 28	0.867 \pm 0.24	123.1 \pm 23
	0.874 \pm 0.25	115.8 \pm 31	0.957 \pm 0.27	102.6 \pm 34	0.970 \pm 0.24	101.4 \pm 34*
F8	0.651 \pm 0.26	141.8 \pm 28	0.805 \pm 0.22	127.8 \pm 26	0.784 \pm 0.26	129.1 \pm 30
	0.751 \pm 0.21	138.6 \pm 26	0.828 \pm 0.21	128.8 \pm 31	0.822 \pm 0.22	130.6 \pm 31
	0.831 \pm 0.25	122.2 \pm 26	0.887 \pm 0.27	111.6 \pm 31	0.928 \pm 0.21	108.1 \pm 28
C4	0.795 \pm 0.29**	125.7 \pm 32*	0.926 \pm 0.16	115.6 \pm 23*	0.874 \pm 0.22*	119.5 \pm 25**
	0.912 \pm 0.19	118.2 \pm 29	0.929 \pm 0.17	115.6 \pm 23	0.887 \pm 0.25	118.8 \pm 35**
	1.015 \pm 0.18**	101.5 \pm 28*	1.025 \pm 0.26	92.2 \pm 34*	1.064 \pm 0.20*	88.2 \pm 30**
T4	0.798 \pm 0.21*	132.8 \pm 27	0.851 \pm 0.20	128.5 \pm 29	0.841 \pm 0.18	130.2 \pm 27*
	0.809 \pm 0.21	129.9 \pm 29	0.861 \pm 0.18	124.5 \pm 28	0.780 \pm 0.27*	129.7 \pm 32
	0.960 \pm 0.18*	113.3 \pm 27	0.946 \pm 0.27	110.2 \pm 31	0.977 \pm 0.20*	107.1 \pm 28*
P4	0.872 \pm 0.23**	118.8 \pm 31*	0.974 \pm 0.15	107.5 \pm 23	0.944 \pm 0.17	109.2 \pm 25
	0.881 \pm 0.27	119.6 \pm 33	0.946 \pm 0.18	115.3 \pm 24*	0.936 \pm 0.24	114.7 \pm 34*
	1.064 \pm 0.17**	95.1 \pm 28*	1.051 \pm 0.26	91.0 \pm 34*	1.072 \pm 0.22	88.8 \pm 31*
T6	0.876 \pm 0.26	115.5 \pm 32	0.914 \pm 0.20	114.5 \pm 29	0.899 \pm 0.21	117.9 \pm 26
	0.884 \pm 0.24	119.5 \pm 27	0.892 \pm 0.25	119.6 \pm 32	0.915 \pm 0.23	116.5 \pm 34
	1.001 \pm 0.21	105.8 \pm 29	1.004 \pm 0.31	97.9 \pm 35	1.0343 \pm 0.24	94.6 \pm 35
O2	0.894 \pm 0.22	117.0 \pm 30	0.935 \pm 0.12	112.9 \pm 19	0.948 \pm 0.16	112.0 \pm 24*
	0.906 \pm 0.18	120.4 \pm 28*	0.916 \pm 0.17	118.0 \pm 26	0.944 \pm 0.17	115.6 \pm 26*

	1.041±0.18	95.5±30*	1.029±0.28	94.6±37	1.080±0.20	88.9±32*
Fp1	0.386±0.21	161.8±22*	0.536±0.28	151.0±21**	0.543±0.28	146.2±22
	0.469±0.28	157.4±26	0.710±0.25	140.7±27	0.611±0.26	150.5±25
	0.577±0.36	138.0±34*	0.734±0.34	123.5±35**	0.731±0.31	127.9±34
F3	0.708±0.23	136.0±26*	0.801±0.25*	126.0±29**	0.781±0.31*	125.5±34**
	0.800±0.24	128.4±27	0.925±0.24	114.8±38	0.907±0.18	115.7±30
	0.885±0.27	110.3±32*	1.007±0.27*	91.6±34**	1.005±0.25*	95.6±32**
F7	0.610±0.27	144.6±25	0.711±0.24	137.9±28*	0.705±0.29	134.3±33
	0.733±0.25	137.4±25	0.802±0.25	130.7±30	0.811±0.26	130.2±29
	0.786±0.30	124.0±33	0.906±0.29	109.9±37*	0.895±0.29	112.0±35
C3	0.820±0.30	121.1±32	0.910±0.20	119.1±23**	0.914±0.26	114.3±32*
	0.922±0.27	121.1±32	0.977±0.22	101.7±31	0.958±0.15	113.3±30
	1.002±0.22	100.6±29	1.051±0.25	85.5±35**	1.062±0.25	85.9±34*
T3	0.800±0.28	121.1±32	0.845±0.27	120.0±30	0.801±0.29	128.3±30*
	0.843±0.25	121.1±32	0.905±0.25	117.9±33	0.911±0.25	116.4±30
	0.937±0.26	100.6±29	0.992±0.30	96.3±32	0.994±0.27	103.5±31*
P3	0.887±0.26	120.0±36	0.843±0.23*	124.6±27**	0.920±0.23	114.3±31**
	0.928±0.19	114.8±28	0.984±0.17	104.8±28	0.983±0.16	106.3±31
	1.027±0.21	96.9±27	1.055±0.29*	88.6±35**	1.087±0.24	83.5±35**
T5	0.880±0.23	119.1±27	0.838±0.24*	121.2±28**	0.886±0.27	116.5±31*
	0.927±0.21	114.8±35	0.954±0.19	113.5±32	0.950±0.27	112.3±35
	0.968±0.24	103.2±30	1.041±0.29*	89.9±33**	1.054±0.26	90.1±31*
O1	0.874±0.23	120.7±30*	0.887±0.23	112.2±27*	0.878±0.24*	117.8±30**
	0.935±0.25	110.1±31	0.948±0.20	109.5±32	0.997±0.18	103.7±31
	1.007±0.23	96.2±30*	1.064±0.25	87.1±33*	1.075±0.26*	86.7±33**
Fz	0.662±0.26**	138.4±24**	0.848±0.18	119.6±20*	0.855±0.22	117.6±32*
	0.770±0.19	129.1±22	0.901±0.16	118.4±25	0.890±0.17	117.5±28*
	0.883±0.25**	111.8±31**	0.966±0.30	94.4±35*	1.027±0.27	87.6±38*
Cz	0.863±0.22**	121.9±29*	0.952±0.18	106.6±21	0.929±0.19	110.7±25*
	0.936±0.15	113.2±21	0.991±0.10	104.9±23	0.940±0.19	113.5±32*
	1.026±0.18**	97.9±29*	1.040±0.29	86.8±33	1.083±0.25	84.8±33*
Pz	0.854±0.24**	122.6±31**	0.908±0.19	113.5±23**	0.918±0.23*	111.3±29*
	0.921±0.17	117.2±26	0.957±0.17	107.9±29	0.962±0.19	108.9±32
	1.069±0.15**	89.8±26**	1.052±0.30	83.6±37**	1.089±0.22*	84.6±34*

Figures



Figure 1 Electrocardiography (ECG) and electroencephalography (EEG). One cycle of ECG includes various deflections, P, Q, R, S (QRS complex) and T. All R peaks of ECG recordings were detected to obtain the RR interval (RRI) time series. Each EEG recording includes brain waves from 19 electrode sites, one ECG recording and one trace of photic stimulation (PS).

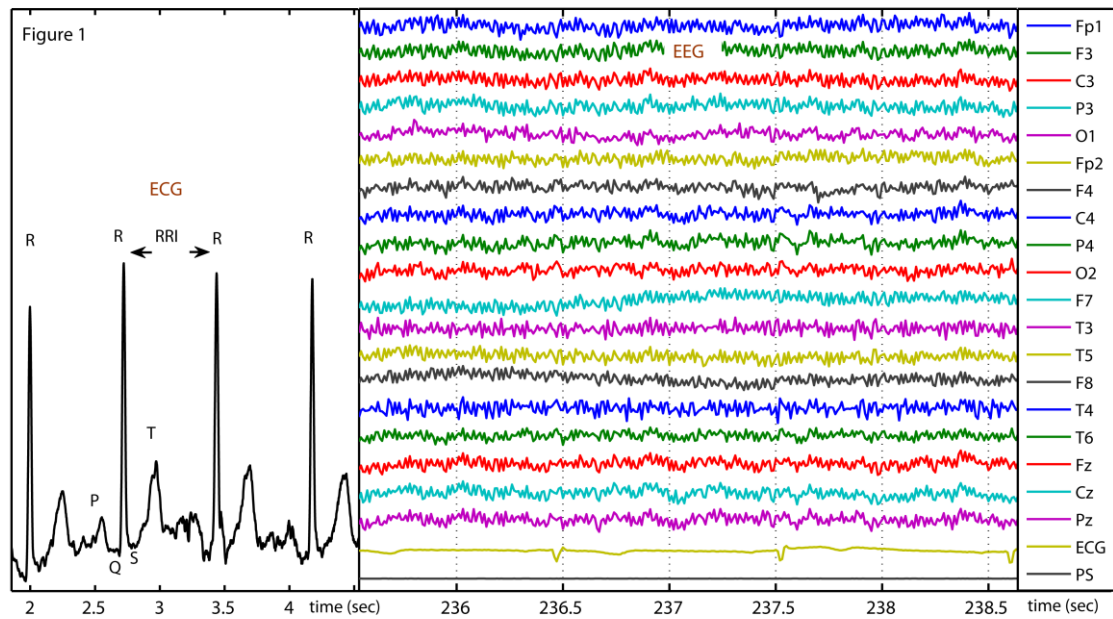


Figure 2 (a) Local peaks of a filtered EEG were detected according to the empirical mode decomposition (EMD) method to make two sequences of the local-peak voltage and interpeak interval. (b) Natural cubic splines were applied to the local maximal and local minimal points respectively according to the sifting procedure of the EMD. The upper and lower EEG envelopes were formed from the maximal points and minimal points, respectively. (c) The EEG excursion amplitude (AMPeeg) was defined as the difference between the upper and lower envelopes. The local peaks of the AMPeeg were again detected to form another two sequences of the local-peak voltage and interpeak interval. (d) Any normalized sequence formed from (a) and (c) was uniformly spread on 6 levels (from 0 to 5) and transformed into a series of symbols from the limited alphabet of symbols $\{0,1,\dots,5\}$.

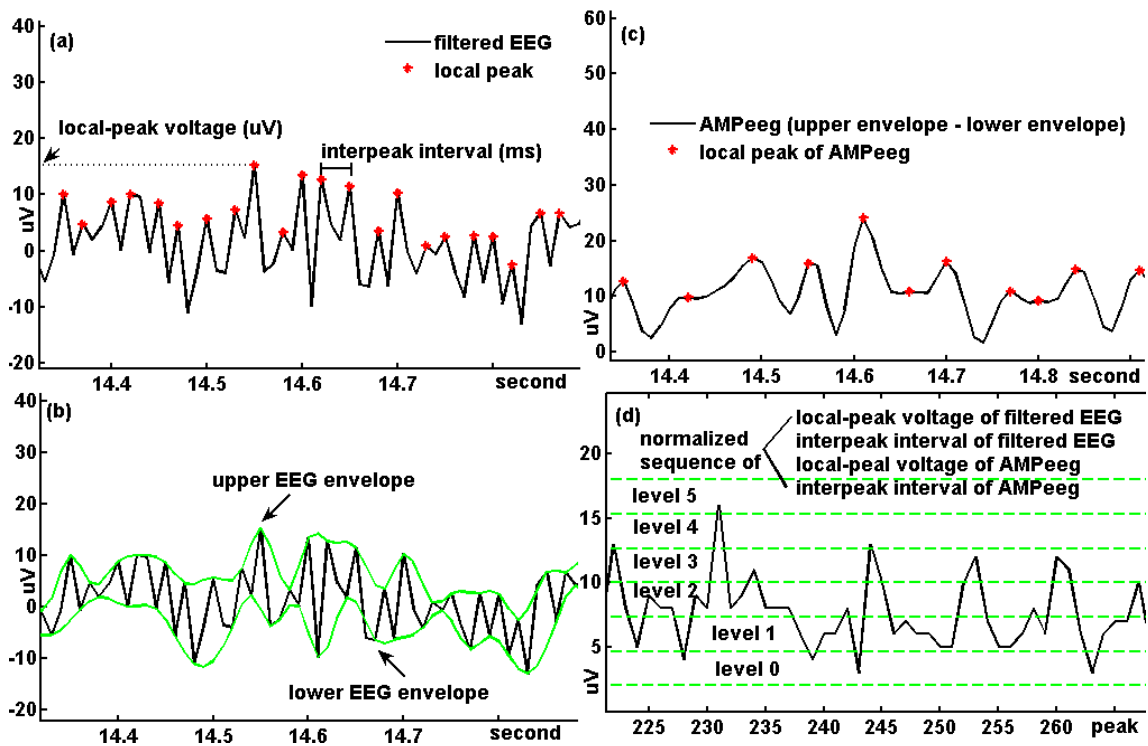


Figure 3 (a) The R-peak detection was performed by an automated arrhythmia detection algorithm and corrected by visual inspection. (b) The normalized RRI series was uniformly spread on 6 levels (from 0 to 5) and transformed into a series of symbols from the limited alphabet of symbols $\{0,1,\dots, 5\}$. (c) From a symbolic sequence, patterns of three delayed samples were constructed. The overlapping triplet symbols of the constructed pattern were codified in decimal format.

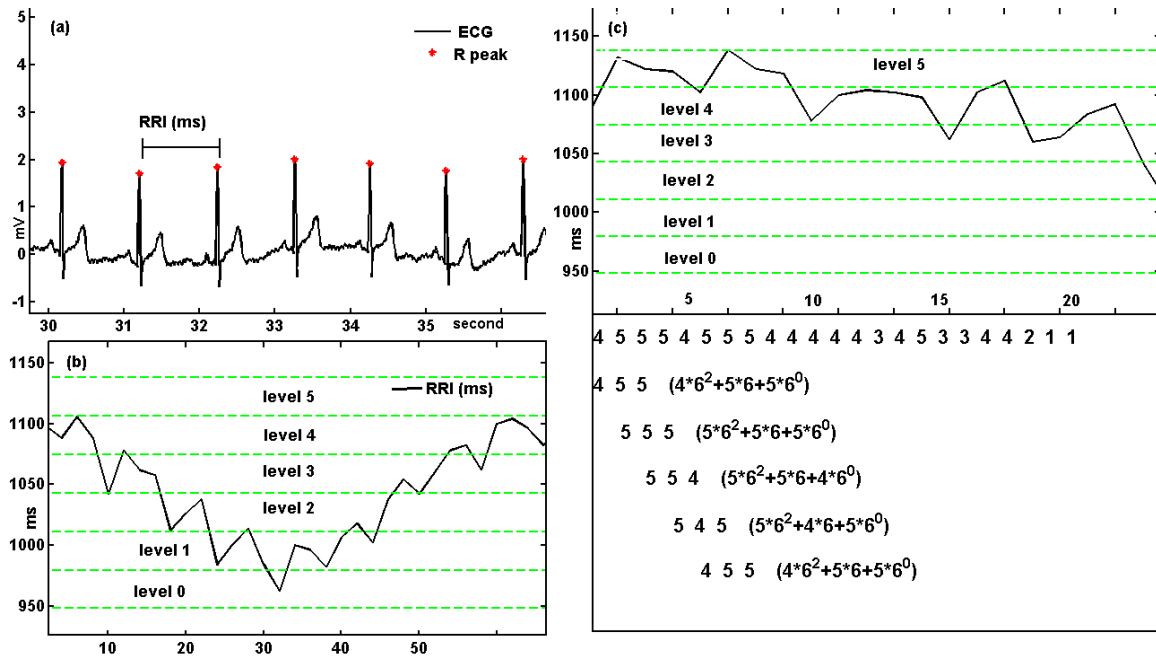


Figure 4 Examples of RR interval (RRI), detrended EEG and the multiscale entropy (MSE) profiles of them. One RRI time series and one detrended EEG signal are shown on the left-hand side of the figure. MSE-RRI 1-3 are examples of the MSE profiles showing the MSE values of RRI from scale 1 to scale 20, while MSE-EEG 1-3 are examples of the MSE profiles showing the MSE values of EEG from scale 1 to scale 20. All the MSE-profiles show an initial increasing before a plateau or a fall.

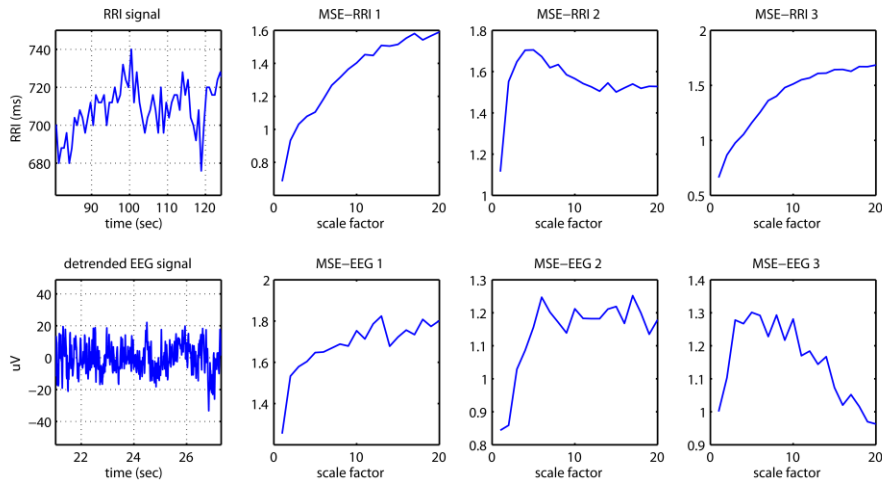


Figure 5 Inverse association between the multiscale entropy (MSE) values of the wakeful RRI and wakeful resting EEG. (a) Regions with significant inverse correlation between the summed MSE values on the scales 11-20 of the wakeful RRI and the summed MSE values on the scales 6-20 of the wakeful resting EEG after Bonferroni corrections (corrected p -values = original p -values * 19, alpha = 0.05). r and p denote the Pearson's partial correlation coefficient and corrected significance level, respectively. (b) The brain map illustrates regions with significant association. The relative brightness is according to the sequential p -values from the smallest one (Fp2, C4, T6 and T4).

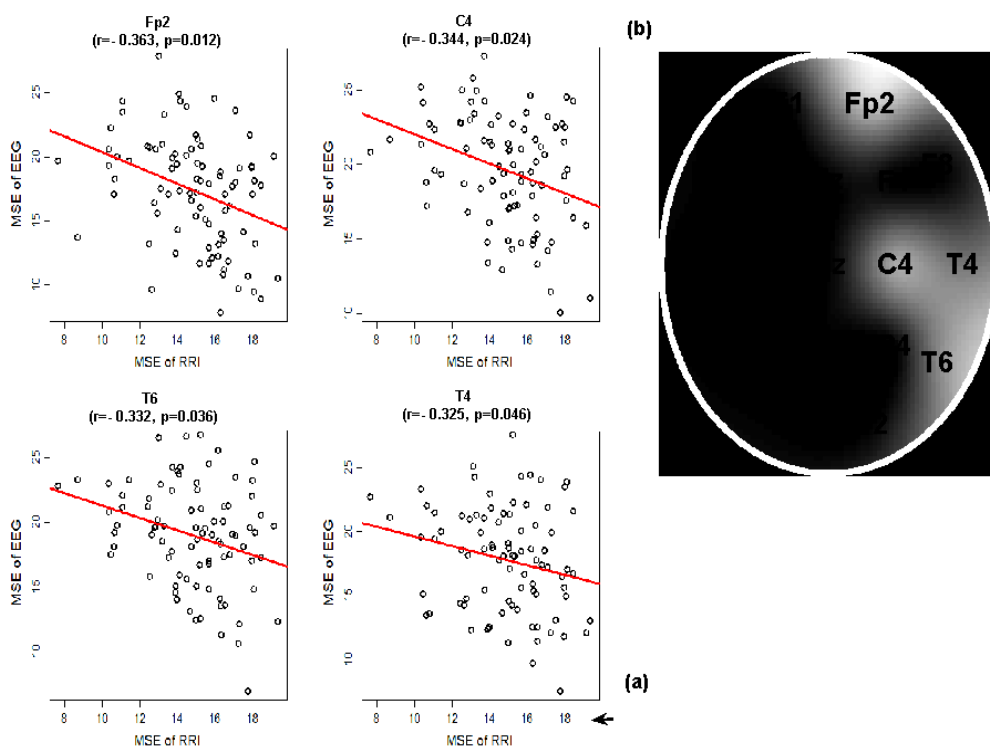


Figure 6 Inverse association between the multiscale entropy (MSE) values of the wakeful RRI and fast-PS EEG. (a) Regions with significant inverse correlation between the summed MSE values on the scales 11-20 of the wakeful RRI and the summed MSE values on the scales 6-20 of the photic-simulated EEG at frequency 12, 15, 18 and 24 Hz (fast-PS, duration 10 seconds and interval 10 seconds) after Bonferroni corrections (corrected p -values = original p -values * 19, alpha = 0.05). r and p denote the Pearson's partial correlation coefficient and corrected significance level, respectively. (b) The brain map illustrates regions with significant association. The relative brightness is according to the sequential p -values from the smallest one (O1, O2 and C4).

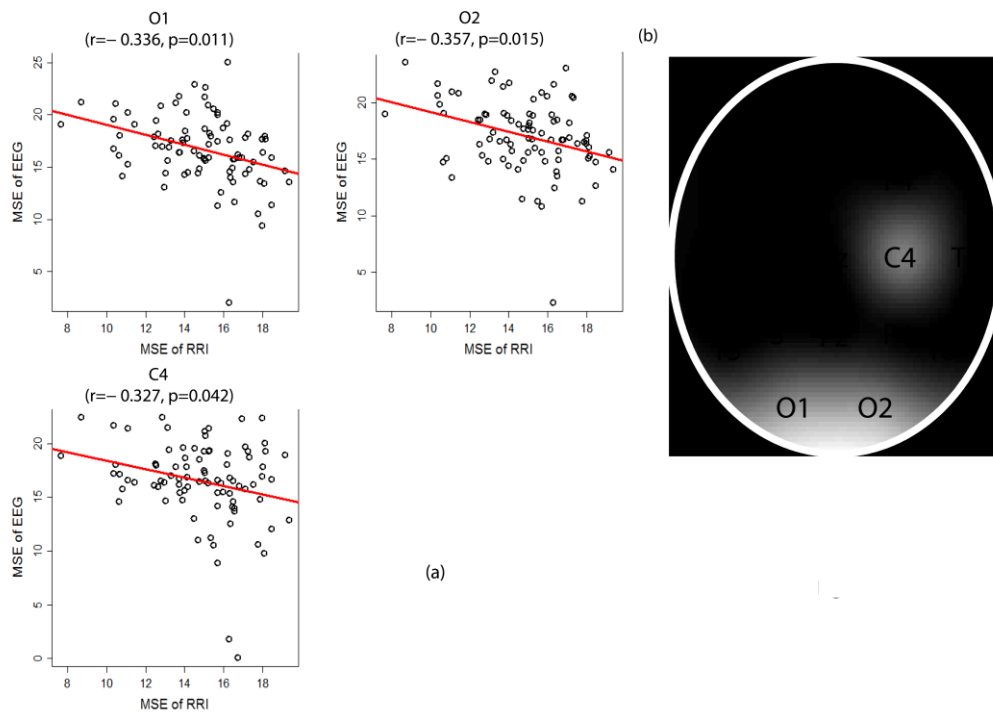


Figure 7 Topographic maps of the significant findings from the post-hoc analyses of one-way multivariate analysis of variance (MANOVA) in the analysis of the filtered EEG whole tracings. The relative brightness is correlated with the p -values as the brightest the smallest p -value. (a1-3) Brain regions showing significant lower number of forbidden words (NumFW) in patients with vascular dementia (VD, $n = 38$) compared with the control group ($n = 29$) in three conditions (resting:wakeful resting, slowPS: slow photic stimulation, fastPS: fast photic stimulation).(b1-3) Brain regions showing significant higher sample entropy (SampEn, $m = 2$) in the VD compared with the control group. (c1-3) Brain regions showing significant lower NumFW in the VD compared with the Alzheimer's group (AD, $n = 22$). (d1-3) Brain regions showing significant higher SampEn in the VD compared with the AD.

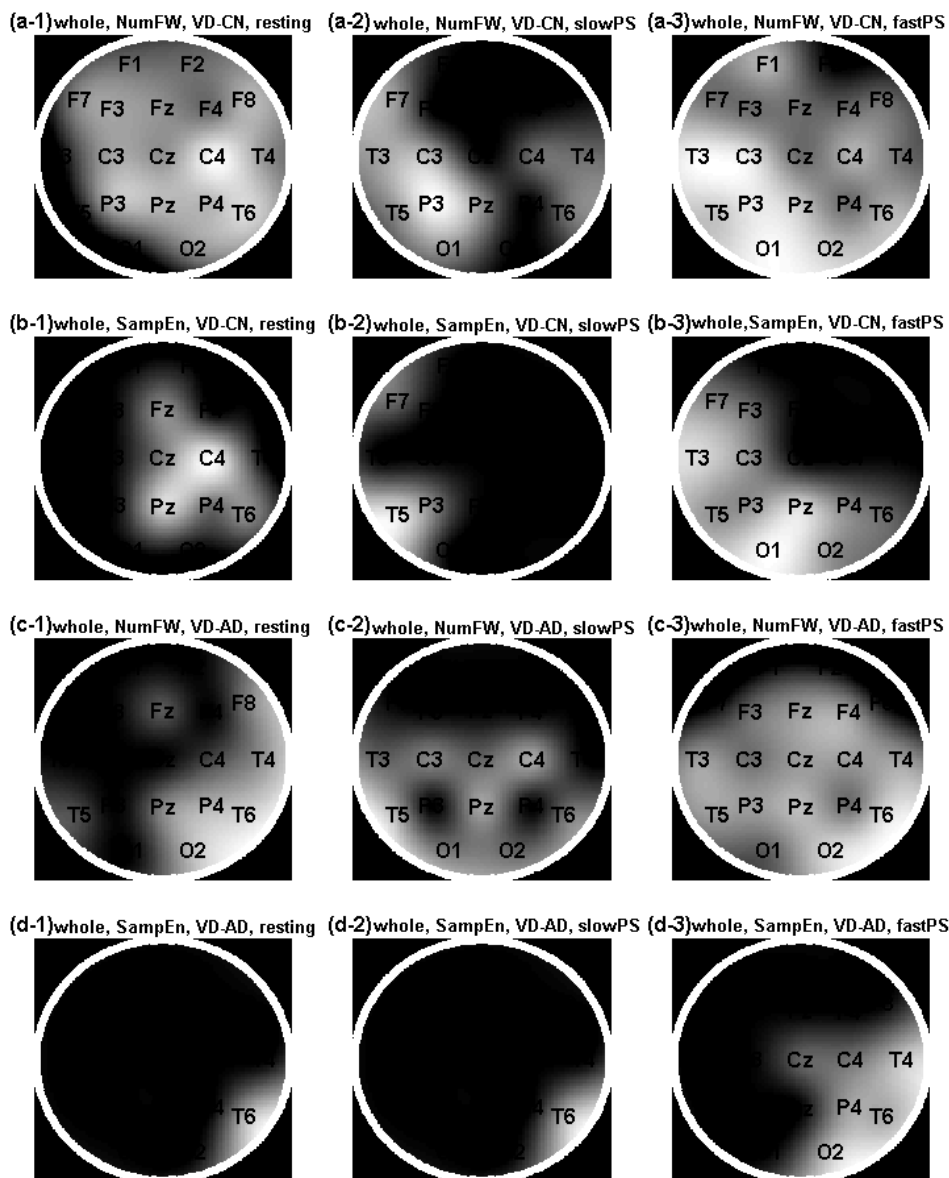
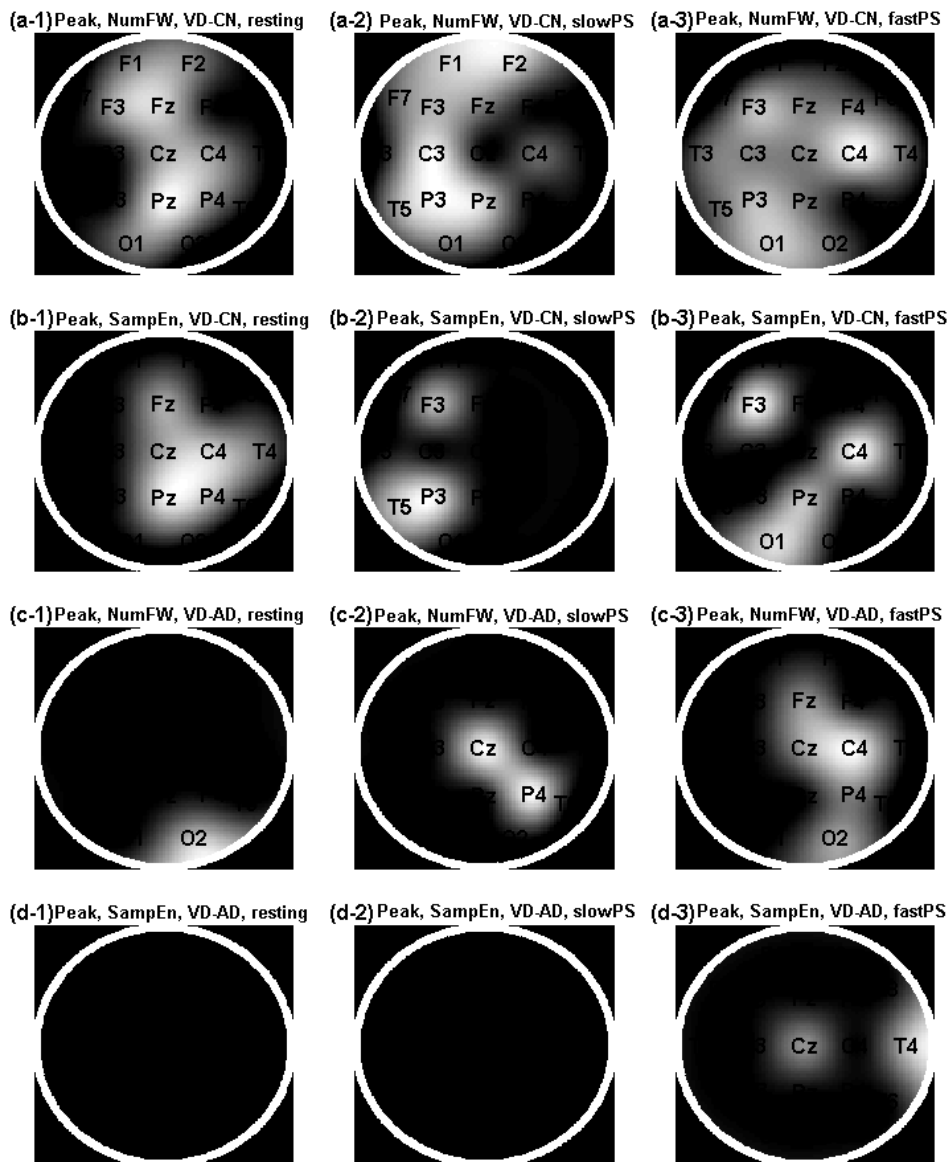
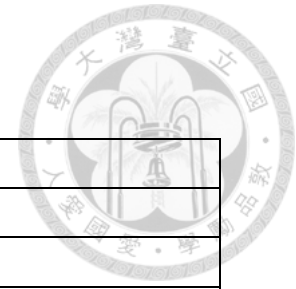


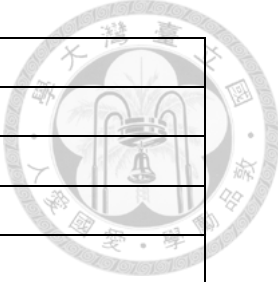
Figure 8 Topographic maps of the significant findings from the post-hoc analyses of one-way multivariate analysis of variance (MANOVA) for the analyses of the local-peak voltage sequences of the filtered EEGs. The relative brightness is correlated with the p -values as the brightest the smallest p -value. (a1-3) Brain regions showing significant lower NumFW in patients with VD ($n = 38$) compared with the control group ($n = 29$) in three conditions (resting: wakeful resting (a1), slowPS: slow photic stimulation (a2), fastPS: fast photic stimulation (a3)). (b1-3) Brain regions showing significant higher sample entropy (SampEn, $m = 2$) in the VD compared with the control group. (c1-3) Brain regions showing significant lower NumFW in the VD compared with the AD ($n = 22$). (d1-3) Brain regions showing significant higher SampEn in the VD compared with the AD.



English Abbreviation



AD	Alzheimer's disease
AAFT	Amplitude adjusted Fourier transform
aEEG	Amplitude integrated EEG
ApEn	Approximate entropy
CNS	Central nervous system
DFA	Detrended fluctuation analysis
ECG	Electrocardiography
EEG	Electroencephalography
EMD	Empirical mode decomposition
EMG	Electromyography
EOG	Electroculograph
ERP	Event-related brain potentials
D_{μ}	Dimension of the natural measure
D_2	Correlation dimension
D_F	Fractal dimension
fMRI	Functional magnetic resonance imaging
HF	High frequency power
HHT	Hilbert-Huang transform
HRV	Heart rate variability
H	Hurst exponent
IAAFT	Iterated amplitude adjusted Fourier transform
IMF	Intrinsic mode function
i.i.d.	Independent and identically distributed
(K-S) entropy	Kolmogorov–Sinai entropy
LF	Low frequency power
LF/HF	Low /high frequency power ratio
MANOVA	Multivariate analysis of variance
mAA	The integrated magnitude of the analytic associate of the EEG
MMSE	Mini-mental status examination
MSE	Multiscale entropy
NumFW	Number of forbidden words
RMS	Root mean square
RS	Rescaled range analysis



RRI	RR interval
SampEn	Sample entropy
SCP	Slow cortical potential
SNR	Signal to noise ratio
SE	Shannon entropy
SOC	Self-organized criticality
SUDEP	Sudden unexpected death in epilepsy
TLE	Temporal lobe epilepsy
VD	Vascular dementia